Mon. Not. R. Astron. Soc. **000**, 1–34 (2015) Printed 4 March 2015 (MN LaTeX style file v2.2)

arXiv:1503.00724v1 [astro-ph.SR] 2 Mar 2015

The M-dwarfs in Multiples (MinMs) survey - I. Stellar multiplicity among low-mass stars within 15 pc*

K. Ward-Duong[1]†, J. Patience[1], R. J. De Rosa[1,2,3], J. Bulger[1], A. Rajan[1],
S. P. Goodwin[4], Richard J. Parker[5], D. W. McCarthy[6] & C. Kulesa[6]
[1]*School of Earth and Space Exploration, Arizona State University, Tempe, AZ 85287, USA*
[2]*Astrophysics Group, School of Physics, University of Exeter, Stocker Road, Exeter EX4 4QL, UK*
[3]*Department of Astronomy, University of California, Berkeley, CA 94720, USA*
[4]*Department of Physics and Astronomy, University of Sheffield, Hounsfield Road, Sheffield, S3 7RH, UK*
[5]*Astrophysics Research Institute, Liverpool John Moores University, 146 Brownlow Hill, L3 5RF, UK*
[6]*Steward Observatory, University of Arizona, 933 N. Cherry Ave., Tucson, AZ 85721, USA*

Accepted 20 February 2015. Received 19 February 2015; in original form 9 June 2014

ABSTRACT
We present a large-scale, volume-limited companion survey of 245 late-K to mid-M (K7-M6) dwarfs within 15 pc. Infrared adaptive optics (AO) data were analysed from the Very Large Telescope, Subaru Telescope, Canada-France-Hawaii Telescope, and MMT Observatory to detect close companions to the sample from $\sim$1 au to 100 au, while digitised wide-field archival plates were searched for wide companions from $\sim$100 au to 10,000 au. With sensitivity to the bottom of the main sequence over a separation range of 3 au to 10,000 au, multiple AO and wide-field epochs allow us to confirm candidates with common proper motions, minimize background contamination, and enable a measurement of comprehensive binary statistics. We detected 65 co-moving stellar companions and find a companion star fraction of 23.5 ± 3.2 per cent over the 3 au to 10,000 au separation range. The companion separation distribution is observed to rise to a higher frequency at smaller separations, peaking at closer separations than measured for more massive primaries. The mass ratio distribution across the $q = 0.2 - 1.0$ range is flat, similar to that of multiple systems with solar-type primaries. The characterisation of binary and multiple star frequency for low-mass field stars can provide crucial comparisons with star forming environments and hold implications for the frequency and evolutionary histories of their associated disks and planets.

Key words: techniques: high angular resolution - binaries: close - binaries: general - binaries: visual - stars: late-type - stars: low-mass

1 INTRODUCTION

Among the nearest stars, the large majority are M-dwarfs (e.g. Reid & Gizis 1997), with a recent accounting indicating that M-dwarfs outnumber higher mass stars by a factor of $\sim$3 (Lépine & Gaidos 2011). Ongoing parallax programs designed to survey the Solar Neighborhood continue to discover additional nearby M-dwarfs, increasing the proportion of the lowest mass members among the nearest stars (e.g. Henry et al. 2006). The nearest star-forming regions are also dominated by low-mass stars; for example, $\sim$50 per cent of the known members of Taurus have spectral types later than M3, the spectral type that will correspond to M0 and later after contraction onto the main sequence (Luhman et al. 2010). The preponderance of the low-mass population of stars highlights the importance of understanding their properties, including the statistics of their companions. As they represent a common outcome of star formation, multiple star systems provide key signatures of the physical processes which affect both star and planet formation.

One of the key scientific questions of star-formation is the universality of the process, and the distribution of binary stars and the initial mass function (IMF) are among the main observational products that can be used to investigate this area (King et al. 2012a). There is no evidence that the IMF varies systematically between different environments (e.g. Luhman et al. 2003; Bastian, Covey & Meyer 2010), indicating that determinations of the IMF are unable to probe the universality or diversity of star-formation. An alternate approach is the analysis of binary populations, since observed differences in binary populations in independent regions suggest differences in the star-formation process (e.g. Goodwin 2010; King et al. 2012a,b; Parker & Meyer 2014). A well-characterised field

---

[*] Based on observations collected at the European Organisation for Astronomical Research in the Southern Hemisphere, Chile (programme 091.D-0804), and observations obtained at the MMT Observatory, a joint facility of the University of Arizona and the Smithsonian Institution.

† E-mail: kwardduo@asu.edu

M-dwarf binary sample is essential for comparison with the full membership of star-forming regions.

In addition to the importance for understanding the products and process of star-formation, companion stars may critically impact planet formation and evolution. A companion star is expected to gravitationally truncate a protoplanetary disk to a radius of approximately one-third the binary star orbital semi-major axis (Artymowicz & Lubow 1994), thereby limiting the amount of material and the region over which planet formation can occur. Determining the population of companions with separations comparable to or less than typical disk sizes of $\sim$100 au (Andrews et al. 2009) are particularly important in considering dynamical effects on the disk, and nearby stars are ideal targets to probe the disk-sized separation range with imaging.

Once planets form, the presence of even a distant companion can alter the dynamics of a planetary system through the Kozai mechanism (Kozai 1962; Lidov 1962). There are indications that some exoplanet systems have been impacted by this dynamical effect (e.g. Wu & Murray 2003), and simulations of early dynamical interactions in star-forming regions have shown that the Kozai mechanism could be induced in up to 20 per cent of field binaries (Parker & Goodwin 2009), subsequently affecting a sizable fraction of the exoplanet population. Determining the binarity of the field population and comparing with primordial binary distributions are critical to determining the fraction of stable stellar systems amenable to hosting planets, as demonstrated recently for G-dwarfs (Parker & Quanz 2013). As the population statistics of exoplanets around low-mass stellar hosts are explored, an understanding of the stellar companions to M-dwarfs represents an important comparison and environmental factor.

Existing M-dwarf binary surveys have sample sizes or selection criteria that impact the interpretation of the population statistics of the companions. The benchmark survey of nearby M-dwarfs by Fischer & Marcy (1992) remains the only survey with complete separation coverage by combining radial velocity, speckle, and direct imaging, however the sample size is restricted to fewer than 65 stars per technique, resulting in large uncertainties on the distributions of mass ratio and separations relative to surveys of more massive primaries (e.g. Raghavan et al. 2010; De Rosa et al. 2014). While more recent M-dwarf surveys include larger samples, the selection criteria include a mixed collection of distances (often based on photometry) or activity indicators, and only the single technique of adaptive optics (AO) or lucky imaging was employed, so the separation range coverage was limited (Bergfors et al. 2010; Janson et al. 2012).

To develop comprehensive population statistics on the companions to a large-scale volume-limited sample of nearby low-mass stars, we have conducted a binary survey of 245 K7-M6 dwarfs within 15 pc based on *Hipparcos* parallaxes. By combining archive and new observations with high resolution and wide-field imaging, the study spans three and a half orders of magnitude in separation. In Section 2, the definition and characteristics of the M-dwarfs in Multiples (MINMS) sample are presented. In Section 3, the new and archival observations are described. The data reduction and analysis method are explained in Section 4. The results and discussion are explored in Section 5. Finally, Section 6 reports a summary of the results.

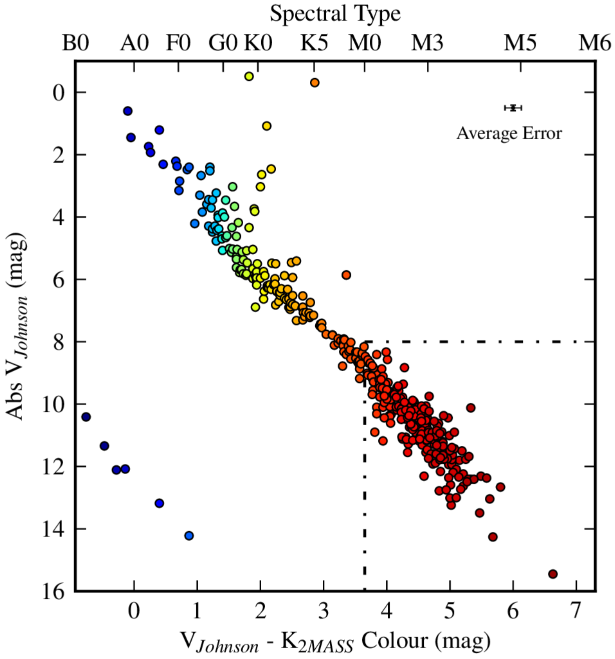

Figure 1. Colour-magnitude diagram of all 449 stars within 15 pc meeting our *Hipparcos* parallax error ($\sigma_\pi/\pi \leqslant 10$ per cent) and photometry criteria. The colour and magnitude criteria used to select our sample of 245 M-dwarfs ($V - K_{\rm S} \geqslant 3.65$, $M_V > 8$) are shown with dashed-dotted lines enclosing our sample space on the CMD. The stars are colour-coded by spectral type, with the paucity of lowest-mass/reddest M-dwarfs at far distances indicative of the sensitivity limit of the *Hipparcos* catalog. An example of the typical errorbar size is shown in the upper right corner of the figure.

2 SAMPLE

2.1 Sample selection

The MINMS sample is derived from the new reduction of the *Hipparcos* catalogue (van Leeuwen 2007). We selected all stars with parallaxes greater than $\pi \geqslant 66.67$ mas, corresponding to stars located within a distance limit of $D \leqslant 15$ pc. In order to obtain precise distances and absolute magnitudes, stars with parallax errors larger than $\sigma_\pi/\pi \geqslant 0.10$ were excluded from the sample. Johnson V-band magnitudes were obtained from the original *Hipparcos* catalogue (Perryman et al. 1997), which comprises ground and space-based photometry with uncertainties $\leqslant 0.08$ mag, and $K_{\rm S}$-band magnitudes were obtained from the Two Micron All Sky Survey (2MASS; Cutri et al. 2003), providing $V - K_{\rm S}$ colours.

Stars with $K_{\rm S}$ magnitudes with significant errors and/or poor quality flags ("X", "U", or "F") were excluded from the sample selection. We also excluded five stars identified as companions to earlier spectral types, as given in the Washington Double Star catalogue (WDS; Mason et al. 2001) and confirmed by common proper motion (see Section 4.3): HIP83599, HIP26801, HIP42762, HIP45343/HIP120005. The parallax and photometric quality criteria provided an all-sky, volume-limited sample of 449 stars of over a wide range of spectral types, as shown in the colour-magnitude diagram (CMD) in Figure 1. M-dwarfs were then selected from this sample by adopting a colour cut of $V - K_{\rm S} > 3.65$, corresponding to spectral class M0 and later (Kenyon & Hartmann 1995). Additionally, only stars with $M_V > 8$ were included to remove any possibility of contamination from evolved stars. The combined par-

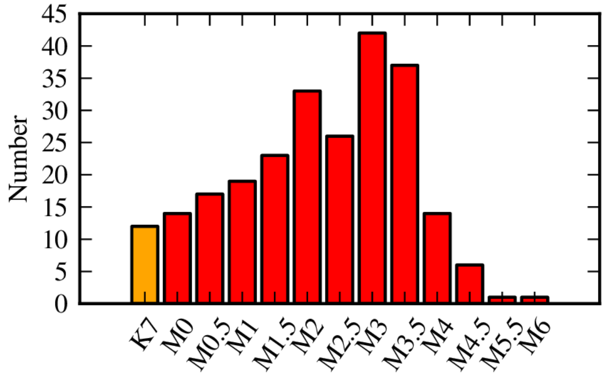

Figure 2. The spectral type distribution of the 15 pc volume-limited 245 M-dwarf sample. The sample has a higher proportion of early-type M-dwarfs, owing to the sensitivity limit of the *Hipparcos* instrument. One star in the sample, HIP 117828, has an early spectral type of "Ma" as classified by Houk & Cowley (1975) but lacks a more recent classification, and is not included in this histogram.

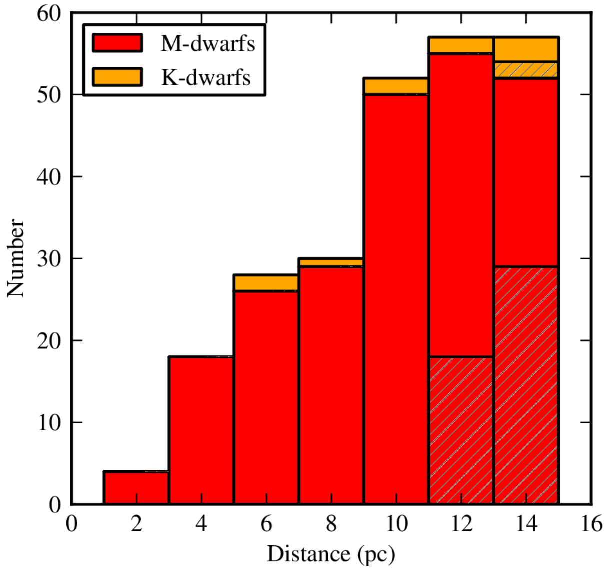

Figure 3. The distance distribution of the 15 pc volume-limited 245 star sample. The darker, hatched portion of the histogram represents stars without new and/or archival adaptive optics data. All of the K and M-dwarfs in our sample up to 11 pc (189 targets) have high-resolution imaging data, covering projected separations of $\sim 1-100$ au. Archival digitised photographic plates were analysed for the entire sample (both darker and lighter solid regions), covering projected separations of $\sim 100-10,000$ au.

allax, colour, and magnitude criteria define a total sample of 245 K and M-dwarfs, of which over 95 per cent are M spectral types.

2.2 Sample properties

The spectral type distribution of the sample is shown in Figure 2, with the majority (94 per cent) of the sample spectral type classifications obtained from the Palomar/MSU Nearby Star Spectroscopic Survey (PMSU, Reid, Hawley & Gizis 1995; Hawley, Gizis & Reid 1996). The spectral types of the remaining stars without PMSU classifications were obtained from the SIMBAD database (individual references listed in Table 1). Uncertainties on the colours and a spread in metallicity led to the inclusion of 12 K7 spectral types, as shown in Figure 3 (discussed in further detail in Section 5.2). Given the limiting magnitudes of the *Hipparcos* catalogue of $V = 12.4$ (ESA 1997), the latest M spectral types were too faint to be detected, leading to the larger frequency of early M-dwarfs in the sample. The distance distribution of the sample is shown in Figure 3. The mass of each primary was estimated from theoretical mass-magnitude relations (Baraffe et al. 1998), with the resulting distribution shown in Figure 4.

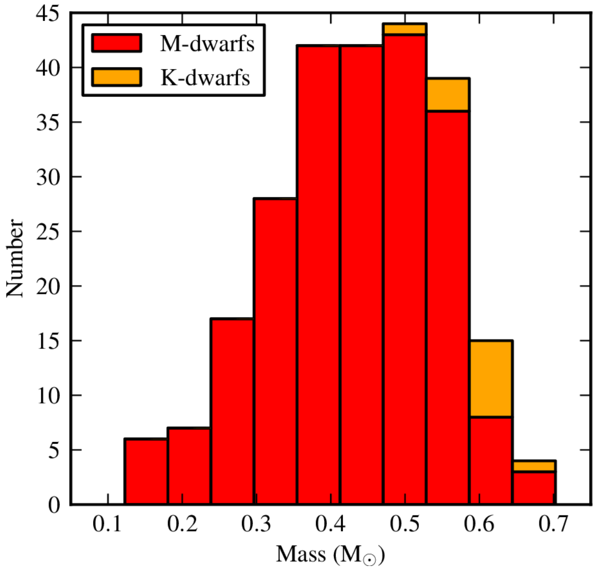

Figure 4. The distribution of primary masses for the targets within the sample. The masses were estimated by comparing the absolute K_S magnitude of each target with theoretical solar-metallicity mass magnitude relations (Baraffe et al. 1998).

Table 1: The 245 K7-M6 dwarf sample within 15 pc

HIP	α (J2000.0)	δ (J2000.0)	μ_α (mas yr^{-1})	μ_δ (mas yr^{-1})	V (mag)	J (mag)	H (mag)	K_S (mag)	π (mas)	Distance (pc)	SpTy.	[Fe/H] (dex)	Ref.
428	1.295368	45.786567	869.7	-151	9.95	6.704±0.021	6.098±0.024	5.853±0.018	88.88±1.42	11.25±0.18	M1	-0.01	2
439	1.351784	-37.357361	5634.4	-2336.4	8.56	5.328±0.019	4.828±0.076	4.523±0.017	230.42±0.90	4.34±0.02	M1.5	-0.45	1
1242	3.873033	-16.133639	-32.1	-149.7	11.49	7.215±0.019	6.712±0.034	6.390±0.016	200.53±9.41	4.99±0.23	M4		
1475	4.595353	44.022949	2887.5	408.9	8.09	5.252±0.264	4.476±0.200	4.018±0.020	278.76±0.77	3.59±0.01	M3.5	-0.26	2
2552	8.122664	67.235616	1741.1	-246.8	10.27	6.844±0.023	6.268±0.021	6.037±0.023	99.35±2.17	10.07±0.22	M2	-0.28	3
3937	12.63845	24.816829	223.7	-40.9	12.01	7.951±0.023	7.350±0.015	7.119±0.020	84.42±4.65	11.85±0.65	M3.5		
4569	14.616383	-27.857032	1293.4	-298.9	11.77	7.763±0.023	7.203±0.051	6.892±0.021	80.95±3.21	12.35±0.49	M3.5		
4856	15.6343	71.679816	1745.3	-380.9	9.98	6.301±0.034	5.699±0.049	5.449±0.017	121.41±1.25	8.24±0.08	M3		
4872	15.661952	62.345041	730.3	88.4	9.56	6.230±0.021	5.582±0.024	5.371±0.020	100.40±1.52	9.96±0.15	M1.5	0.15	2
5496	17.595382	-67.444937	386.3	580	9.8	5.997±0.019	5.409±0.026	5.132±0.024	122.04±2.42	8.19±0.16	M2.0		
5643	18.127668	-16.998967	1210.1	647	12.1	7.258±0.020	6.749±0.033	6.420±0.017	271.01±8.36	3.69±0.11	M4.5	-0.38	1
8051	25.83408	4.321657	-422.2	-764.4	10.93	7.370±0.024	6.809±0.042	6.516±0.023	87.62±2.00	11.41±0.26	M2	-0.13	2
8768	28.204883	-22.434856	844.2	-0.6	8.89	6.064±0.021	5.405±0.026	5.178±0.020	90.86±1.16	11.01±0.14	K7		
9291	29.847979	58.521134	322	-194.8	12.21	7.790±0.019	7.224±0.061	6.961±0.024	81.65±4.06	12.25±0.61	M4		
9724	31.27018	-17.614632	1311.5	-174	10.19	6.542±0.021	5.898±0.024	5.662±0.020	109.38±1.92	9.14±0.16	M2.5		
9786	31.452304	-30.176649	-527.8	100.1	12.15	8.367±0.024	7.867±0.038	7.558±0.024	107.81±2.92	9.28±0.25	M2.5		
10279	33.08745	3.575621	-1761.5	-1852.3	10.04	6.830±0.019	6.321±0.034	6.077±0.020	96.02±1.66	10.41±0.18	M1.5	-0.32	1
10395	33.473436	-32.041237	758.9	-530.5	10.31	6.961±0.020	6.327±0.026	6.093±0.016	79.68±1.69	12.55±0.27	M1.5		
10617	34.171684	-30.988491	687.2	247.5	12.02	7.987±0.029	7.320±0.027	7.131±0.021	69.81±3.10	14.32±0.64	M3.0		
10812	34.791992	-36.778083	1394.1	550	11.59	7.924±0.032	7.317±0.063	7.031±0.020	71.06±3.23	14.07±0.64	M2.5		
11048	35.561017	47.880027	216.6	40.2	9.4	6.377±0.019	5.770±0.038	5.554±0.026	83.75±1.14	11.94±0.16	M0.5	0.14	2
11964	38.594024	-43.796344	58.1	-287.4	8.89	5.795±0.018	5.126±0.027	4.885±0.016	86.18±0.78	11.60±0.11	M0.0		
12097	38.972113	20.219881	250.1	-141.8	10.68	7.208±0.020	6.572±0.020	6.328±0.020	73.56±1.85	13.59±0.34	M2		
12781	41.064632	25.523374	862.5	-360.7	10.55	6.752±0.018	6.197±0.017	5.961±0.021	133.16±2.26	7.51±0.13	M3	-0.1	2
13218	42.540549	-53.138971	-117.4	502.9	10.72	7.349±0.024	6.753±0.036	6.495±0.020	77.19±1.64	12.96±0.28	M1.5		
13389	43.092367	-63.67982	979.1	630.6	11.36	7.671±0.024	7.115±0.029	6.829±0.017	85.87±1.99	11.65±0.27	M2.5		
15220	49.057609	58.167329	445.6	-340.3	10.53	7.344±0.020	6.759±0.055	6.566±0.024	69.51±3.37	14.39±0.70	M2		
15638	50.340755	79.967257	410.4	284.7	11.21	7.704±0.027	7.117±0.036	6.890±0.024	71.21±1.56	14.04±0.31	M2		
16536	53.232738	-44.701952	-311.8	131.2	11.47	7.741±0.020	7.213±0.036	6.907±0.016	93.11±1.94	10.74±0.22	M2.5	-0.28	1
17609	56.583918	26.215502	387.2	-197.6	9.61	6.689±0.021	6.046±0.018	5.844±0.018	67.80±2.06	14.75±0.45	M0		
19337	62.155823	33.637038	525	126.7	10.18	7.016±0.020	6.395±0.044	6.178±0.020	74.37±2.71	13.45±0.49	M0.5		
19394	62.315272	-53.373698	1043.7	582	11.79	7.948±0.026	7.428±0.040	7.135±0.021	66.69±1.82	14.99±0.41	M3.5	0.07	1
21088	67.805446	58.976153	-4.7	2.6	10.82	6.622±0.021	6.012±0.020	5.717±0.021	179.27±3.23	5.58±0.10	M4	0.36	3
21556	69.424445	-11.038877	-225.1	-194.5	10.34	6.943±0.019	6.331±0.026	6.091±0.021	90.10±1.74	11.10±0.21	M1.5	-0.04	2
21932	70.732396	18.958165	656.9	-1117.3	9.95	6.462±0.024	5.824±0.033	5.607±0.034	107.83±2.85	9.27±0.25	M2	-0.01	1
22627	73.023864	6.476539	146.1	-310.1	11.94	7.814±0.024	7.209±0.046	6.942±0.018	81.38±4.04	12.29±0.61	M3.5	0.12	1
22738	73.379934	-55.860294	129.1	68.5	10.73	7.197±0.027	6.623±0.055	6.338±0.021	90.02±1.98	11.11±0.24	M2.0		
22762	73.458249	-17.773421	408.4	-645.1	10.9	7.413±0.020	6.860±0.038	6.598±0.021	82.52±2.40	12.12±0.35	M2	-0.24	2
23452	75.618384	-21.256729	-153.4	-257.7	8.31	5.450±0.021	4.853±0.017	4.600±0.018	116.59±1.51	8.58±0.11	K7		
23512	75.833701	-17.373562	-228.8	-444.5	11.71	7.819±0.023	7.242±0.034	6.936±0.021	108.61±2.66	9.21±0.23	M3	-0.19	1
23518	75.84959	53.128469	1304.2	-1537.6	9.96	7.001±0.023	6.414±0.034	6.172±0.021	73.41±1.97	13.62±0.37	M0.5		
23932	77.146023	-18.172047	503.9	-1399.8	10.28	6.175±0.018	5.591±0.031	5.314±0.018	107.85±2.10	9.27±0.18	M3.5		
24186	77.919074	-45.018405	6499.1	-5722.6	8.86	5.821±0.026	5.316±0.027	5.049±0.021	255.66±0.91	3.91±0.01	sdM1	-0.85	1
24284	78.175937	19.665657	278	241.2	10.82	7.299±0.024	6.695±0.040	6.470±0.024	81.35±4.07	12.29±0.62	M2	-0.09	2
25578	82.000627	9.643928	-194.1	-767.9	12.48	8.311±0.021	7.840±0.033	7.542±0.017	113.50±5.01	8.81±0.39	M3.5	-0.22	1
25878	82.864154	-3.677228	763.9	-2092.4	7.97	4.999±0.300	4.149±0.212	4.039±0.260	176.77±1.18	5.66±0.04	M1.5	0.19	1
25953	83.061072	9.820808	-177.9	-219.4	11.55	7.423±0.032	6.876±0.034	6.560±0.036	78.16±3.70	12.79±0.61	M3.5		
26801	85.378074	53.48985	4.3	-512.2	9.78	6.586±0.021	5.963±0.016	5.759±0.016	80.40±1.69	12.44±0.26	M0.5	0.11	2
26857	85.538611	12.489337	1998.6	-1570.6	11.56	7.124±0.021	6.627±0.018	6.389±0.016	171.55±3.99	5.83±0.14	M4	-0.11	1
28035	88.930057	-26.856507	315	-10.5	10.7	7.175±0.029	6.475±0.023	6.288±0.020	68.57±2.17	14.58±0.46	M2.5V^a		
28368	89.907339	58.593019	12.3	-255.6	10.25	7.068±0.021	6.416±0.023	6.212±0.018	73.89±1.64	13.53±0.30	M0.5		
29052	91.932237	-25.744864	-184.2	-204	11.87	8.018±0.032	7.499±0.061	7.169±0.023	88.14±2.50	11.35±0.32	M4^b	-0.15	2
29277	92.582693	82.106756	50.1	-1335.9	10.48	6.869±0.023	6.295±0.017	6.061±0.018	106.69±1.31	9.37±0.12	M2		
29295	92.644232	-21.864621	-136.8	-706.1	8.15	5.104±0.037	4.393±0.254	4.166±0.232	173.81±0.99	5.75±0.03	M0.5	-0.03	1
29316	92.728307	10.318029	51.9	-941.2	10.41	6.795±0.024	6.306±0.040	6.032±0.023	91.65±3.50	10.91±0.42	M2.5		
30920	97.348084	-2.810504	-53.4	4.6	11.12	6.376±0.023	5.754±0.034	5.486±0.016	242.32±3.12	4.13±0.05	M4.5	0.13	3
31292	98.444972	-75.624946	-328.1	272.1	11.41	7.410±0.030	6.850±0.031	6.558±0.021	115.19±10.61	8.68±0.80	M3V^a	-0.06	1
31293	98.430286	-75.629965	-299.4	283	10.35	6.725±0.023	6.146±0.026	5.862±0.024	110.88±2.25	9.02±0.18	M2V^c	-0.05	1
31635	99.295001	17.564815	-765.4	338.1	9.63	6.674±0.024	6.031±0.016	5.862±0.024	102.60±1.65	9.75±0.16	K7	-0.34	2
31862	99.906836	-55.609673	-394.4	12.7	9.8	6.861±0.020	6.276±0.031	6.027±0.017	75.19±1.10	13.30±0.19	M0Vk^a		
33142	103.517713	60.871769	518	-998.5	11.01	7.128±0.020	6.604±0.017	6.345±0.016	95.43±2.36	10.48±0.26	M3		
33226	103.703986	33.268174	-728.7	-399.7	9.89	6.104±0.024	5.526±0.016	5.275±0.023	179.01±1.60	5.59±0.05	M3	0	2
33499	104.447007	-44.284818	263.2	109.2	10.81	6.883±0.019	6.365±0.044	6.056±0.018	124.85±2.13	8.01±0.14	M3.0		
34115	106.108087	68.2888	345.7	53.7	11.95	8.170±0.034	7.594±0.026	7.269±0.020	66.98±2.65	14.93±0.59	M3		
34603	107.507653	38.529459	-445.4	-943.3	11.65	6.731±0.026	6.152±0.047	5.846±0.018	158.87±3.35	6.29±0.13	M4.5	0.1	3
35191	109.082402	27.142502	-38.5	-194.5	10.83	7.013±0.026	6.436±0.027	6.187±0.023	83.09±2.84	12.04±0.41	M2.5		
35353	109.534092	39.274814	-213	-114.4	10.3	7.209±0.023	6.588±0.026	6.369±0.023	69.01±2.07	14.49±0.43	M0		
36208	111.852081	5.225786	571.6	-3693.6	9.84	5.714±0.032	5.219±0.063	4.857±0.023	262.98±1.39	3.80±0.02	M3.5	-0.01	1
36338	112.189321	-3.298157	435.6	-794.4	11.47	7.544±0.020	6.976±0.031	6.704±0.027	81.38±2.49	12.29±0.38	M3	-0.01	2
36626	112.990436	36.219407	-251.4	-250.6	10.52	6.771±0.019	6.179±0.024	5.927±0.017	84.26±3.45	11.87±0.49	M2.5		
36627	112.988838	36.229824	-277.9	-259	11.82	7.571±0.020	6.985±0.020	6.755±0.021	83.46±4.07	11.98±0.58	M3.5		
36834	113.614295	62.941501	-497.1	-104.7	10.4	7.340±0.026	6.782±0.016	6.556±0.018	87.15±2.31	11.47±0.30	M0.5	-0.37	2
36915	113.841133	54.849726	-120.2	18.5	11.36	7.772±0.024	7.222±0.033	6.955±0.023	78.14±2.69	12.80±0.44	M2		
36985	114.02949	-3.110779	36.3	-253.5	9.87	6.791±0.034	6.155±0.036	5.934±0.018	70.55±1.64	14.17±0.33	M1.5V^d		
37217	114.670663	-21.224577	454.2	-474.5	11.68	7.848±0.019	7.334±0.036	7.063±0.023	94.31±3.31	10.60±0.37	M3	-0.22	1
37288	114.845994	2.183663	-147.8	-246.7	9.66	6.769±0.027	6.092±0.036	5.872±0.021	68.58±1.47	14.58±0.31	K7		
37766	116.167387	3.552458	-347.3	-448.8	11.19	6.581±0.024	6.005±0.038	5.698±0.017	167.88±2.31	5.96±0.08	M4.5	4	1
38082	117.068278	20.368135	1452.1	-988.3	11.46	8.120±0.024	7.610±0.024	7.396±0.024	67.69±2.65	14.77±0.58	M1		
38956	119.559465	41.301835	-0.2	-6.7	12.02	7.734±0.023	7.133±0.034	6.878±0.031	116.06±3.67	8.62±0.27	M3.5	0.24	4
40501	124.033259	1.302572	-374.7	59.7	10.08	6.625±0.026	6.036±0.031	5.766±0.024	109.62±1.54	9.12±0.13	M2	-0.17	1

Table 1: continued.

HIP	α	δ	μ_α	μ_δ	V	J	H	K_S	π	Distance	SpTy.	[Fe/H]	Ref.
	(J2000.0)	(J2000.0)	(mas yr^{-1})	(mas yr^{-1})	(mag)	(mag)	(mag)	(mag)	(mas)	(pc)		(dex)	
41824	127.906464	19.391178	-23.6	20.1	11.9	7.509±0.020	6.894±0.024	6.603±0.024	90.37±8.22	11.07±1.01	M3.5		
42220	129.106067	67.295071	-1062.9	47.7	9.28	6.425±0.029	5.782±0.015	5.580±0.015	72.59±1.26	13.78±0.24	K7	-0.06	2
42762	130.719369	9.549654	1.2	-6.3	11.83	8.122±0.026	7.490±0.038	7.283±0.018	66.96±3.91	14.93±0.87	M2.5		
44722	136.688956	-8.806837	-304.3	209.4	9.5	6.641±0.018	5.982±0.040	5.757±0.017	68.69±1.29	14.56±0.27	K7		
45908	140.406683	-60.281953	-838.5	182	9.49	6.442±0.023	5.793±0.033	5.587±0.021	95.58±0.91	10.46±0.10	M0.0	-0.14	1
46655	142.685768	0.322661	-569.9	-552.2	11.71	7.697±0.020	7.182±0.029	6.871±0.024	103.46±3.94	9.67±0.37	M3.5	-0.09	1
46706	142.830928	-13.488726	730.3	23.1	10.06	6.361±0.020	5.755±0.029	5.511±0.020	99.88±3.60	10.01±0.36	M3		
46769	142.984726	36.320228	-207.9	-524.7	10.19	7.121±0.023	6.569±0.055	6.302±0.020	71.91±1.82	13.91±0.35	M0	-0.2	2
47103	144.006819	-21.660796	137.8	-989.1	10.91	7.337±0.034	6.740±0.033	6.475±0.017	110.82±1.92	9.02±0.16	M2.5	-0.3	1
47425	144.943206	-41.067558	-526.6	356.4	10.72	6.902±0.029	6.321±0.049	6.056±0.023	105.63±1.64	9.47±0.15	M2.0	-0.01	1
47513	145.293167	13.209563	-660.7	-142.9	10.38	6.971±0.020	6.369±0.044	6.128±0.020	88.81±1.68	11.26±0.21	M1.5	-0.05	2
47620	145.645136	70.033884	-672.2	-268.3	10.56	6.917±0.018	6.326±0.015	6.075±0.017	81.37±1.77	12.29±0.27	M2		
47650	145.715596	70.039402	-667.3	-268.5	11.19	7.326±0.020	6.731±0.018	6.469±0.016	88.07±2.41	11.35±0.31	M3		
47741	145.981716	26.969006	-581.6	-100	12.08	8.035±0.026	7.461±0.024	7.190±0.023	71.29±4.49	14.03±0.88	M3.5		
47780	146.124302	-45.776502	-464.2	-582.1	10.22	6.632±0.023	6.045±0.044	5.780±0.020	101.31±3.18	9.87±0.31	M1.0	-0.07	1
48336	147.790173	-12.32987	1140	-1457.5	10.04	6.988±0.024	6.400±0.036	6.150±0.026	72.92±1.82	13.71±0.34	M0.5		
48659	148.849425	-27.261306	-103.7	-154.2	12.04	8.032±0.023	7.433±0.038	7.143±0.021	88.32±3.18	11.32±0.41	M3V^a		
48714	149.036126	62.788463	-304.5	-583.2	8.99	6.030±0.024	5.369±0.044	5.200±0.024	94.68±1.26	10.56±0.14	M0	0.11	2
49969	153.019527	-2.684739	511.4	-603.8	10.64	7.021±0.023	6.471±0.049	6.193±0.026	81.08±2.87	12.33±0.44	M2.5		
49986	153.07362	-3.745664	-151.8	-243.8	9.26	5.888±0.021	5.258±0.016	5.015±0.020	127.08±1.90	7.87±0.12	M1.5	0.02	1
50341	154.191447	-11.96178	-420.1	-604.8	10.99	7.323±0.019	6.711±0.042	6.452±0.018	73.30±2.62	13.64±0.49	M3		
51007	156.295159	-10.228694	-691.6	120.5	10.15	6.895±0.019	6.264±0.033	6.032±0.017	81.00±1.91	12.35±0.29	M1	-0.02	2
51317	157.231466	0.840995	-601.7	-733.9	9.65	6.176±0.021	5.605±0.033	5.311±0.023	141.50±2.22	7.07±0.11	M2	-0.2	1
52190	159.934843	-37.920484	192.2	-124	11.02	7.211±0.018	6.629±0.023	6.381±0.023	71.51±2.48	13.98±0.48	M2Ve^c		
52596	161.319558	-30.807499	-28.9	-236.5	11.22	7.816±0.020	7.216±0.036	6.992±0.016	71.41±2.37	14.00±0.46	M1.5V^a		
53020	162.71425	6.810202	-3.4	-41.6	11.64	7.319±0.023	6.707±0.051	6.371±0.016	147.92±3.52	6.76±0.16	M4	0.03	1
53985	165.659754	21.96714	141.2	-51.2	9.57	6.522±0.020	5.899±0.018	5.688±0.021	84.95±1.05	11.77±0.15	M0		
54035	165.834147	35.96987	-578.6	-4771.4	7.49	4.203±0.242	3.640±0.202	3.254±0.306	392.64±0.67	2.55±0.00	M2	-0.3	2
54211	166.369055	43.526771	-4417.9	943.3	8.82	5.538±0.019	5.002±0.021	4.769±0.020	206.27±1.00	4.85±0.02	M6	-0.32	2
54532	167.380601	-24.598641	-798	-445.5	10.44	6.948±0.021	6.358±0.038	6.097±0.023	93.00±1.69	10.75±0.20	M2	-0.1	1
55042	169.000866	-57.547668	-2464.8	1179.5	11.66	7.811±0.020	7.304±0.053	7.035±0.031	78.91±2.60	12.67±0.42	M3.5		
55360	170.02011	65.846487	-2948	183.9	9.31	6.306±0.018	5.730±0.020	5.534±0.017	112.13±1.03	8.92±0.08	M0	-0.41	2
56157	172.67427	-8.095262	-354.8	262.5	11.98	8.033±0.019	7.457±0.026	7.152±0.017	75.75±4.22	13.20±0.74	M3V^a		
56244	172.943811	-41.046437	-715.8	171.5	11.55	7.366±0.027	6.765±0.038	6.511±0.034	96.56±2.39	10.36±0.26	M3.5		
56528	173.862282	-32.539971	-71.3	-850.1	9.81	6.471±0.018	5.856±0.036	5.623±0.021	112.58±1.44	8.88±0.11	M1.5	-0.17	1
57050	175.435971	42.751974	-579.7	-89.6	11.86	7.608±0.018	7.069±0.023	6.822±0.016	90.06±2.75	11.10±0.34	M4	-0.04	2
57087	175.546226	26.70657	896.4	-813.7	10.67	6.900±0.024	6.319±0.023	6.073±0.016	98.61±2.33	10.14±0.24	M2.5	-0.03	1
57544	176.92241	78.691159	743.9	479.8	10.8	6.724±0.024	6.217±0.044	5.954±0.027	186.86±1.70	5.35±0.05	M3.5	-0.25	3
57548	176.934985	0.804563	605.6	-1219.2	11.12	6.505±0.023	5.945±0.024	5.654±0.024	298.04±2.30	3.36±0.03	M4	-0.17	1
57802	177.780573	35.272017	-272	254.8	9.76	6.419±0.020	5.828±0.020	5.606±0.017	116.48±1.19	8.59±0.09	M1	-0.27	4
59406	182.798989	-19.960581	-227.3	-189.4	11.67	7.895±0.027	7.359±0.034	7.044±0.016	79.43±2.36	12.59±0.37	M3		
60444	185.888379	67.188425	235.4	-106.7	11.19	7.598±0.020	7.086±0.024	6.807±0.015	77.54±3.23	12.90±0.54	M2.5		
60559	186.218774	-18.24228	1096.2	-2304.9	11.28	7.734±0.021	7.247±0.021	6.950±0.021	112.98±2.51	8.85±0.20	M2	-0.62	1
60910	187.249512	8.427484	0.9	-35.5	11.99	7.844±0.035	7.203±0.053	6.956±0.026	75.85±3.99	13.18±0.69	M3.5		
61094	187.815854	8.810603	-636.3	-521.2	9.74	6.782±0.034	6.091±0.027	5.892±0.020	73.28±1.31	13.65±0.24	K7		
61629	189.467578	-52.001476	-1032.2	30.5	10.65	6.864±0.019	6.285±0.027	6.020±0.021	103.18±2.31	9.69±0.22	M2.0	0.01	1
61706	189.718504	11.696166	-1156.2	-244.9	11.49	7.581±0.019	6.939±0.036	6.691±0.036	69.59±2.79	14.37±0.58	M3		
61874	190.19287	-43.566377	-782	693.5	12.24	8.217±0.029	7.703±0.044	7.413±0.021	128.52±3.90	7.78±0.24	M3.0	-0.48	1
62452	191.985937	9.751397	-1007.7	-461	11.39	7.195±0.026	6.666±0.046	6.362±0.018	119.47±2.69	8.37±0.19	M3.5	0.03	1
62556	192.261472	66.110186	-437.2	-104.7	10.94	6.880±0.024	6.299±0.046	6.070±0.024	97.91±1.83	10.21±0.19	M3		
63510	195.194055	12.375693	-640.1	-25.1	9.76	6.437±0.021	5.786±0.017	5.578±0.016	85.54±1.53	11.69±0.21	M0.5	0.25	2
65011	199.889958	35.110163	386.7	-774.9	9.48	6.383±0.021	5.788±0.026	5.560±0.016	75.38±1.54	13.27±0.27	M0.5	-0.05	4
65026	199.940367	47.778028	152.9	-17.4	8.48	5.338±0.026	4.721±0.018	4.494±0.018	93.40±2.21	10.71±0.25	M0.5		
65714	202.087868	-2.360286	153	-491.8	11.23	7.515±0.021	6.913±0.051	6.613±0.023	72.00±2.83	13.89±0.55	M3		
65859	202.499107	10.377162	1127.5	-1074.2	9.05	5.902±0.018	5.300±0.033	5.036±0.027	130.62±1.05	7.66±0.06	M0.5	-0.16	1
66625	204.850421	46.186493	-43.6	390.5	10.24	7.054±0.018	6.513±0.036	6.284±0.017	76.87±1.61	13.01±0.27	M1		
66906	205.680288	33.290104	-111.5	-706.7	12.03	7.787±0.020	7.212±0.024	6.982±0.020	107.77±3.22	9.28±0.28	M3.5	0.14	4
67155	206.432399	14.891522	1777.1	-1454.5	8.46	5.181±0.037	4.775±0.206	4.415±0.017	185.49±1.10	5.39±0.03	M1.5	-0.22	1
67164	206.4613	-17.968219	-311.6	-549.4	11.81	7.745±0.021	7.192±0.046	6.902±0.044	97.62±5.03	10.24±0.53	M3.5		
68469	210.263284	-2.654865	-825	599	9.71	6.516±0.018	5.935±0.036	5.683±0.020	99.72±1.57	10.03±0.16	M1	-0.14	1
69454	213.303642	-56.742059	355.1	178.7	10.2	6.951±0.026	6.394±0.047	6.136±0.027	85.62±1.94	11.68±0.26	M2V^e		
70475	216.233264	8.887619	546.3	158.2	12.23	8.420±0.034	7.802±0.038	7.590±0.027	70.03±4.89	14.28±1.00	M2.5	-0.15	4
70865	217.373742	15.532644	-1053.7	1301.4	10.67	7.229±0.021	6.605±0.031	6.393±0.018	71.39±2.10	14.01±0.41	M2		
70890	217.428921	-62.679477	159.2	-67.3	11.01	5.357±0.023	4.835±0.057	4.384±0.033	771.64±2.60	1.30±0.00	M5.5	0.16	1
70975	217.754844	-12.2961	-405.2	-400.2	11.92	7.803±0.026	7.259±0.049	6.961±0.021	92.44±3.94	10.82±0.46	M3.5		
71253	218.570042	-12.519555	-357.5	595.1	11.32	6.838±0.019	6.262±0.044	5.939±0.034	164.99±3.29	6.06±0.12	M4	0.14	1
71898	220.589896	66.055783	-307.5	-33.9	10.88	7.306±0.024	6.733±0.026	6.491±0.024	93.17±1.30	10.73±0.15	M1.5		
72896	223.464449	23.555806	-715.8	106.4	11.53	7.438±0.020	6.828±0.020	6.572±0.020	98.40±4.42	10.16±0.46	M3.5		
72944	223.621833	16.101052	277.4	-132.3	10.11	6.633±0.023	5.990±0.021	5.770±0.018	103.59±1.72	9.65±0.16	M2	-0.06	1
73470	225.231544	45.426209	236.2	325.3	9.15	6.198±0.023	5.604±0.034	5.383±0.018	84.79±1.07	11.79±0.15	K7		
74190	227.398303	3.166823	-601.1	482.5	11.46	7.720±0.024	7.134±0.034	6.858±0.018	69.19±2.60	14.45±0.54	M3		
74995	229.861771	-7.72228	-1224.5	-99.5	10.57	6.706±0.026	6.095±0.033	5.837±0.023	160.91±2.62	6.21±0.10	M3	-0.2	1
75187	230.470546	20.977754	79.4	128.6	10.66	6.610±0.021	5.960±0.016	5.756±0.018	87.63±1.81	11.41±0.24	M1.5		
76074	233.053887	-41.275588	-1175.9	-1029.6	9.31	5.647±0.021	5.025±0.024	4.759±0.024	168.66±1.30	5.93±0.05	M2.5	0.06	1
76832	235.319304	75.992776	808.2	-739.8	12.22	8.260±0.018	7.716±0.020	7.442±0.023	75.13±2.40	13.31±0.43	M3		
76901	235.529261	-19.470833	20.3	-95.9	11.83	7.920±0.019	7.421±0.036	7.168±0.027	95.90±5.59	10.43±0.61	M3		
78353	239.972426	-8.253201	203.5	-23.5	10.49	7.185±0.030	6.601±0.047	6.343±0.029	71.95±1.88	13.90±0.36	M1		
79431	243.174062	-18.875503	24.8	-210.8	11.34	7.555±0.026	6.855±0.044	6.589±0.018	69.46±3.12	14.40±0.65	M3V^a	0.46	3
79755	244.178136	67.238847	-494.6	84.4	8.61	5.779±0.019	5.136±0.034	4.953±0.018	93.57±0.95	10.69±0.11	K7		
79762	244.188838	67.256248	-477.8	91.1	10.69	6.908±0.021	6.300±0.021	6.066±0.020	93.09±1.48	10.74±0.17	M3		
80018	245.014621	-37.529006	-740.1	997.4	10.56	6.793±0.023	6.223±0.021	5.950±0.021	119.85±2.52	8.34±0.18	M2.0	-0.06	1

Table 1: continued.

HIP	α (J2000.0)	δ (J2000.0)	μ_α (mas yr^{-1})	μ_δ (mas yr^{-1})	V (mag)	J (mag)	H (mag)	K_S (mag)	π (mas)	Distance (pc)	SpTy.	[Fe/H] (dex)	Ref.
80346	246.038842	48.352901	1144.2	-450.8	10.27	6.638±0.024	6.141±0.021	5.915±0.023	124.12±1.16	8.06±0.08	M2.5		
80459	246.352598	54.304102	432.6	-171.2	10.13	6.608±0.020	6.063±0.018	5.833±0.024	153.46±0.99	6.52±0.04	M1.5	-0.23	3
80824	247.575251	-12.662596	-91.3	-1185.8	10.1	5.950±0.024	5.373±0.040	5.075±0.024	232.98±1.60	4.29±0.03	M3.5	-0.02	1
82809	253.855399	-8.326946	-631.5	-90.8	11.73	7.555±0.024	7.056±0.061	6.724±0.017	148.92±4.00	6.72±0.18	M3.5	-0.26	1
82817	253.869858	-8.336376	-811.8	-890.5	9.02	5.270±0.037	4.775±0.017	4.403±0.036	161.41±5.64	6.20±0.22	M3	-0.39	3
83043	254.536879	25.74416	-113.3	-507.7	9.7	6.448±0.021	5.865±0.020	5.624±0.016	96.67±1.39	10.34±0.15	M1	-0.04	3
83599	256.303349	-5.095949	-223.9	219.7	10.08	6.780±0.029	6.193±0.021	5.975±0.026	94.59±1.85	10.57±0.21	M2		
83762	256.7812	21.554011	-465.7	-29.4	11.61	7.875±0.020	7.289±0.021	7.042±0.016	74.84±3.07	13.36±0.55	M3		
83945	257.381451	43.681386	335.9	-284.8	11.77	7.380±0.019	6.757±0.016	6.485±0.016	134.31±1.99	7.45±0.11	M3.5	0.33	3
84051	257.746466	-52.515508	-250	158	10.05	6.866±0.024	6.229±0.024	6.026±0.021	80.17±1.84	12.47±0.29	M1V^e		
84099	257.894779	38.442757	211.4	-46.1	11.54	7.630±0.023	7.041±0.016	6.801±0.021	83.31±1.98	12.00±0.29	M3.5		
84140	258.032559	45.666125	249.8	-1572.6	9.31	5.552±0.030	5.066±0.016	4.834±0.023	167.29±5.02	5.98±0.18	M3.5	-0.31	3
84521	259.170749	8.058392	-280.7	-67.1	11.49	7.933±0.019	7.389±0.027	7.106±0.020	67.08±2.69	14.91±0.60	M2		
84790	259.969642	41.71382	285.8	-823.4	11.37	7.712±0.024	7.132±0.020	6.915±0.018	80.77±1.66	12.38±0.25	M2.5		
84794	259.975883	26.50087	-217.2	350.8	11.26	7.273±0.020	6.710±0.031	6.422±0.018	86.27±4.10	11.59±0.55	M3.5	0.28	4
85523	262.166444	-46.895189	573.8	-879.4	9.38	5.711±0.019	5.154±0.033	4.855±0.018	220.24±1.42	4.54±0.03	M2.5	-0.23	1
85665	262.594699	5.548514	29.4	-251.4	9.33	6.240±0.020	5.654±0.042	5.422±0.029	100.23±1.07	9.98±0.11	M0	-0.14	1
86057	263.806659	-48.680873	63.7	453.3	10.13	6.667±0.023	6.080±0.029	5.829±0.021	102.83±2.75	9.72±0.26	M1.5	-0.19	1
86087	263.893669	61.681564	263.3	-514.2	9.98	6.884±0.032	6.271±0.017	6.066±0.018	70.93±0.95	14.10±0.19	M0.5		
86162	264.107994	68.339231	-318.9	-1267.2	9.15	5.335±0.021	4.766±0.033	4.548±0.021	220.84±0.94	4.53±0.02	M3	-0.09	3
86214	264.265256	-44.319215	-710.1	-938	10.94	6.544±0.023	5.917±0.038	5.606±0.020	196.90±2.15	5.08±0.06	M3.5	0.1	1
86287	264.472279	18.591708	926.9	982.7	9.62	6.360±0.023	5.790±0.020	5.572±0.020	123.67±1.61	8.09±0.11	M1	-0.35	1
86776	265.983178	43.378613	9.9	-602.5	10.49	6.812±0.024	6.221±0.018	5.964±0.020	105.50±1.18	9.48±0.11	M2.5		
86990	266.642573	-57.319049	-1120.3	-1353	10.75	6.855±0.021	6.297±0.036	6.016±0.017	171.48±2.31	5.83±0.08	M2.0	-0.28	1
87937	269.452072	4.693391	-800.2	10328	9.54	5.244±0.020	4.834±0.034	4.524±0.020	548.31±1.51	1.82±0.01	M4	-0.51	1
87938	269.462348	46.588641	-17.7	575.7	11.79	7.847±0.020	7.254±0.023	7.000±0.017	70.99±1.86	14.09±0.37	M3		
88574	271.28158	-3.031321	570.9	-333.4	9.37	6.161±0.019	5.571±0.040	5.306±0.021	128.89±1.43	7.76±0.09	M1	-0.27	1
91430	279.686466	-14.49055	113	-571	11.28	7.661±0.024	7.060±0.040	6.849±0.018	77.60±2.79	12.89±0.46	M2.5		
91699	280.495973	31.83049	-303.3	8.6	11.27	7.523±0.020	6.977±0.016	6.722±0.020	87.36±2.66	11.45±0.35	M3		
91768	280.694565	59.630434	-1313.2	1807.1	8.94	5.189±0.017	4.741±0.036	4.432±0.020	280.18±2.18	3.57±0.03	M3	-0.49	3
91772	280.695581	59.626895	-1391.9	1838.6	8.94	5.721±0.020	5.197±0.024	5.000±0.023	280.18±2.18	3.57±0.03	M3		
92403	282.455684	-23.836233	640	-192.7	10.37	6.222±0.018	5.655±0.034	5.370±0.016	336.72±2.03	2.97±0.02	M3.5	-0.4	1
92871	283.864213	8.402504	92.8	-70.9	10.1	6.311±0.019	5.680±0.021	5.434±0.020	84.94±1.72	11.77±0.24	M3		
93069	284.377481	-55.991946	5	-468.8	8.86	5.873±0.024	5.250±0.061	5.025±0.027	81.40±1.95	12.29±0.29	M0.0		
93101	284.500571	5.908123	-195.1	-1220.7	9.22	6.239±0.019	5.587±0.029	5.357±0.021	91.68±1.54	10.91±0.18	M0.5		
93206	284.781069	-48.274468	149.8	-494.9	11.13	7.520±0.023	6.932±0.047	6.700±0.024	70.95±2.56	14.09±0.51	M2.0		
93873	286.773191	20.888031	-473.7	-350.3	10.77	7.295±0.020	6.726±0.061	6.521±0.021	117.45±2.28	8.51±0.17	M1.5	-0.47	4
93899	286.805009	20.877017	-479.3	-333.4	10.76	7.278±0.021	6.752±0.051	6.517±0.023	114.25±2.30	8.75±0.18	M2		
94349	288.060778	2.887322	-40.6	-11.4	11.09	7.087±0.020	6.572±0.018	6.294±0.024	97.84±2.95	10.22±0.31	M3.5		
94761	289.230208	5.168902	-582.4	-1336.8	9.12	5.583±0.030	4.929±0.027	4.673±0.020	170.36±1.00	5.87±0.03	M2.5	0.05	1
97241	296.457265	32.38712	395.2	198.3	10.61	7.572±0.020	7.030±0.024	6.774±0.021	86.99±7.52	11.50±0.99	M1		
97292	296.599859	32.016946	348.8	-277.5	9.74	6.883±0.032	6.215±0.020	6.041±0.017	73.46±1.79	13.61±0.33	M1		
99150	301.938326	-31.752508	-498.5	-235.1	12.19	8.274±0.026	7.679±0.038	7.397±0.023	67.08±5.02	14.91±1.12	M3.0		
99701	303.472484	-45.164019	778.1	-159.4	7.97	5.122±0.023	4.525±0.228	4.281±0.024	161.34±1.00	6.20±0.04	K7.0		
100923	306.923501	-27.747743	-206.6	-882.6	11.41	7.706±0.020	7.083±0.029	6.864±0.027	67.38±3.01	14.84±0.66	M3		
101180	307.633524	65.449559	443.7	283.7	10.54	6.735±0.021	6.136±0.046	5.933±0.023	125.07±1.08	8.00±0.07	M2.5	-0.09	2
102141	310.463151	-32.435208	261.3	-344.8	10.27	5.807±0.026	5.201±0.046	4.944±0.042	93.50±3.67	10.70±0.42	M4.5		
102401	311.267079	44.499071	433.5	272	10.79	7.329±0.018	6.769±0.023	6.533±0.016	81.17±1.73	12.32±0.26	M1.5	-0.15	2
102409	311.289714	-31.3409	279.7	-360.3	8.81	5.436±0.017	4.831±0.016	4.529±0.020	100.91±1.06	9.91±0.10	M0.0		
103039	313.137573	-16.974738	-306.7	30.8	11.41	7.090±0.023	6.517±0.044	6.199±0.021	175.03±3.40	5.71±0.11	M4V^a	-0.07	1
103096	313.332458	62.15439	1	-774.3	8.55	5.429±0.029	4.919±0.059	4.618±0.024	141.87±0.64	7.05±0.03	M0.5	-0.01	2
103441	314.355654	22.362727	771.5	-212.6	11.98	8.410±0.030	7.868±0.053	7.640±0.024	72.58±3.16	13.78±0.60	M2	-0.28	3
103800	315.494341	-6.318749	-229.2	-445.2	11.23	7.563±0.017	6.952±0.026	6.692±0.018	69.53±2.93	14.38±0.61	M3		
103910	315.808107	-56.963432	-358	353.2	12.88	8.730±0.024	8.175±0.029	7.902±0.024	78.61±5.92	12.72±0.96	M3.0		
104432	317.322613	-13.302503	714.5	-1994.3	10.87	7.688±0.029	7.121±0.036	6.909±0.029	82.18±2.17	12.17±0.32	M1	-0.45	2
104644	317.956535	-43.613649	215.1	-689.5	11.98	8.478±0.024	7.919±0.042	7.667±0.021	67.55±3.74	14.80±0.82	M1.5		
106106	322.403391	17.643291	1010	376.3	10.33	6.249±0.021	5.737±0.024	5.453±0.020	149.15±1.81	6.70±0.08	M3.5	-0.13	3
106255	322.828329	-9.791191	28.3	-218.1	11.96	7.316±0.023	6.701±0.034	6.379±0.020	120.52±5.98	8.30±0.41	M4.5		
106440	323.391563	-49.009006	-46.2	-818	8.66	5.349±0.032	4.766±0.256	4.501±0.018	201.87±1.01	4.95±0.02	M1.5	-0.17	1
106811	324.501592	27.7238	462.9	-48.9	9.83	6.809±0.035	6.154±0.067	5.922±0.023	75.09±1.89	13.32±0.34	M0		
108159	328.688818	-46.992734	-311.7	-365.6	11.99	8.393±0.026	7.816±0.033	7.576±0.023	68.33±3.84	14.63±0.82	M2.5		
108569	329.8946	-59.752815	886.9	-125.9	9.74	6.613±0.021	5.990±0.023	5.757±0.021	83.43±1.77	11.99±0.25	M0.5		
108706	330.304684	28.306906	372.1	36.5	11.99	7.635±0.026	7.035±0.031	6.777±0.021	112.33±3.05	8.90±0.24	M4	0.11	4
108782	330.542812	1.400232	-452.8	-278.5	9.17	6.196±0.023	5.562±0.051	5.322±0.023	97.61±1.53	10.24±0.16	M0	0.01	1
109388	332.418111	-4.64073	1135.9	-20.3	10.41	6.510±0.024	5.899±0.044	5.594±0.017	109.94±2.07	9.10±0.17	M3.5	0.22	1
109555	332.875393	18.426194	329.2	179.8	10.25	6.725±0.037	6.035±0.036	5.823±0.016	86.08±1.38	11.62±0.19	M2	0.26	2
109638	333.149794	8.55325	116	-661.5	11.99	8.277±0.021	7.681±0.024	7.472±0.027	66.84±4.41	14.96±0.99	M3		
110893	336.998171	57.695918	-806.8	-399.1	9.59	5.575±0.027	5.038±0.034	4.777±0.029	249.94±1.87	4.00±0.03	M3	-0.08	2
111313	338.259274	9.377978	537.3	141.3	10.36	7.208±0.024	6.604±0.040	6.356±0.023	78.68±2.69	12.71±0.43	M1		
111766	339.623935	-65.378479	817.5	-156.8	11.5	7.271±0.021	6.721±0.034	6.428±0.024	75.87±5.83	13.18±1.01	M3.5		
111802	339.68989	-20.621132	447.7	-80.8	9.06	5.669±0.019	5.108±0.049	4.800±0.016	115.01±1.32	8.69±0.10	M1.5		
112460	341.707201	44.333999	-709.6	-459.7	10.29	6.106±0.030	5.554±0.031	5.299±0.024	195.22±1.87	5.12±0.05	M3.5	-0.03	2
112774	342.580937	-7.090105	-105.5	103.8	9.86	6.932±0.023	6.324±0.029	6.104±0.020	70.77±1.85	14.13±0.37	K7		
112909	342.973065	31.754212	524.8	-51.7	11.66	7.697±0.020	7.129±0.018	6.874±0.021	68.78±2.77	14.54±0.59	M3		
113020	343.319724	-14.263697	960.1	-674	10.16	5.934±0.019	5.349±0.049	5.010±0.021	213.28±2.12	4.69±0.05	M4	0.14	1
113229	343.939626	-75.458671	-1027.5	-1061.4	10.42	6.616±0.018	6.084±0.027	5.811±0.021	116.07±1.19	8.62±0.09	M2.5	0	1
113296	344.145022	16.553432	-1033.3	-284	8.68	5.360±0.020	4.800±0.036	4.523±0.016	146.09±1.00	6.85±0.05	M1.5	0.03	1
114046	346.466815	-35.853071	6766.9	1328	7.35	4.338±0.258	3.608±0.230	3.465±0.200	305.26±0.70	3.28±0.01	M0.5	-0.24	1
115332	350.406036	17.29038	-536.5	-1385.2	11.7	7.391±0.029	6.771±0.024	6.507±0.016	91.00±2.89	10.99±0.35	M4	0.23	1
115562	351.127141	57.854307	-62.2	-283.3	10.03	6.795±0.032	6.097±0.034	5.871±0.021	77.15±1.29	12.96±0.22	M1	0.24	2
116132	352.967381	19.937293	543.2	-44.6	10.05	6.162±0.024	5.575±0.021	5.326±0.018	161.76±1.66	6.18±0.06	M3.5	0.15	3

Table 1: continued.

HIP	α (J2000.0)	δ (J2000.0)	μ_α (mas yr^{-1})	μ_δ (mas yr^{-1})	V (mag)	J (mag)	H (mag)	K_S (mag)	π (mas)	Distance (pc)	SpTy.	[Fe/H] (dex)	Ref.
116317	353.5079	0.179431	-491.4	-661.8	11.16	7.664±0.024	7.070±0.034	6.828±0.020	71.54±3.27	13.98±0.64	M2.5		
117473	357.302193	2.401225	994.2	-967.4	8.98	5.827±0.023	5.282±0.031	5.043±0.020	167.29±1.23	5.98±0.04	M1	-0.44	1
117828	358.458795	-75.63253	243.4	-378.3	9.99	6.450±0.019	5.783±0.017	5.549±0.027	100.07±1.05	9.99±0.10	Ma[f]	0.17	1

References (metallicities). – [1] Neves et al. (2014); [2] Gaidos & Mann (2014); [3] Rojas-Ayala et al. (2012); [4] Newton et al. (2014)

Spectral type references for targets without PMSU classifications. – [a] Gray et al. (2006); [b] Browning et al. (2010); [c] Torres et al. (2006); [d] Poveda et al. (2009); [e] Koen et al. (2010); [f] Houk & Cowley (1975)

3 DATA SOURCES AND ACQUISITION

The MINMS survey made use of new and archival AO observations and archival digitised photographic plates to detect companions to M-dwarfs. The AO data provide the capacity to search for companions at high angular resolution, while the plate data provide a complementary widefield search space. Combined, the two detection techniques provide nearly continuous angular separation coverage for companions from $\sim$0.1 arcsec to $\sim$10 arcmin. In this section, we describe the archival data origins and the newly-obtained AO observations.

3.1 Archival high-resolution imaging data

To search for companions at projected separations of $\sim 1 - 100$ au from their host stars, we queried all publicly-available high-resolution and adaptive optics (AO) archives. Of the 245 star total sample, 181 stars had previous high-resolution AO imaging. We obtained archival near-infrared AO imaging data from the following instruments/facilities: NAOS-CONICA (NaCo: Nasmyth Adaptive Optics System Near-Infrared Imager and Spectrograph, Lenzen et al. 2003; Rousset et al. 2003) on the Very Large Telescope (VLT); the AOB/PUEO KIR camera (Doyon et al. 1998) on the Canada-France-Hawaii Telescope (CFHT); and CIAO (Coronagraphic Imager; Murakawa et al. 2003, 2004), HiCIAO (High Contrast Instrument for the Subaru Next Generation Adaptive Optics; Hodapp et al. 2008), and IRCS (Infrared Camera and Spectropgrah; Tokunaga et al. 1998; Kobayashi et al. 2000) on Subaru. Table 2 provides a summary of the telescopes and instruments used to obtain the first epoch data. Archive AO data from three sources – CFHT, VLT, and Subaru – combined with new AO images from MMT, covered 196 of the 245-star MINMS sample. Some of the targets have additional archive data, and the data used in this study were selected based on the availability of unsaturated images, with preference given to the three instruments that observed the largest number of targets in archives. Existing observations and their corresponding calibration files were downloaded from the Canadian Astronomy Data Centre, the European Southern Observatory Science Archive Facility, and the Subaru-Mitaka-Okayama-Kiso Archive System. Detailed information on the observations, including observation, filter, exposure time, date, programme ID and project PI for each target are provided in Table 2.

Table 2: High-resolution imaging data

HIP	Telescope	Instrument	Filter	Exp. time (s)	Programme ID	PI	UT Date
428	CFHT	PUEO/KIR	Brγ	6	00BF25	Perrier-Bellet	2000-08-21
439	VLT	NaCo/S13	NB1.64	8	072.C-0570(A)	Beuzit	2003-12-08
1242	VLT	NaCo/S13	NB1.64	0.7	072.C-0570(A)	Beuzit	2003-12-10
1475	CFHT	PUEO/KIR	Fe II	0.5	99IID409	Ménard	1999-08-25
2552	CFHT	PUEO/KIR	Brγ	10	07AF12	Forveille	2007-01-28
3937	CFHT	PUEO/KIR	H	10	h8	Jewitt	2000-08-19
4856	CFHT	PUEO/KIR	$H_2(\nu = 1-0)$	4	03BD2	Forveille	2003-10-16
4872	CFHT	PUEO/KIR	Fe II	2	97IIF28	Beuzit	1997-12-27
5496	VLT	NaCo/S13	H	5	382.D-0754(A)	Bean	2008-10-17
5643	CFHT	PUEO/KIR	K	1	00BH12	Roddier	2000-12-12
8051	CFHT	PUEO/KIR	Fe II	3	97IIF28	Beuzit	1997-12-28
8768	CFHT	PUEO/KIR	Brγ	2	01BF50	Perrier-Bellet	2001-08-06
9291	CFHT	PUEO/KIR	Fe II	15	04BF8	Catala	2004-09-28
9724	VLT	NaCo/S13	NB1.64	0.345	072.C-0570(A)	Beuzit	2003-12-09
9786	VLT	NaCo/S13	NB1.64	3.5	072.C-0570(A)	Beuzit	2003-12-08
10279	CFHT	PUEO/KIR	Brγ	4	01BF50	Perrier-Bellet	2001-08-06
10395	CFHT	PUEO/KIR	Brγ	10	00BF25	Perrier-Bellet	2000-08-21
10617	VLT	NaCo/S27	K_S	0.6	077.C-0483(A)	Melo	2006-07-28
10812	VLT	NaCo/S54	NB2.12	0.9	381.C-0235(A)	Kuerster	2008-07-04
11048	CFHT	PUEO/KIR	Brγ	2.5	01BD03	Forveille	2001-08-31
11964	VLT	NaCo/S13	NB2.12	0.6	074.C-0074(A)	Udry	2004-11-10
12097	Subaru	IRCS	K	3	o08184	Dello Russo/Vervack	2008-08-05
12781	CFHT	PUEO/KIR	$H_2(\nu = 1-0)$	8	03BD2	Forveille	2003-10-15
13389	VLT	NaCo/S13	NB1.64	1	072.C-0570(A)	Beuzit	2003-12-09
16536	VLT	NaCo/S13	NB1.64	4	073.C-0155(A)	Beuzit	2004-09-23
17609	MMT	ARIES	$K_{C\ 2.09}$	1.4	UAO-S10/S11	De Rosa/Ward-Duong	2013-09-18
21088	CFHT	PUEO/KIR	Brγ	4	F123	Perrier	2000-02-18
21556	CFHT	PUEO/KIR	$H_2(\nu = 1-0)$	4	02BE03	Forveille	2002-09-18
21932	VLT	NaCo/S27	NB2.17	0.4	079.C-0216(A)	Montagnier	2007-09-15
22627	VLT	NaCo/S13	NB2.12	0.4	70.C-0777(D)	Mundt	2003-01-23
22738	VLT	NaCo/S13	NB1.64	3	073.C-0155(A)	Beuzit	2004-09-23
23452	CFHT	PUEO/KIR	$H_2(\nu = 1-0)$	1.5	02BE03	Forveille	2002-09-18
23512	CFHT	PUEO/KIR	$H_2(\nu = 1-0)$	15	03BD2	Forveille	2003-10-15
23518	MMT	ARIES	$K_{C\ 2.09}$	1.4	UAO-S10/S11	De Rosa/Ward-Duong	2013-09-18
23932	VLT	NaCo/S27	K_S	0.5	70.C-0738(A)	Beuzit	2003-03-16
24186	VLT	NaCo/S13	H	0.35	70.C-0738(A)	Beuzit	2003-03-18
24284	Subaru	CIAO	H	10	o04203	Itoh	2004-11-20
25578	VLT	NaCo/S27	K_S	2	079.C-0216(A)	Montagnier	2007-09-15
25878	CFHT	PUEO/KIR	Fe II	1	03BH10D	Liu	2004-01-05
26857	CFHT	PUEO/KIR	Fe II	3	97IIF28	Beuzit	1997-12-29
28368	Subaru	HiCIAO	H	1.5	o11302	Bowler	2011-12-27
29052	VLT	NaCo/S13	NB1.64	1.5	072.C-0570(A)	Beuzit	2003-12-08
29277	CFHT	PUEO/KIR	Fe II	4	03AF26	Beuzit	2003-03-16
29295	CFHT	PUEO/KIR	H_2	0.7	97IIF28	Beuzit	1997-12-29
29316	CFHT	PUEO/KIR	Brγ	10	03BD10	Forveille	2004-01-06
30920	VLT	NaCo/S13	K_S	2	077.C-0783(A)	Forveille	2006-04-11
31292	VLT	NaCo/S13	NB1.64	1.5	072.C-0570(A)	Beuzit	2003-12-09
31293	VLT	NaCo/S13	NB1.64	1.3	072.C-0570(A)	Beuzit	2003-12-09
31635	VLT	NaCo/S13	NB1.64	0.345	072.C-0570(A)	Beuzit	2003-12-09
33142	CFHT	PUEO/KIR	Fe II	6	05AF19	Forveille	2005-04-26
33226	CFHT	PUEO/KIR	Fe II	1	97IIF28	Beuzit	1997-12-29
33499	VLT	NaCo/S13	NB1.64	1	072.C-0570(A)	Beuzit	2003-12-08
34603	CFHT	PUEO/KIR	Fe II	2	98IF58	Beuzit	1998-03-07
35191	VLT	NaCo/S13	NB1.26	0.75	072.C-0570(A)	Beuzit	2003-12-10
36208	VLT	NaCo/S13	H	0.345	072.C-0570(A)	Beuzit	2003-12-11
36626	CFHT	PUEO/KIR	Brγ	5	F58	Perrier-Bellet	2000-04-19
36627	CFHT	PUEO/KIR	Brγ	10	F58	Perrier-Bellet	2000-04-19

Table 2: continued.

HIP	Telescope	Instrument	Filter	Exp. time (s)	Programme ID	PI	UT Date
37217	VLT	NaCo/S13	NB1.64	1	072.C-0570(A)	Beuzit	2003-12-08
37288	VLT	NaCo/S13	NB1.64	1	70.C-0777(E)	Mundt	2003-02-19
37766	VLT	NaCo/S13	K_{S}	2.7	077.C-0783(A)	Forveille	2006-04-11
38956	CFHT	PUEO/KIR	H_2	15	97IID06	Richer/Beuzit	1997-12-26
40501	VLT	NaCo/S13	H	0.8	70.C-0738(A)	Beuzit	2003-03-16
41824	CFHT	PUEO/KIR	Brγ	10	07AF12	Forveille	2007-01-29
45908	VLT	NaCo/S13	NB1.64	0.5	072.C-0570(A)	Beuzit	2003-12-09
46655	CFHT	PUEO/KIR	Fe II	2	03BH10D	Liu	2004-01-06
46706	CFHT	PUEO/KIR	H_2	2.5	04AD8	Forveille	2004-04-04
46769	MMT	ARIES	$K_{\mathrm{C}\ 2.09}$	1.4	UAO-S2	De Rosa	2013-05-24
47103	VLT	NaCo/S13	H	8	079.C-0216(A)	Montagnier	2007-04-10
47425	VLT	NaCo/S13	NB1.26	1	70.C-0738(A)	Beuzit	2003-03-17
47513	VLT	NaCo/S13	NB1.64	0.5	072.C-0570(A)	Beuzit	2003-12-10
47620	MMT	ARIES	$K_{\mathrm{C}\ 2.09}$	1.4	UAO-S2	De Rosa	2013-05-24
47780	VLT	NaCo/S13	NB1.75	0.5	70.C-0738(A)	Beuzit	2003-03-17
48659	VLT	NaCo/S13	K_{S}	0.5	60.A-9800(J)	–^{a}	2010-02-08
48714	CFHT	PUEO/KIR	H_2	0.5	04AD8	Forveille	2004-04-04
49969	VLT	NaCo/S13	NB2.12	0.4	70.C-0738(A)	Beuzit	2003-03-18
49986	CFHT	PUEO/KIR	J_{cont}	1	F58	Perrier-Bellet	2000-04-18
51007	CFHT	PUEO/KIR	Fe II	2	03BH10D	Liu	2004-01-06
51317	VLT	NaCo/S54	NB2.17	0.3454	079.C-0216(A)	Montagnier	2007-04-10
53020	VLT	NaCo/S27	K_{S}	0.5	079.C-0216(A)	Montagnier	2007-05-06
53985	CFHT	PUEO/KIR	Brγ	3.5	F58	Perrier-Bellet	2000-04-19
54035	CFHT	PUEO/KIR	Fe II	0.2	H1A	Roddier	2000-04-13
54211	CFHT	PUEO/KIR	K$'$	0.1	00BH12	Roddier	2000-12-13
54532	CFHT	PUEO/KIR	$H_2(\nu = 1-0)$	10	05AF19	Forveille	2005-04-26
55360	CFHT	PUEO/KIR	Fe II	1.5	98IF58	Beuzit	1998-03-07
56244	VLT	NaCo/S13	K_{S}	0.347	074.C-0084(B)	Neuhäuser	2005-01-07
56528	CFHT	PUEO/KIR	Fe II	2	99IF59	Perrier	1999-04-04
57050	CFHT	PUEO/KIR	$H_2(\nu = 2-1)$	15	05AF19	Forveille	2005-04-25
57087	VLT	NaCo/L27	L$'$	0.2	081.C-0430(A)	Apai	2008-04-06
57544	CFHT	PUEO/KIR	H_2	8	98IF58	Beuzit	1998-03-07
57548	CFHT	PUEO/KIR	Fe II	1	03BH10D	Liu	2004-01-06
57802	CFHT	PUEO/KIR	Fe II	1.5	98IF58	Beuzit	1998-03-08
59406	VLT	NaCo/S13	NB2.17	2	60.A-9800(J)	–	2010-02-08
60559	CFHT	PUEO/KIR	Fe II	7	98IF58	Beuzit	1998-03-08
60910	VLT	NaCo/S13	K_{S}	0.3454	080.C-0424(A)	Vogt	2008-02-19
61094	VLT	NaCo/S27	K_{S}	0.347	077.D-0179(A)	Neuhäuser	2006-04-22
61629	VLT	NaCo/S27	NB2.17	0.4	077.C-0483(A)	Melo	2006-04-29
61874	VLT	NaCo/S13	NB1.64	3	70.C-0738(A)	Beuzit	2003-03-14
62452	CFHT	PUEO/KIR	Fe II	2	03BH10D	Liu	2004-01-06
62556	CFHT	PUEO/KIR	Fe II	5	03AF26	Beuzit	2003-03-17
63510	VLT	NaCo/S13	K_{S}	8	077.C-0783(A)	Forveille	2006-05-23
65011	MMT	ARIES	$K_{\mathrm{C}\ 2.09}$	1.4	UAO-S2	De Rosa	2013-05-24
65026	CFHT	PUEO/KIR	$H_2(\nu = 2-1)$	8	05AF19	Forveille	2005-04-27
65859	CFHT	PUEO/KIR	H_2	0.5	97IIF09	Bouvier	1998-01-14
66625	MMT	ARIES	$K_{\mathrm{C}\ 2.09}$	1.4	UAO-S2	De Rosa	2013-05-24
66906	CFHT	PUEO/KIR	Brγ	10	F123	Perrier	2000-02-19
67155	VLT	NaCo/S13	K_{S}	2	077.C-0783(A)	Forveille	2006-05-23
67164	CFHT	PUEO/KIR	Brγ	15	03AF26	Beuzit	2003-03-21
68469	CFHT	PUEO/KIR	Brγ	3	F58	Perrier-Bellet	2000-04-20
69454	VLT	NaCo/S13	NB1.64	1	70.C-0738(A)	Beuzit	2003-03-14
70890	VLT	NaCo/S13	H	1	075.C-0733(A)	Beuzit	2005-05-01
70975	VLT	NaCo/S13	K_{S}	10	078.C-0441(A)	Forveille	2007-02-23
71253	CFHT	PUEO/KIR	H_2	10	98IF58	Beuzit	1998-03-08
71898	CFHT	PUEO/KIR	H_2	8	02AF43	Beuzit	2002-06-24
72896	VLT	NaCo/S13	K_{S}	1.5	091.D-0804(A)	De Rosa	2013-04-19
72944	VLT	NaCo/S13	K_{S}	0.5	076.C-0139(A)	Bouy	2006-03-01

Table 2: continued.

HIP	Telescope	Instrument	Filter	Exp. time (s)	Programme ID	PI	UT Date
73470	CFHT	PUEO/KIR	$H_2(\nu = 2-1)$	8	05AF21	Beuzit	2005-04-25
74190	Subaru	IRCS	K	3	o06101	Imanishi	2006-07-20
74995	VLT	NaCo/S27	$K_{\rm S}$	5	081.C-0600(A)	Lagrange	2008-06-29
75187	CFHT	PUEO/KIR	Brγ	3	02BE03	Forveille	2002-09-18
76074	VLT	NaCo/S13	NB1.64	0.35	075.C-0733(A)	Beuzit	2005-05-02
76832	MMT	ARIES	$K_{\rm C\ 2.09}$	1.4	UAO-S2	De Rosa	2013-05-24
76901	CFHT	PUEO/KIR	Brγ	15	F58	Perrier-Bellet	2000-04-19
78353	Subaru	CIAO	K	30	o05104	Nakajima	2005-07-13
79755	CFHT	PUEO/KIR	$H_{\rm cont}$	1	01AH25B	Baudoz	2001-05-03
79762	CFHT	PUEO/KIR	Brγ	10	F58	Perrier-Bellet	2000-04-20
80018	VLT	NaCo/S13	NB1.64	1	079.C-0216(A)	Montagnier	2007-05-19
80346	CFHT	PUEO/KIR	Brγ	5	07AF12	Forveille	2007-01-29
80459	CFHT	PUEO/KIR	$J_{\rm cont}$	1.5	01BF51	Gallant	2001-08-03
80824	CFHT	PUEO/KIR	K$'$	0.1	01AH25B	Baudoz	2001-05-01
82809	VLT	NaCo/S13	NB1.64	10	71.C-0388(A)	Beuzit	2003-07-20
82817	VLT	NaCo/S27	NB1.64	0.345	71.D-0465(A)	Forveille	2003-05-29
83043	CFHT	PUEO/KIR	$H_2(\nu = 1-0)$	5	05AF19	Forveille	2005-04-26
83599	VLT	NaCo/S13	NB1.64	0.5	71.C-0388(A)	Beuzit	2003-07-19
83762	MMT	ARIES	$K_{\rm C\ 2.09}$	1.4	UAO-S2	De Rosa	2013-05-24
83945	CFHT	PUEO/KIR	Brγ	10	01AD01	Forveille	2001-07-07
84099	MMT	ARIES	$K_{\rm C\ 2.09}$	1.4	UAO-S2	De Rosa	2013-05-24
84140	CFHT	PUEO/KIR	$H_2(\nu = 1-0)$	6	04AD8	Forveille	2004-04-05
84790	MMT	ARIES	$K_{\rm C\ 2.09}$	1.4	UAO-S2	De Rosa	2013-05-24
85523	VLT	NaCo/S27	$K_{\rm S}$	0.35	084.C-0443(A)	Lagrange	2010-03-20
85665	CFHT	PUEO/KIR	$H_2(\nu = 1-0)$	15	05AF19	Forveille	2005-04-26
86057	VLT	NaCo/S13	NB1.64	1.8	079.C-0216(A)	Montagnier	2007-05-14
86087	MMT	ARIES	$K_{\rm C\ 2.09}$	1.4	UAO-S2	De Rosa	2013-05-24
86162	CFHT	PUEO/KIR	Brγ	1	01BF51	Gallant	2001-08-03
86214	VLT	NaCo/S13	H	2.5	075.C-0733(A)	Beuzit	2005-05-01
86287	CFHT	PUEO/KIR	Brγ	7	F58	Perrier-Bellet	2000-04-19
86776	CFHT	PUEO/KIR	$H_2(\nu = 2-1)$	5	02AF43	Beuzit	2002-07-23
86990	VLT	NaCo/S13	NB1.64	1	71.C-0388(A)	Beuzit	2003-07-19
87937	VLT	NaCo/L27	L$'$	0.2	081.C-0430(C)	Apai	2008-07-03
87938	MMT	ARIES	$K_{\rm C\ 2.09}$	1.4	UAO-S2	De Rosa	2013-05-24
88574	CFHT	PUEO/KIR	Brγ	6	F58	Perrier-Bellet	2000-04-20
91699	CFHT	PUEO/KIR	$H_2(\nu = 2-1)$	10	05AF19	Forveille	2005-04-26
91768	CFHT	PUEO/KIR	$H_2(\nu = 1-0)$	0.5	09BC06	DeRosa	2009-09-01
91772	CFHT	PUEO/KIR	Brγ	1	01AH25B	Baudoz	2001-05-04
92403	VLT	NaCo/S27	IB2.18	0.3454	091.D-0804(A)	De Rosa	2013-05-11
92871	CFHT	PUEO/KIR	$H_2(\nu = 1-0)$	3	05AF19	Forveille	2005-04-27
93101	CFHT	PUEO/KIR	Paβ	3	02BE03	Forveille	2002-09-18
93873	CFHT	PUEO/KIR	Brγ	5	00AD99	Forveille	2000-08-15
93899	CFHT	PUEO/KIR	K$'$	10	00AD99	Forveille	2000-08-15
94349	VLT	NaCo/S13	NB1.64	7	079.C-0216(A)	Montagnier	2007-05-14
94761	CFHT	PUEO/KIR	Brγ	1.5	00BF25	Perrier-Bellet	2000-08-20
97241	CFHT	PUEO/KIR	Fe II	8	02BF27	Beuzit	2002-09-10
97292	MMT	ARIES	$K_{\rm C\ 2.09}$	1.4	UAO-S10/S11	De Rosa/Ward-Duong	2013-09-18
99150	VLT	NaCo/S27	$K_{\rm S}$	4.7	077.C-0483(A)	Melo	2006-06-09
99701	VLT	NaCo/S13	NB1.64	10	71.C-0388(A)	Beuzit	2003-07-19
101180	CFHT	PUEO/KIR	Brγ	4	00AD99	Forveille	2000-08-16
102141	VLT	NaCo/S13	$K_{\rm S}$	5	083.C-0659(A)	Patience	2009-06-01
102401	MMT	ARIES	$K_{\rm C\ 2.09}$	1.4	UAO-S10/S11	De Rosa/Ward-Duong	2013-09-18
102409	VLT	NaCo/S13	$K_{\rm S}$	0.5	71.C-0029(A)	Mundt	2003-07-21
103039	CFHT	PUEO/KIR	Brγ	4	01BF50	Perrier-Bellet	2001-08-06
103096	CFHT	PUEO/KIR	Brγ	1	00BF25	Perrier-Bellet	2000-08-21
103441	VLT	NaCo/S13	NB1.64	0.9	71.C-0029(A)	Mundt	2003-07-23
106106	CFHT	PUEO/KIR	Fe II	3	97IIF28	Beuzit	1997-12-28
106255	VLT	NaCo/S13	NB1.64	1.5	075.C-0733(A)	Beuzit	2005-05-02

Table 2: continued.

HIP	Telescope	Instrument	Filter	Exp. time (s)	Programme ID	PI	UT Date
106440	VLT	NaCo/S27	K_{S}	0.35	083.C-0599(A)	Lagrange	2009-09-28
106811	Subaru	CIAO	K	5	o05136	Nakajima	2005-11-14
108159	VLT	NaCo/S27	K_{S}	2	60.A-9800(J)	–	2008-10-23
108706	CFHT	PUEO/KIR	Paβ	10	02BF27	Beuzit	2002-09-10
108782	CFHT	PUEO/KIR	Brγ	3	01BD02	–	2001-08-07
109388	VLT	NaCo/S27	K_{S}	0.5	083.C-0151(A)	Lagrange	2009-08-27
109555	CFHT	PUEO/KIR	Fe II	3	97IIF28	Beuzit	1997-12-28
110893	CFHT	PUEO/KIR	Brγ	2	01BF50	Perrier-Bellet	2001-08-04
111313	Subaru	CIAO	K	10	o05104	Nakajima	2005-07-09
111766	VLT	NaCo/S27	K_{S}	0.7	077.C-0483(A)	Melo	2006-05-26
111802	VLT	NaCo/S13	NB2.12	0.5	075.C-0112(A)	Udry	2005-07-08
112460	CFHT	PUEO/KIR	Fe II	1.6	97IIF28	Beuzit	1997-12-28
112774	Subaru	CIAO	K	5	o04104	Nakajima	2004-09-01
112909	MMT	ARIES	$K_{\mathrm{C}\ 2.09}$	1.4	UAO-S10/S11	De Rosa/Ward-Duong	2013-09-18
113020	CFHT	PUEO/KIR	Brγ	3	01BF50	Perrier-Bellet	2001-08-04
113229	VLT	NaCo/S13	NB1.64	0.345	072.C-0570(A)	Beuzit	2003-12-08
113296	CFHT	PUEO/KIR	Brγ	1	00AD99	Forveille	2000-08-15
114046	VLT	NaCo/S13	NB1.64	3.5	072.C-0570(A)	Beuzit	2003-12-09
115332	VLT	NaCo/S13	NB1.64	1	073.C-0124(A)	Udry	2004-06-23
115562	MMT	ARIES	$K_{\mathrm{C}\ 2.09}$	1.4	UAO-S2	De Rosa	2013-05-24
116132	CFHT	PUEO/KIR	Brγ	2	00BF25	Perrier-Bellet	2000-08-21
117473	CFHT	PUEO/KIR	Fe II	2	98IIF65	Perrier	1998-09-07
117828	VLT	NaCo/S13	NB1.64	0.345	072.C-0570(A)	Beuzit	2003-12-08

[a] Observatory technical time.

Table 3. Adaptive optics observations summary

Telescope	Instrument	1st Epoch	2nd Epoch	Filters (bandpass)	Pixel Scale (mas px^{-1})	Unique Programmes
CFHT	AOBIR	94	23	JHK	38	34
VLT	NaCo	79	24	$JHKL'$	13, 27, 54	31
MMT	ARIES	16	10	K	20, 40	2
Subaru	CIAO	5	0	HK	22	4
Subaru	HiCIAO	1	0	H	10	1
Subaru	IRCS	2	0	K	21	2

3.2 New AO observations

In addition to the existing archival observations of the sample, 32 dedicated observations – 16 new first-epoch imaging, and 16 follow-up second epoch imaging – were obtained. New and follow-up observations for 26 stars were taken in March, May, and September of 2013 using the Arizona Infrared imager and Echelle Spectrograph (ARIES; McCarthy et al. 1998) at the MMT Observatory. We also obtained second-epoch confirmation imaging for an additional 6 southern targets in our sample from March 2013 through September 2013 with VLT/NaCo (programme ID: 091.D-0804). The details of these observations are listed in Table 3. When possible, follow-up second-epoch images were obtained with similar configurations as the discovery epochs. New observations of targets from the MINMS sample were taken in the $K_{\rm S}$ filter, as the majority of the existing archival observations (64 per cent) were taken in $K_{\rm S}$ band.

3.3 Archival photographic plates

In order to extend the AO imaging survey with a wider search for companions at separations from $\sim 100 - 10,000$ au, we used the SuperCOSMOS Sky Survey Science Archive (Hambly et al. 2001) to obtain scans of plates from the UK Schmidt (UKST), ESO Schmidt, and Palomar Oschin Schmidt (POSS) sky surveys for the full 245-star sample. The archival plates provide multiple epochs of observation for each target, taken with the $BVRI$ filters at a pixel scale of 0.67 arcsec px^{-1}. With time baselines spanning from 10 to 50 years between the initial and final epochs, and the extremely high proper motions of the targets in our sample (sample median proper motion of 0.63 arcsec yr^{-1}), it is possible to search for common proper motion pairs. Mosaics of the plates were made to provide a search radius around each M-dwarf, and the mosaic dimensions correspond to a projected separation of 10,000 au from each primary star.

4 DATA REDUCTION AND ANALYSIS

4.1 Adaptive optics data

4.1.1 Image reduction

For all AO datasets, standardised data reduction techniques of dark subtraction, bad pixel rejection, flat fielding, and sky subtraction were applied. Unsaturated science frames were aligned by fitting a Gaussian to the point spread function (PSF) of the primary in each image to determine the centroid and align on the peak of that fit. After alignment, the individual frames were median combined to form a final reduced science image for each of the 196 M-dwarfs with new or archival AO imaging. The typical combined integration time for a given target was ∼60 seconds, with individual exposure times ranging from $0.3 - 15$ seconds.

4.1.2 Sensitivity and completeness estimation

Given the heterogeneous origins of the AO datasets, the contrast limits of the observations differ between targets. To assess the sensitivity of the full sample to detecting companions over a range of separations, we generated contrast curves for each target. The ensemble of contrast values was used to estimate the completeness of the study. For each reduced, combined science image, the contrast as a function of separation was measured by first determining the standard deviation of the background level within a five pixel annulus over a range of separations from the primary star, and then calculating the corresponding magnitude difference between the peak value of the primary star PSF and 3σ over the background, as tabulated in Table 7 (Appendix). The maximum angular separation at which a companion could be detected in the image was considered to be the limit where 95 per cent of the pixels within that radius were within the boundaries of the image field of view.

4.1.3 Companion detection, photometry and mass estimates

For each K7-M6 dwarf, the reduced, combined image was carefully visually inspected for candidate stellar companions. Previous comparisons with automated detection procedures have verified the reliability of visual inspection (Metchev & Hillenbrand 2009), and we repeated the inspection multiple times for each target on both individual and combined frames. Examples of detected companions are shown in Figure 5. After identification, the fluxes of the candidates and their host stars were measured using aperture photometry in IDL. An aperture with radius 2.5 times the average full width at half maximum (FWHM) was chosen in order to measure the total flux associated with the star or candidate in question, with the sky contribution subtracted by defining an annulus of radius 3-9 times the FWHM outside of this aperture. Measurement of the flux ratio between the primary and companion allowed us to derive the magnitude difference of the two objects; any stars unresolved in the 2MASS photometry (with $\Delta m < 4$ and $\rho < 10$ arcsec) were corrected for the individual contributions from each of the stellar components (De Rosa et al. 2011). The centroids of the primary target and candidate companion were found with a Gaussian fit, providing an accurate measurement of the pixel separation between the pair of objects. This was converted to an angular separation between the objects using the known pixel scales of the instruments, given in Table 3. We converted angular separation using the *Hipparcos* parallax-based distance measurements into projected separation in au.

To determine the masses of stellar components in a system, we utilised the low-mass, solar-metallicity evolutionary models of Baraffe et al. (1998), assuming a standard field star age of 5 Gyr. Using the absolute magnitudes of the primaries, these models were also applied to the sensitivity curves calculated in Section 4.1.2 to determine the completeness of the AO imaging in terms of detectable companion mass.

4.2 Archival plate analysis

4.2.1 Companion detection algorithm

Detection of co-moving companion candidates within the mosaiced plates was performed by measuring all objects within the plates using Source Extractor (Bertin & Arnouts 1996). With these parameters, we derived the proper motion for each object with respect

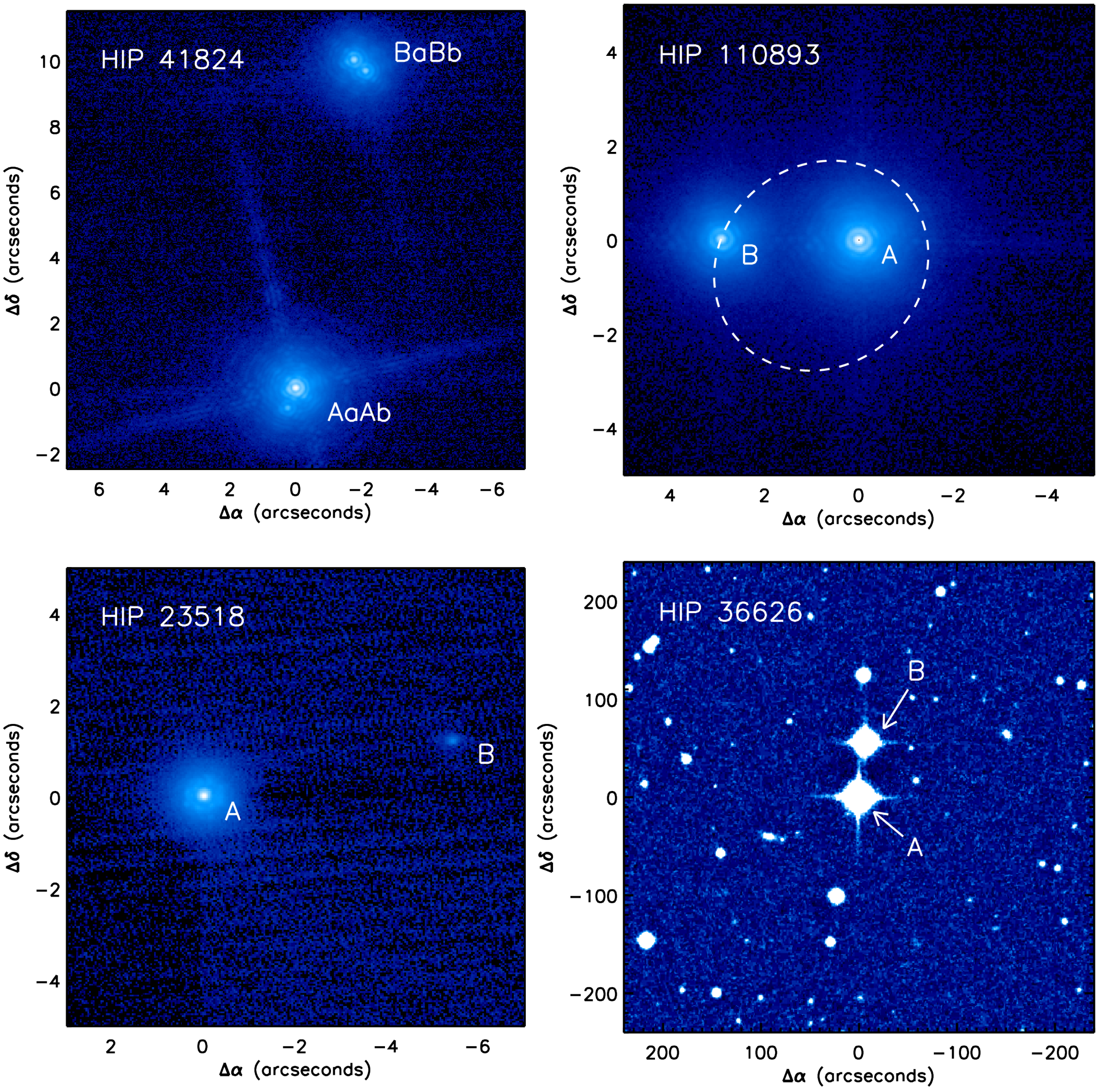

Figure 5. Four of the companions identified or recovered within this study. (*top left*) A CFHT/AOBIR image of the hierarchical quadruple system HIP 41824 (CU Cnc), originally discovered by Beuzit et al. (2004), which consists of four M-dwarfs in an ϵ Lyr-like configuration (e.g. Tokovinin 2008). (*top right*) A CFHT/AOBIR image of the HIP 110893 binary system. The measured separation and position angle is consistent with the orbital fit given in Heintz (1986), which is over-plotted (white dashed curve). (*bottom left*) An MMT/ARIES image of the newly-discovered binary companion to HIP 23518. With an estimated mass of 0.08 $M_{\odot}$, HIP 23518 B is at the canonical stellar/substellar boundary. (*bottom right*) A photographic plate from the Palomar telescope, obtained from the SuperCOSMOS Sky Survey, showing the two components of the wide HIP 36626 (VV Lyn) binary system (Worley 1962).

to the stationary background stars in the field. An object was considered a common proper motion (CPM) candidate if its measured proper motion with respect to the background field stars was within 5σ of the *Hipparcos*-measured proper motion of the primary. These candidates were then visually inspected by blinking the plates from different epochs to eliminate false positives, such as artefacts from the plate scanning process. As noted in Section 2, any stars within our *Hipparcos*-selected sample which were themselves companions to earlier spectral types were excluded from our analysis and statistics.

4.2.2 *Sensitivity and completeness estimation*

To determine the sensitivity of the plate images, we calculated radial contrast curves using the same method applied to the AO data, starting at an annulus of five pixels from the centroid position of the primary. The B-band images were chosen for the sensitivity estimates as they provided the highest resolution and minimal saturation of the primary. The depth of the plates provided many faint unassociated objects within the field, and the catalogued magnitudes of these unassociated objects corresponded to magnitudes far below the substellar limit for associated objects. Given the depth of the plates, any stellar companions were readily identified by visual inspection. To determine the minimum detection separation for a stellar companion at the bottom of the main sequence, the expected B-band magnitude of a 0.08 $M_{\odot}$ star was estimated from models, and the corresponding level of pixel counts in the plate was determined by matching to a star in the PPMXL catalogue (Roeser, Demleitner & Schilbach 2010) with the same apparent magnitude.

4.2.3 Photometry and mass estimates

For each comoving companion identified within the plate images, angular separations and magnitude differences from the primary M-dwarfs were derived from the 2MASS catalogue astrometry and $K_{\rm S}$-band photometry. As in the AO data analysis, the magnitude differences between the components were converted into component masses using 5 Gyr isochrones (Baraffe et al. 1998). The identified CPM companions were then cross-referenced against binary component identifications in the Washington Double Star catalogue (WDS; Mason et al. 2001). Detected companions were also cross-checked against known catalogues of white dwarf/M-dwarf pairs (Silvestri et al. 2001) and white dwarf catalogues (McCook & Sion, 1999) to remove any contamination from systems with known higher-mass companions.

4.3 Astrometric confirmation

To confirm or reject detected AO and plate CPM candidates, we compared the second-epoch positions with the motion of a background object. The expected motion of a background object was calculated using the *Hipparcos* proper motion and parallax of the primary. In each case, the representative errors in the expected motion of a background object were determined from the first epoch measured uncertainties in position angle and separation. Due to the range of projected separations probed, any resolved companion within the AO images can have measurable orbital motion over the time baseline between the two epochs of observations. In order to estimate a range of possible orbital motions, two scenarios are considered: a face-on, or edge-on circular orbit. For the representative change in the position angle, a face-on circular orbit is used with a semi-major axis equal to the observed projected separation. The period of the orbit is then derived from Kepler's third law, using the masses of the two components given in Table 5, from which the change in the position angle is calculated.

In order to estimate the expected change in the separation for a bound component, an edge-on circular orbit is used. As the projected separation does not correspond to a unique value of the semi-major axis (a), and the rate of change of the separation depends on both a and the location of the companion within the orbit (characterised by the true anomaly, ν), a large number of orbits were simulated. For a given projected separation ($a_{\rm proj}$), the four unique values of ν are calculated as

$$\nu = \pm \cos^{-1}\left(\pm\sqrt{\frac{a_{\rm proj}^2}{a^2}}\right). \tag{1}$$

The limiting case for an edge-on circular orbit is when $a = a_{\rm proj}$, with ν becoming undefined when $a < a_{\rm proj}$. For a given value of a, the four values of the true anomaly were increased from ν to $\nu + 2\pi$ over the period determined from Kepler's third law using the masses for each component given in Table 5. The projected separation at each time step was then calculated as

$$a_{\rm proj} = a|\cos(\nu)|. \tag{2}$$

As the maximal change in the projected separation as a function of time depends on the true semi-major axis, 10,000 simulations were run where the value of a was increased from $a_{\rm proj}$ until the maximum value of $da_{\rm proj}/dt$ was reached (typically between $a = 2-3 \times a_{\rm proj}$). These two representative bounds for the change in projected separation and position angle for a bound companion are shown for four examples given in Figure 6, 7, 8, 9, and are shown for all companions which are detected in at least two epochs in Figure 21 (Appendix). The motion of the candidate companion was compared with the expected motion for a background source, and checked for consistency with the expected change for a bound component, within the uncertainties on position angle and separation available from the second epoch measurement. For the the large majority of the historic WDS measurements, no uncertainties are available for additional epochs.

For three of the targets with companions detected at close angular separations ($\rho \lesssim 0.2$ arcsec) – HIP 36208, HIP 86214, and HIP 114046 – the candidate is not detected within the second epoch. Given the proper motion of the primary, a background object should have been visible in the field in each of these cases. The lack of detection of the companion in the vicinity of the expected location of a background object is used as evidence for the bound nature of the companion, and they are therefore considered bound for the purposes of this study. Continued monitoring of these targets would be required in order to confirm the physical association of these companion by imaging the companion as it passes through apastron.

4.3.1 Assessment of binary sample contamination

We performed two analyses to determine the likelihood of background interlopers contaminating the binary sample. We first determined the background point source density for each of the stars in our sample from the 2MASS catalogue by selecting targets within a 10,000 au radius and within the Ks-band magnitude limits for potential stellar companions, i.e., fainter than the primary star but brighter than the $K{\rm s} = 10$ substellar limit. We find a median number of 10.5 candidate sources per 10,000 au radius (median of 3.46×10^{-6} sources arcsec^{-2} in a five degree search radius) for the full MinMs sample. The nearby distances of stars in our sample lead to the large number of background sources within the full companion search radius. While the maximum separation of an AO-detected binary ($\sim$ 35 arcsec) has a very low typical probability of background contamination (often $<<$ 1 per cent), the source count method yields significantly higher predictions on the order of a few to 10 per cent for background sources when considering the wider ($>$ 35 arcsec) plate-detected candidates.

In addition to the background source estimation, we determined the likelihood of unassociated field stars sharing similar 2D proper motions with our sample targets, as such systems would also appear as false positives in the binary statistics. Using the online Besançon stellar population synthesis tools (Robin et al. 2003), we generated catalogues of over 12,000,000 stars spanning large fields ($0.0 < \alpha < 360$, $-60 < \delta < +60$), with distance and magnitude limits corresponding to the expected companion properties. As seen

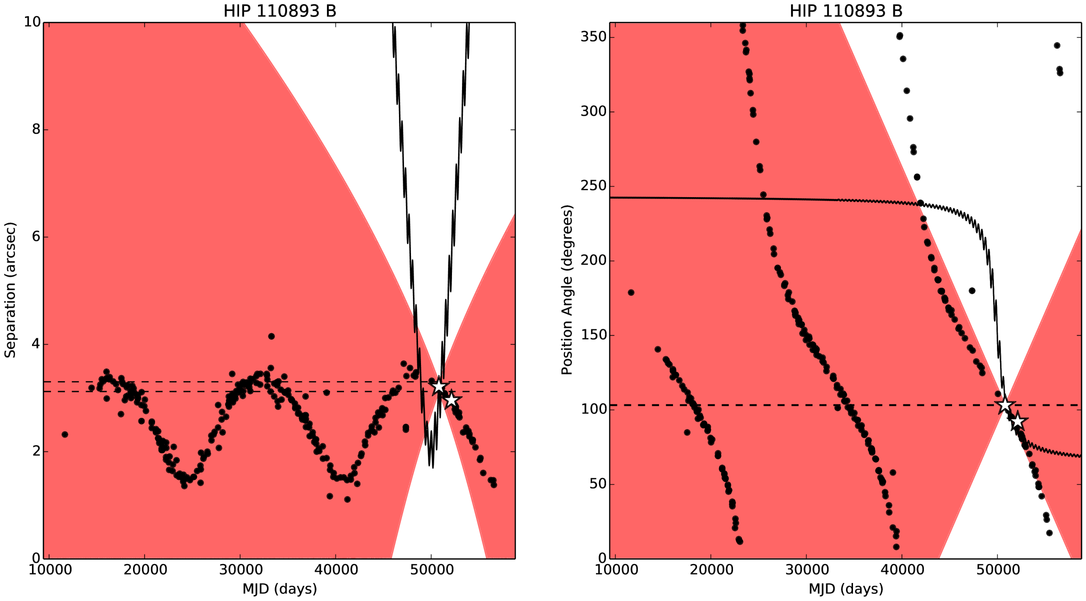

Figure 6. Proper motion diagram showing the change in separation (left panel) and position angle (right panel) between the two components of the HIP 110893 binary system. In both diagrams the measurements presented within this study are denoted by large white stars, with the measurements obtained from the WDS catalogue plotted as small circles (Mason et al. 2001). The dashed horizontal lines denote the upper and lower bounds of the separation and position angle measurement within the first epoch. The expected motion of a stationary background object, given the proper motion and parallax of the M3 dwarf target, is enclosed by the solid black lines. Given the maximal change in separation and position angle for circular orbits calculated in Section 4.3, indicative ranges of allowed separations and position angles are denoted by the red shaded region.

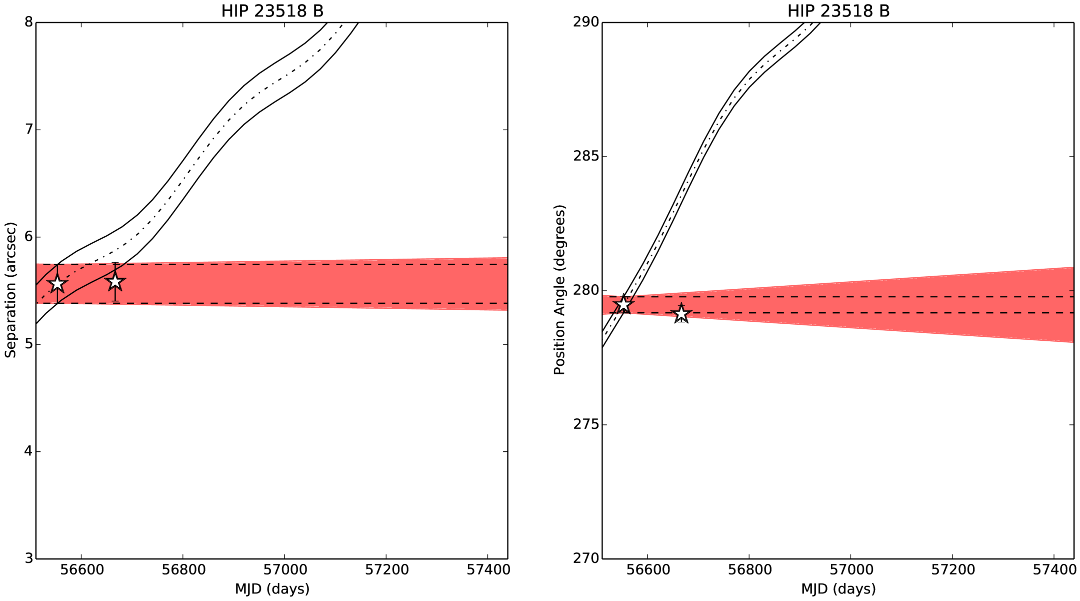

Figure 7. Proper motion diagram for the newly-discovered bound companion HIP 23518 B, identified within MMT/ARIES images presented within this study. Symbols, curves, and shading are as with Figure 6.

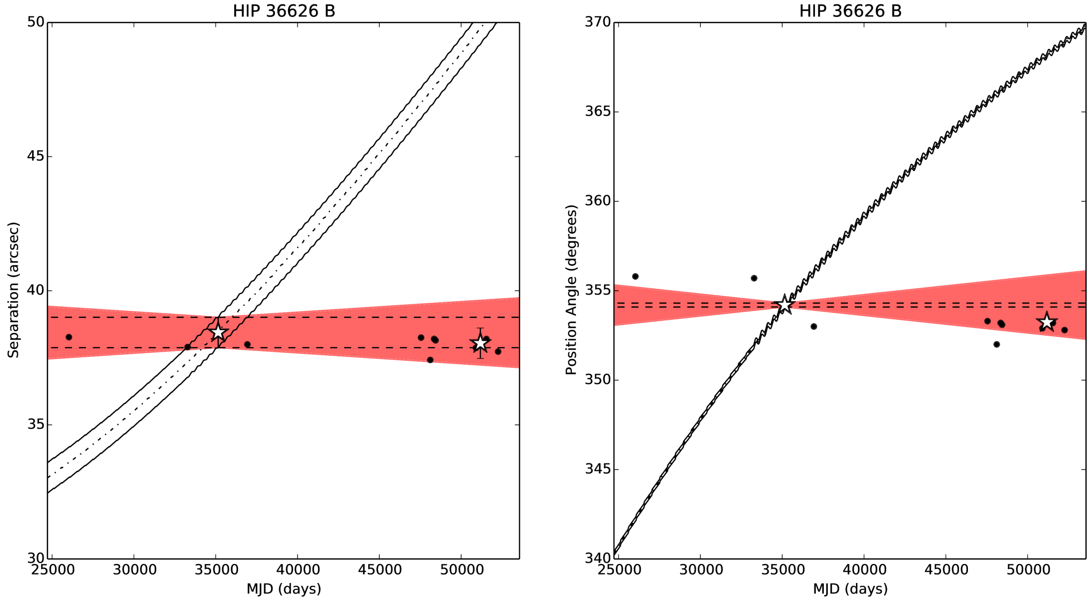

Figure 8. Proper motion diagram for the bound companion HIP 36626 B (VV Lyn B) identified within the photographic plates. Symbols, curves, and shading are as with Figure 6.

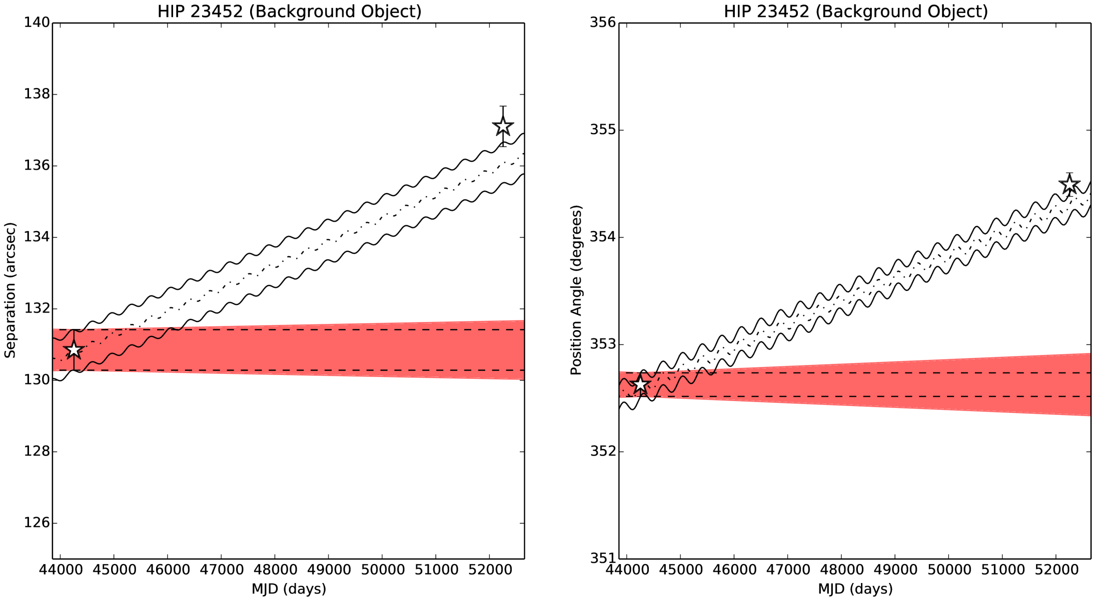

Figure 9. Proper motion diagram for a background object within the vicinity of HIP 23452 identified within the photographic plates. Symbols, curves, and shading are as with Figure 6.

in Figure 10, the extremely high proper motion of our sample leads to small overlap with the synthetic population proper motion distribution (even considering only the magnitude of the total proper motion vector and not the constituent 2D vectors, which would further narrow possible matches). For each star in our full sample, we determined the number of proper motion and Ks-magnitude matches in the synthetic population by selecting on proper motion in both right ascension and declination at various levels of confidence. This yielded the following average numbers of matching synthetic stars over the full sample per target: $1\sigma - 0.08$; $3\sigma - 0.69$; $5\sigma - 1.86$; $10\sigma - 8.23$. Of these, each system with a non-zero number of synthetic proper motion matches was selected to check physical association. As shown in Table 4, while these systems may share similar proper motions with some stars in the synthetic sample, the probability

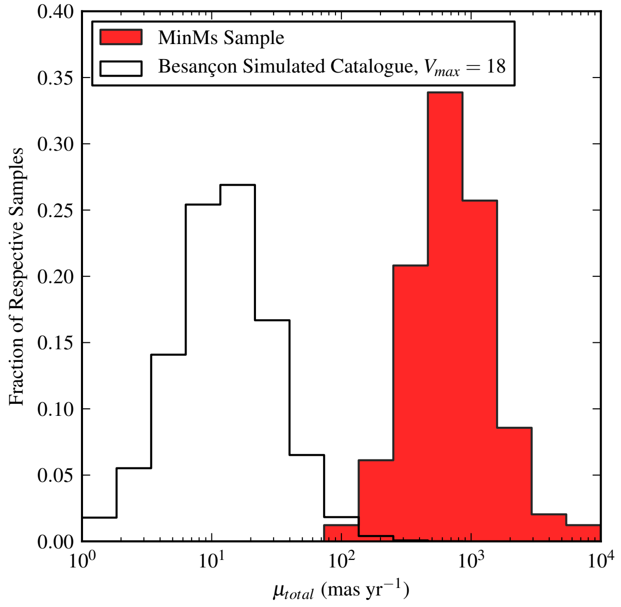

Figure 10. The relative proper motion distribution fractions for the MINMS sample and a comparable synthetic Besançon stellar catalogue (Robin et al. 2003), generated with similar sample properties.

Table 4. Likelihood of chance proper motion and position matches for low proper motion binaries

HIP	# 5σ synth. μ matches	# 10σ synth. μ matches	ρ (asec)	Source Density (counts asec^{-2})	# Bg. Sources (counts)
3937	28	127	1.68	3.15×10^{-3}	2.80×10^{-5}
15220	0	1	4.5	3.21×10^{-5}	2.04×10^{-3}
22738	27	82	7.65	3.02×10^{-6}	5.55×10^{-4}
23452	0	1	0.81	2.15×10^{-6}	4.44×10^{-6}
28368	3	11	163.15	9.54×10^{-6}	7.98×10^{-1}
35191	7	37	0.05	7.28×10^{-6}	5.72×10^{-1}
36626	1	5	0.68	5.28×10^{-6}	7.67×10^{-6}
41824	6	39	11.04	3.42×10^{-6}	1.31×10^{-3}
59406	0	1	84.7	3.24×10^{-6}	7.31×10^{-2}
65026	200	942	0.63	1.56×10^{-6}	1.95×10^{-6}
65714	0	1	8.86	2.87×10^{-6}	7.07×10^{-4}
72944	1	7	4.98	1.59×10^{-6}	1.21×10^{-4}
97292	0	1	5.62	1.06×10^{-4}	1.05×10^{-8}
102141	3	6	2.82	4.21×10^{-6}	1.05×10^{-2}
111802	0	1	25.86	1.50×10^{-6}	3.15×10^{-4}

of background source contamination from 2MASS in all cases is $<<$ 1 per cent. The combination of these analyses, particularly when coupled with previous orbital parameter measurements, supports the hypothesis of the physical association of all detected wide systems in our survey.

5 RESULTS AND DISCUSSION

Table 5: Confirmed companions - measured and derived properties

HIP	WDS[a] desig.	UT Date	ρ (arcsec)	a_{proj} (au)	θ (deg)	Δm (mag)	Broadband filter	M_{prim} ($M_\odot$)	M_{sec} ($M_\odot$)	Epoch
1242	–[b]	2003-12-10	0.21 ± 0.05	1.0 ± 0.3	158.0 ± 1.0	0.93	H	0.15	0.11	1
		2008-06-22	0.19 ± 0.01	0.9 ± 0.0	167.6 ± 3.2	0.58	H	0.18	0.14	2
1475	B	1954-10-03	37.40 ± 0.60	134.1 ± 2.0	59.5 ± 0.1	2.71	K_S	0.42	0.16	1
		1995-10-13	36.28 ± 0.70	130.2 ± 2.0	61.1 ± 0.2	2.71	K_S	0.42	0.16	2
2552	Ab	2001-08-05	0.40 ± 0.10	4.0 ± 1.0	320.0 ± 4.0	1.28	K_S	0.40	0.21	1
		2007-01-29	0.39 ± 0.02	3.9 ± 0.2	72.5 ± 1.7	1.21	K_S	0.46	0.25	2
2552	B	2001-08-05	4.01 ± 0.09	40.0 ± 1.0	177.1 ± 0.2	1.35	K_S	0.40	0.22	1
		2007-01-29	3.99 ± 0.06	40.2 ± 0.6	171.8 ± 1.1	1.35	K_S	0.40	0.22	2
3937	–	2000-08-19	1.68 ± 0.09	20.0 ± 2.0	322.3 ± 0.5	0.61	H	0.26	0.19	1
		2013-09-18	1.03 ± 0.18	12.1 ± 2.1	319.8 ± 0.7	0.61	K_S	0.26	0.19	2
4872	B	1952-09-15	296.40 ± 0.60	2,952.0 ± 45.0	75.5 ± 0.3	0.61	K_S	0.56	0.2	1
		1995-09-14	295.50 ± 0.60	2,943.5 ± 45.0	75.5 ± 0.3	0.61	K_S	0.56	0.2	2
5496	–	2003-12-09	0.07 ± 0.07	$0.5^{+0.6}_{-0.5}$	165.0 ± 2.0	0.44	H	0.43	0.36	1
		2008-10-17	0.09 ± 0.01	0.7 ± 0.1	73.7 ± 1.8	0.26	H	0.52	0.45	2
9724	–	2003-12-09	0.52 ± 0.05	4.8 ± 0.5	102.1 ± 0.4	3.25	H	0.47	0.11	1
		2013-07-03	0.62 ± 0.01	5.7 ± 0.5	102.1 ± 0.4	3.25	H	0.47	0.11	2
10617	–	1986-09-03	105.50 ± 0.60	1,511.0 ± 68.0	312.1 ± 0.1	2.11	K_S	0.40	0.27	1
		1997-11-22	105.60 ± 0.60	1,512.1 ± 68.0	312.1 ± 0.1	2.11	K_S	0.40	0.27	2
15220	B	1954-01-28	6.75 ± 1.00	97.2 ± 15.0	12.9 ± 5.0	0.07	K_S	0.50	0.49	1
		1995-11-12	5.65 ± 1.00	81.2 ± 15.0	6.0 ± 5.0	0.07	K_S	0.50	0.49	2
22738	–	2004-09-23	7.65 ± 0.05	85.0 ± 2.0	314.7 ± 0.1	0.72	H	0.36	0.25	1
		2012-08-24	7.47 ± 0.56	83.1 ± 0.2	314.7 ± 0.1	0.71	H	0.35	0.25	2
23452	B	2002-09-18	0.81 ± 0.09	6.9 ± 0.8	285.4 ± 0.7	1.30	K_S	0.59	0.37	1
		2014-01-13	0.89 ± 0.18	7.6 ± 1.6	335.4 ± 4.8	1.30	K_S	0.59	0.37	2
23518	⋆[c]	2013-09-18	5.60 ± 0.20	76.0 ± 3.0	279.5 ± 0.3	4.81	K_S	0.54	0.08	1
		2014-01-10	5.58 ± 0.20	76.1 ± 2.4	279.1 ± 0.3	4.81	K_S	0.54	0.08	2
23932	–	2003-03-16	0.06 ± 0.05	0.6 ± 0.5	30.0 ± 4.0	0.10	K_S	0.43	0.41	1
		2011-02-16	0.07 ± 0.05	0.7 ± 0.5	44.4 ± 5.5	0.10	K_S	0.43	0.41	2
28368	–	1954-01-05	163.10 ± 0.60	2,208.0 ± 50.0	119.4 ± 0.6	0.20	K_S	0.53	0.22	1
		1996-12-10	162.50 ± 0.60	2,199.6 ± 50.0	119.5 ± 0.6	0.20	K_S	0.53	0.22	2
29316	B	2004-01-07	1.72 ± 0.09	19.0 ± 1.0	30.1 ± 0.2	1.50	K_S	0.45	0.22	1
		2013-09-18	0.58 ± 0.18	6.3 ± 1.9	52.5 ± 1.1	1.50	K_S	0.45	0.22	2
30920	B	2006-04-11	1.37 ± 0.05	5.6 ± 0.2	47.4 ± 0.2	1.24	K_S	0.21	0.1	1
		2009-03-28	1.07 ± 0.01	4.4 ± 0.0	74.6 ± 0.3	1.61	K_S	0.24	0.13	2
31293	–	1977-02-10	23.00 ± 0.60	207.3 ± 7.0	35.3 ± 0.3	0.76	K_S	0.45	0.32	1
		1989-12-31	23.22 ± 0.60	209.4 ± 7.0	34.0 ± 0.3	0.76	K_S	0.45	0.32	2
33142	–	2002-09-12	0.30 ± 0.10	3.0 ± 1.0	250.0 ± 3.0	0.47	H	0.32	0.25	1
		2005-04-27	0.19 ± 0.01	1.9 ± 0.1	160.5 ± 3.9	0.47	H	0.32	0.25	2
33499	–[f]	2003-12-08	0.83 ± 0.05	6.6 ± 0.4	282.9 ± 0.3	0.01	H	0.24	0.24	1
35191	–	2000-02-25	0.06 ± 0.05	0.7 ± 0.6	154.0 ± 6.0	0.32	J	0.39	0.34	1
		2003-12-08	0.06 ± 0.01	0.8 ± 0.1	334.5 ± 6.0	0.32	J	0.39	0.34	2
36208	⋆[e]	2003-12-11	0.17 ± 0.05	0.6 ± 0.2	327.0 ± 4.0	1.07	H	0.24	0.14	1
36626	Ab	2000-04-20	0.70 ± 0.10	8.0 ± 1.0	201.0 ± 4.0	1.87	K_S	0.51	0.21	1
		2013-09-18	1.53 ± 0.01	18.1 ± 0.1	194.4 ± 0.6	1.87	K_S	0.51	0.21	2
36626	B	1955-02-13	38.40 ± 0.60	456.0 ± 20.0	354.2 ± 0.1	3.82	K_S	0.51	0.39	1
		1998-12-28	38.04 ± 0.60	451.5 ± 20.0	353.2 ± 0.1	3.82	K_S	0.51	0.39	2
41824	Ab	1999-02-27	0.67 ± 0.09	7.0 ± 1.0	157.2 ± 0.9	1.48	K_S	0.38	0.11	1
		2007-01-29	0.65 ± 0.09	7.2 ± 1.0	169.9 ± 1.1	1.48	K_S	0.38	0.11	2
41824	Ba	1999-02-27	10.17 ± 0.09	113.0 ± 10.0	348.6 ± 0.1	1.74	K_S	0.38	0.17	1
		2007-01-29	10.32 ± 0.09	114.2 ± 10.0	348.5 ± 0.1	1.74	K_S	0.38	0.17	2
41824	Bb	1999-02-27	9.91 ± 0.09	110.0 ± 10.0	346.2 ± 0.1	2.20	K_S	0.38	0.13	1
		2007-01-29	9.58 ± 0.09	106.0 ± 10.0	346.0 ± 0.1	2.20	K_S	0.38	0.13	2
46706	–	1997-12-28	0.70 ± 0.10	7.0 ± 1.0	239.0 ± 1.0	0.09	K_S	0.42	0.41	1
		2004-04-05	0.52 ± 0.01	5.2 ± 0.0	49.8 ± 0.3	0.09	K_S	0.54	0.53	2
47620	B	1955-01-26	89.10 ± 0.60	1,096.0 ± 25.0	77.1 ± 0.1	0.60	K_S	0.52	0.46	1
		2000-01-13	88.80 ± 0.60	1,091.8 ± 25.0	77.5 ± 0.1	0.60	K_S	0.52	0.46	2
49969	–	2000-02-19	0.20 ± 0.10	2.0 ± 1.0	253.0 ± 8.0	0.81	H	0.43	0.29	1
		2003-03-18	0.16 ± 0.01	1.9 ± 0.0	61.8 ± 1.4	0.51	H	0.49	0.36	2
54211	B	1955-03-19	30.20 ± 0.60	147.0 ± 3.0	131.1 ± 0.2	4.40	K_S	0.40	0.1	1
		2000-03-14	31.91 ± 0.60	154.7 ± 3.0	126.6 ± 0.2	4.40	K_S	0.40	0.1	2
59406	–	1954-04-02	84.70 ± 0.60	1,066.0 ± 32.0	120.9 ± 0.1	1.58	K_S	0.36	0.26	1
		1994-05-18	85.12 ± 0.60	1,071.7 ± 32.0	120.9 ± 0.1	1.58	K_S	0.36	0.26	2
60910	–[f]	2008-02-19	0.07 ± 0.05	0.9 ± 0.7	114.0 ± 5.0	0.70	K_S	0.32	0.22	1
62556	–	1997-12-27	0.20 ± 0.10	2.0 ± 1.0	240.0 ± 7.0	0.55	H	0.37	0.28	1
		2003-03-17	0.32 ± 0.04	3.3 ± 0.4	202.8 ± 4.3	0.55	H	0.37	0.28	2
63510	B	2005-05-01	0.28 ± 0.05	3.2 ± 0.6	357.0 ± 1.0	3.26	K_S	0.58	0.12	1
		2006-05-23	0.24 ± 0.01	2.8 ± 0.1	307.4 ± 4.5	3.71	K_S	0.58	0.12	2
65011	B	1950-05-15	19.60 ± 0.20	260.0 ± 9.0	123.1 ± 0.3	0.66	K_S	0.63	0.3	1
		1990-05-06	17.80 ± 0.20	236.1 ± 9.0	128.9 ± 0.3	0.66	K_S	0.63	0.3	2
65026	B	2000-04-20	0.63 ± 0.09	7.0 ± 1.0	107.0 ± 6.0	0.85	K_S	0.67	0.52	1
		2005-04-27	1.26 ± 0.09	13.5 ± 1.0	94.2 ± 0.2	0.85	K_S	0.67	0.52	2
65714	–	1956-04-08	8.90 ± 0.60	123.0 ± 9.0	45.7 ± 2.0	1.36	K_S	0.48	0.22	1
		1996-04-21	7.65 ± 0.60	106.2 ± 9.0	51.5 ± 2.0	1.36	K_S	0.48	0.22	2
71898	–	2002-06-25	2.88 ± 0.09	31.0 ± 1.0	109.9 ± 0.2	3.94	K_S	0.40	0.08	1
		2004-04-25	2.77 ± 0.01	29.7 ± 0.1	105.8 ± 0.2	3.94	K_S	0.40	0.08	2
72896	–	2001-08-06	1.00 ± 0.10	11.0 ± 1.0	116.0 ± 1.0	0.77	K_S	0.29	0.2	1
		2013-04-19	1.02 ± 0.01	10.3 ± 0.0	93.7 ± 0.0	0.77	K_S	0.37	0.25	2
72944	Ba	2005-06-04	4.92 ± 0.05	47.5 ± 0.9	32.5 ± 0.2	2.66	K_S	0.49	0.09	1
		2006-03-01	4.91 ± 0.01	47.4 ± 0.1	33.4 ± 0.1	2.66	K_S	0.49	0.09	2
72944	Bb	2005-06-04	4.98 ± 0.05	48.1 ± 0.9	32.0 ± 0.2	4.80	K_S	0.49	0.08	1

Table 5: continued.

HIP	WDS desig.	UT Date	ρ (arcsec)	a_{proj} (au)	θ (deg)	Δm (mag)	Broadband filter	M_{prim} $(M_{\odot})$	M_{sec} $(M_{\odot})$	Epoch
		2006-03-01	5.01 ± 0.01	48.4 ± 0.1	32.4 ± 0.1	4.80	K_S	0.49	0.08	2
73470	–	2003-03-17	1.36 ± 0.09	16.0 ± 1.0	179.2 ± 0.2	2.26	K_S	0.60	0.24	1
		2005-04-25	1.54 ± 0.01	18.1 ± 0.1	173.0 ± 0.1	2.26	K_S	0.62	0.25	2
79755	–	1955-04-23	64.00 ± 0.60	684.0 ± 9.0	12.7 ± 0.1	0.99	K_S	0.66	0.47	1
		1994-06-18	64.87 ± 0.60	693.2 ± 9.0	13.5 ± 0.1	0.99	K_S	0.66	0.47	2
80018	–	2007-05-19	4.92 ± 0.05	41.0 ± 1.0	226.9 ± 0.2	3.02	H	0.38	0.1	1
		2013-03-29	4.43 ± 0.02	37.0 ± 0.1	226.0 ± 0.1	3.02	H	0.38	0.1	2
82817	B	2003-05-29	0.11 ± 0.05	0.7 ± 0.3	275.0 ± 2.0	0.28	H	0.43	0.38	1
		2005-07-21	0.22 ± 0.01	1.4 ± 0.1	173.8 ± 0.1	0.28	H	0.43	0.38	2
82817	C	1954-06-01	73.10 ± 0.60	453.0 ± 16.0	313.8 ± 0.1	0.28	H	0.43	0.2	1
		1996-04-25	72.75 ± 0.60	450.7 ± 16.0	313.3 ± 0.1	0.28	H	0.43	0.2	2
82817	F	1954-06-01	232.50 ± 0.60	1,440.0 ± 50.0	155.4 ± 0.4	4.58	K_S	0.43	0.09	1
		1996-04-25	232.01 ± 0.60	1,437.4 ± 50.0	155.4 ± 0.4	4.58	K_S	0.43	0.09	2
84140	B	1999-04-04	1.11 ± 0.09	6.6 ± 0.6	225.0 ± 0.5	0.01	K_S	0.34	0.34	1
		2004-04-05	0.25 ± 0.09	1.5 ± 0.5	166.6 ± 5.5	0.01	K_S	0.47	0.47	2
84794	–	1951-07-05	15.80 ± 0.60	183.0 ± 11.0	267.3 ± 0.2	1.10	K_S	0.44	0.29	1
		1996-08-09	16.81 ± 0.60	194.9 ± 11.0	268.7 ± 0.2	1.10	K_S	0.44	0.29	2
86057	–	2005-05-01	3.76 ± 0.05	37.0 ± 1.0	325.4 ± 0.3	1.93	H	0.45	0.18	1
		2007-05-14	3.94 ± 0.05	38.3 ± 1.0	323.7 ± 0.3	1.93	H	0.45	0.18	2
86214	$\star^{e}$	2005-05-01	0.17 ± 0.05	0.9 ± 0.3	190.0 ± 5.0	1.01	H	0.23	0.14	1
91772	A[d]	2001-05-04	12.53 ± 0.09	44.7 ± 0.5	170.1 ± 0.1	0.60	K_S	0.26	0.19	1
		2009-09-01	11.98 ± 0.04	42.8 ± 0.1	219.4 ± 0.2	0.60	K_S	0.26	0.19	2
93899	–	1951-07-13	116.60 ± 0.60	1,020.0 ± 21.0	290.2 ± 0.5	1.01	K_S	0.32	0.32	1
		1994-06-12	115.40 ± 0.60	1,010.1 ± 21.0	291.0 ± 0.5	1.01	K_S	0.32	0.32	2
94349	–	2003-07-19	0.08 ± 0.05	0.8 ± 0.6	58.0 ± 6.0	0.80	H	0.34	0.23	1
		2007-05-14	0.16 ± 0.01	1.7 ± 0.0	319.7 ± 1.8	0.80	H	0.41	0.28	2
94761	B	1950-08-12	72.90 ± 0.60	428.0 ± 4.0	149.5 ± 0.5	4.64	K_S	0.49	0.09	1
		1995-08-16	75.36 ± 0.60	442.4 ± 4.0	151.6 ± 0.5	4.64	K_S	0.49	0.09	2
97292	B[f]	2013-09-18	5.60 ± 0.20	76.0 ± 3.0	140.1 ± 0.3	0.71	K_S	0.49	0.37	1
99150	–	1976-05-30	41.60 ± 0.60	619.0 ± 47.0	111.0 ± 0.5	1.70	K_S	0.37	0.33	1
		1996-09-17	41.60 ± 0.60	621.0 ± 47.0	109.4 ± 0.5	1.70	K_S	0.37	0.33	2
102141	C	2003-07-21	2.82 ± 0.05	30.0 ± 1.0	171.2 ± 0.2	0.03	K_S	0.54	0.53	1
		2009-06-01	2.51 ± 0.01	26.8 ± 0.0	159.4 ± 0.6	0.03	K_S	0.66	0.65	2
106255	–	2003-12-10	0.19 ± 0.05	1.5 ± 0.4	162.0 ± 1.0	1.12	H	0.27	0.15	1
		2005-05-02	0.16 ± 0.01	1.3 ± 0.0	128.2 ± 0.5	1.12	H	0.31	0.17	2
110893	–	1997-12-28	3.21 ± 0.09	12.9 ± 0.4	103.3 ± 0.2	0.98	K_S	0.27	0.17	1
		2001-08-04	2.96 ± 0.01	11.8 ± 0.1	86.9 ± 0.3	0.98	K_S	0.32	0.2	2
111766	–	2006-05-26	0.78 ± 0.05	10.0 ± 1.0	175.5 ± 0.2	0.24	K_S	0.38	0.34	1
		2013-05-08	0.86 ± 0.01	11.4 ± 0.1	123.0 ± 0.3	0.24	K_S	0.38	0.34	2
111802	–	1984-10-15	25.90 ± 0.60	225.0 ± 6.0	351.6 ± 0.1	0.30	K_S	0.60	0.32	1
		1999-08-11	28.07 ± 0.60	244.1 ± 6.0	352.2 ± 0.1	0.30	K_S	0.60	0.32	2
114046	$\star^{e}$	2003-12-09	0.07 ± 0.05	0.2 ± 0.2	267.0 ± 3.0	1.21	H	0.44	0.25	1
116132	B	1997-12-25	5.18 ± 0.09	32.0 ± 0.7	93.8 ± 0.3	1.37	K_S	0.35	0.17	1
		2000-08-21	5.28 ± 0.01	32.7 ± 0.0	94.0 ± 0.1	1.37	K_S	0.39	0.2	2

[a] WDS catalogue component designation.

[b] targets within the WDS catalog, but without an assigned component designation.

[c] is a newly confirmed companion without a designation in the WDS catalog ($\star$ denotes a new companion).

[d] HIP 91772 is designated as the "B" component in the WDS catalog, but has the largest estimated mass of the system.

[e] denotes a target for which there is no second epoch detection, but instead a non-detection of a background object (Section 4.3).

[f] denotes instance where second epoch data were not available, but multiple confirmation epochs were obtained from previous WDS measurements.

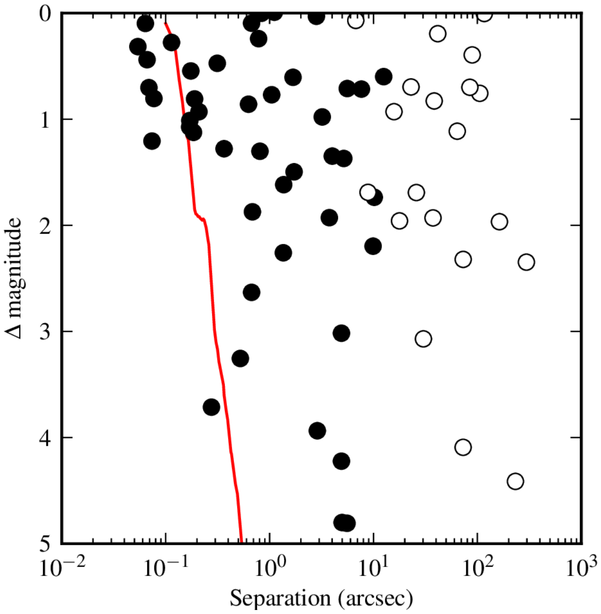

Figure 11. The separations and magnitude differences for the confirmed stellar companions in our survey. Companions shown were detected in either the AO data (in one or more of the $JHK\mathrm{s}$ filters, filled circles), the plate data (only K_S magnitude differences from 2MASS cross-matching shown, open circles), or in a few cases, with both imaging techniques. The red line represents the median 3σ sensitivity of the sample, and continues beyond the canonical substellar limit. The survey is sensitive to companions above, and to the right of, this sensitivity limit.

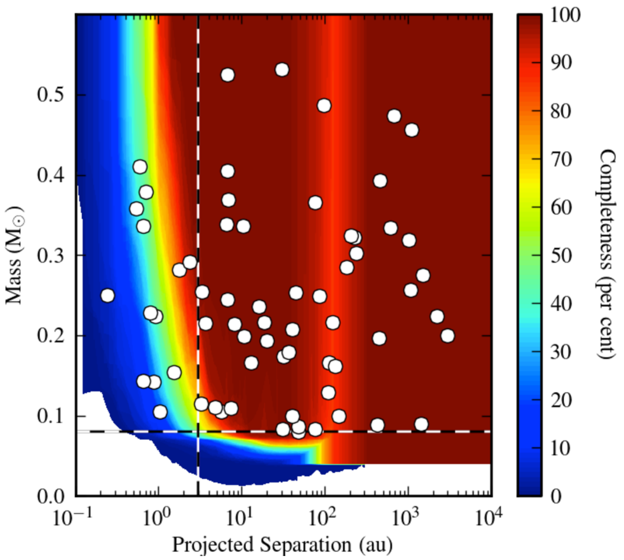

Figure 12. The completeness of the MinMs survey in terms of derived physical parameters. The horizontal black and white dashed line designates the substellar limit of 0.08 $\mathrm{M}_\odot$, while the vertical dashed line at 3 au indicates the minimum interior separation to which the AO subsample is 85 per cent complete. These lines define the minimum mass and separation thresholds used to assess population statistics for a subsample minimizing detection biases. Stellar companions are over-plotted, and span the parameter range of our survey.

5.1 Detected co-moving companions and survey completeness

Based on the multi-epoch AO and wide-field imaging data analysis, a total of 47 AO-detected and 20 wide-field-detected physically associated companions were identified in the MinMs sample (41 systems with one or more companions detected in the close AO data, and 17 systems with one or more companions detected in the wide plate data, for a total of 58 multiple systems and 187 single stars). Due to some overlap in search space between the two types of data, two different companions were detected independently by the two techniques, resulting in 65 unique co-moving companions to the MinMs sample. Among the AO-detected companions, four are newly identified within this study. The measured astrometry and relative photometry for each of the resolved companions are reported in Table 5, along with the inferred masses of each component derived from an evolutionary model (Baraffe et al. 1998), as described in Section 4.2.3. The 65 companions are distributed in 53 binary systems, three triple systems, and two quadruple systems.

The observed angular separations and magnitude differences for all of the companions are plotted in Figure 11, and the 3σ median sensitivity of the sample is also shown. The angular separations range from 0.05 arcsec to 4.94 arcmin. The magnitude differences measured in one of the infrared filters ranged from $\Delta m = 0.0 - 5.0$. Only stellar companions are considered for this study, so the maximum magnitude difference needed for sensitivity to an M9 companion ($M_K \sim 10$ mag) to an M0 primary ($M_K \sim 4.5$ mag) is only 5.5 mag at K_S-band. The limited dynamic range required to reach the bottom of the main sequence, combined with the sensitive observations, results in a very uniform completeness to stellar companions. Detection limits for all targets are reported in Table 7 (Appendix).

The observational properties are transformed into physical properties of mass and projected separation in Figure 12. Wider than a few au, the completeness is very high (typically $>$ 95 per cent), as shown in Figure 12. The detected companions are also included in the figure, and co-moving objects down to the stellar/substellar limit are identified in the MinMs study. The vertical and horizontal dashed lines define the boundaries of the region considered for constructing the distributions of companion separation, secondary mass, and total system mass. The closer pairs ($<$ 3 au) are not included in the population statistics, since the interpretation of the data would be dependent on a large correction factor. A similar plot in terms of mass ratio and projected separation is given in Figure 13, and the dashed lines delineate the systems included in determining the mass ratio distribution of the MinMs sample. Although the sensitivity is very uniform to a companion mass limit of 0.08 $\mathrm{M}_\odot$, the range of target masses makes the lower mass ratio limit of $q \geqslant 0.2$ for uniform completeness in the mass ratio distribution.

5.2 Comparison of sample properties and binary detections

To determine if any selection biases impacted the study, particularly given the magnitude-limited nature of our survey, we analysed binary occurrence against attributes such as distance, magnitude, and metallicity. To test whether observed binaries were consistent with being drawn randomly from the survey sample, all systems were rank-ordered by a given attribute and the binaries were plotted to create a cumulative distribution function, which could then be compared against a random distribution. This was performed using a

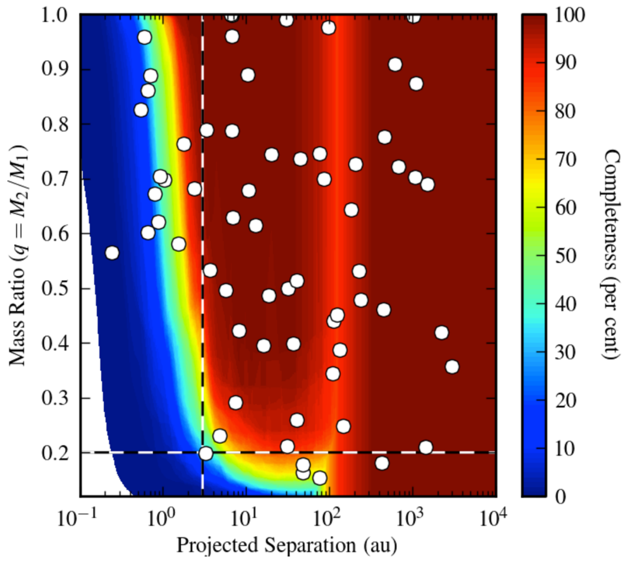

Figure 13. The completeness of the MinMs survey, shown in terms of the mass ratio of the companion to the primary star. The horizontal dashed line at $q = 0.2$ designates the mass ratio limit for uniform completeness, while the vertical dashed line indicates the minimum separation limit of 3 au used to assess population statistics.

method similar to calculating the Gini coefficient, a widely-used statistic in economics measuring wealth distribution within societies (Gini 1955). For each system attribute, the area underneath the binary distribution, normalized to 0.5, was calculated. The error on the area was estimated with a Monte Carlo simulation of 10,000 random distributions, each with the same number of binaries in the same number of total targets. In this study, the 58 multiple systems within 245 total systems leads us to an expected area of 0.5 ± 0.03.

The comparisons for the systems in our survey are shown in Figures 14 for the distances of the systems, and Figure 15, for the magnitude distribution of the target sample. For the distance distribution, we find the area beneath the binary distribution to be 0.54, slightly over 1σ away from the expected area value. This may be seen in a slight overabundance of binaries near rank order 0.5, corresponding to systems at $\sim$8 pc, but is still consistent with a random distribution, and so the sample does not appear to be significantly biased toward systems at closer or further distances. Similarly, for the V-band magnitude distribution in Figure 15, the area was also 0.54, and is again consistent with a random underlying distribution. Similar comparisons were performed for the binaries within only the 196-star AO subsample, with area values of 0.49 for the distance distribution and 0.52 for the magnitude distribution, which are also consistent with selection from a random distribution.

Using literature values for the 124 stars within our sample with previous metallicity measurements (Table 1), subsamples of the binaries and single stars were also compared with the same technique. With 20 observed multiple systems within the 124 star subsample with metallicity measurements, the expected integrated area of the binary distribution function is 0.5 ± 0.06. With an observed value of 0.45, the survey also appears consistent with a random distribution with respect to stellar metallicity, and suggests no dependence of binarity upon the system metallicity. With very few measurements of extremely metal-poor or metal-rich stars within our sample, no binaries were detected at extreme metallicities, underscoring the utility of additional sample metallicity and age estimations in determining robust statistics for various population subsamples.

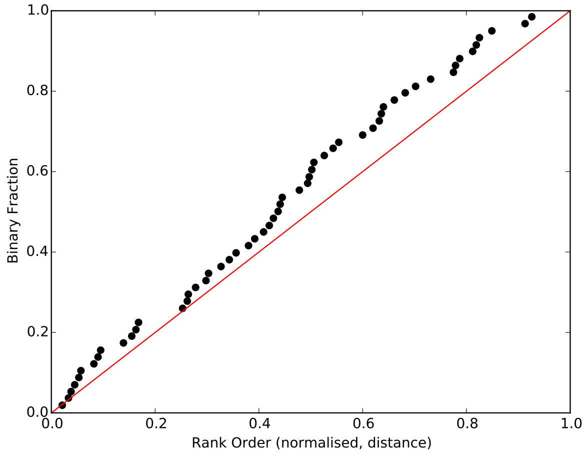

Figure 14. Binary fraction of the stars within our sample at a given distance versus normalized rank-ordered distance of the full sample. The solid red line denotes the expected trend for a random distribution, with integrated area normalised to 0.5 ± 0.03 (errors drawn from Monte Carlo simulations of 10,000 random distributions). The black points show the binary fraction as a function of rank-ordered distance; with an integrated area of 0.54, the binary occurrence is consistent with being drawn from a random distribution, implying an unbiased observation of binaries in the MinMs sample with respect to system distance.

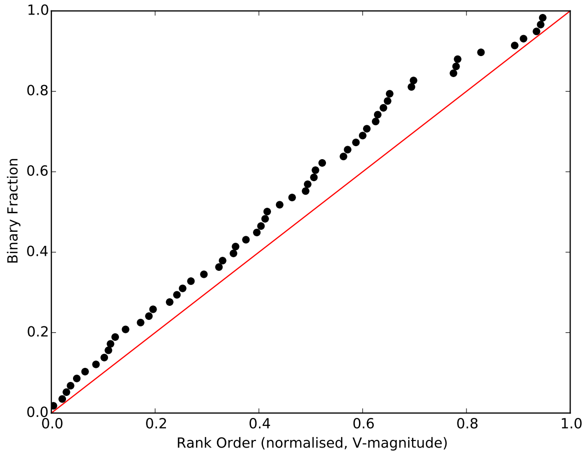

Figure 15. Binary fraction of the stars within our sample with a given V-band magnitude versus normalized rank-ordered magnitude of the full sample. Colors and symbols are as in the preceding figure for distance distribution. The integrated binary distribution with respect to magnitude is also 0.54, and consistent with being drawn randomly, implying an unbiased observation of binaries in the MinMs sample with respect to system brightness.

5.3 Projected separation distribution

The separation range of 3 au defined from the survey completeness to the outer limit of 10,000 au, spans 3.5 orders of magnitude. The distribution of projected separations was constructed over six

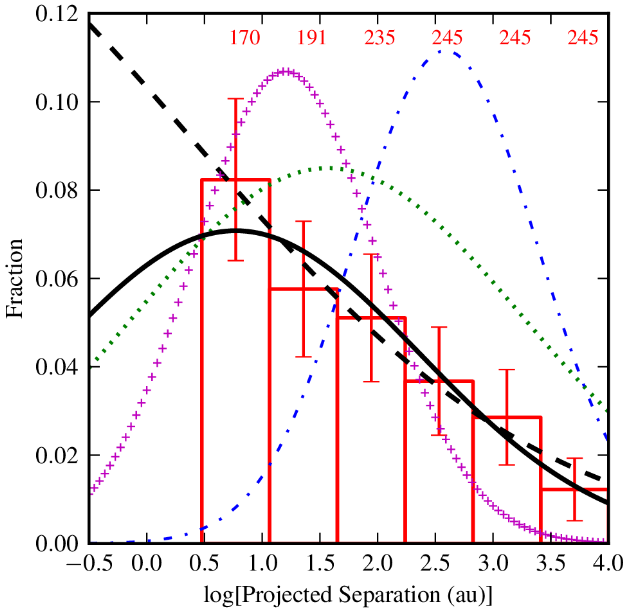

Figure 16. The distribution of projected separations for the companions resolved between 3 and 10,000 au, corrected for incompleteness (red histogram). Assuming a log-normal distribution, a Gaussian was fit to the observed distribution. Allowing all parameters to vary freely, the distribution is best fit by a Gaussian with a mean of $\mu_{\log(a)} = -0.66$ and width of $\sigma_{\log(a)} = 1.86$ (dashed black curve). A restricted fit was also computed by fixing the mean of the distribution to the centre of the first bin of the distribution ($\mu_{\log(a)} = 0.77$), with a best-fitting Gaussian of width $\sigma_{\log(a)} = 1.34$ (solid black curve). These fits represent the two limiting cases of the true distribution, given the observed distribution within the restricted separation range. For comparison, the distribution of companion separations for A-star primaries (blue dot-dash curve, De Rosa et al. 2014), solar-type primaries (green dotted curve, Raghavan et al. 2010), and for M-dwarf primaries in a previous lucky-imaging survey (magenta crosses, Janson et al. 2012).

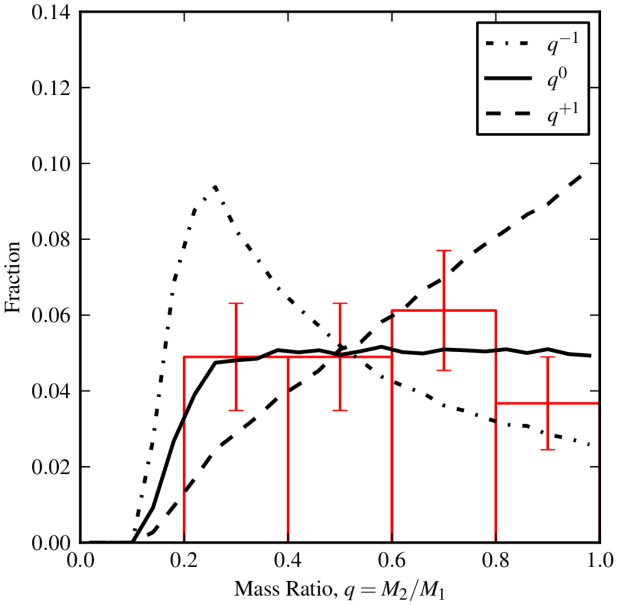

Figure 17. The distribution of companion mass ratios for the companions resolved in the MinMs study. Only those companions with projected separations between $30 - 10,000$ au and mass ratios of $q \geqslant 0.2$ are included to minimize observational biases. The predicted shape of the mass ratio distribution for companions drawn from a distribution rising to more equal-mass companions ($f(q) \propto q^{1}$, dashed curve), a flat distribution ($f(q) \propto q^{0}$, solid curve), and a falling distribution ($f(q) \propto q^{-1}$, dot-dashed curve) are plotted for reference. The observed mass ratio distribution is most consistent with the flat distribution.

equally sized bins from $\log{(a_{\rm proj})}$ of 0.5 to 4.0, and is shown in Figure 16. For each bin, the number of targets in the sample that was sensitive to 95 per cent of the bin range is indicated above each bin, and the companion frequency per bin was determined by dividing the number of resolved companions within the bin by the subset of targets complete to 95 per cent of the bin. The error bars were calculated from Poisson statistics.

Over the range of the survey data, the distribution rises monotonically to the smaller separations covered in the 3 au to 10 au bin. The best-fit log-normal distribution is plotted, and due to the unconstrained location of the peak of the distribution, a best-fitting $\mu_{\log(a)} = -0.66$ and $\sigma_{\log(a)} = 1.86$ is found. Fixing the peak to be at the centre of the first bin of the observed distribution ($\mu_{\log(a)} = 0.77$), a significantly narrower distribution is fit ($\sigma_{\log(a)} = 1.34$). Compared to a previous survey of M-stars at a larger range of distances with less sensitivity to wider companions (Janson et al. 2012), the peak of the restricted fit to the MinMs distribution is lower, but significantly wider (Figure 16). Two additional comparison curves are shown for the distributions of companions to higher mass primaries. The solar-type distribution peak occurs at a somewhat wider separation (Raghavan et al. 2010) and the fit is consistently higher than the corresponding value of the M-star distribution with the exception of the bin for the smallest separations. The fit to the projected separation distribution of A-star systems (De Rosa et al. 2014) is substantially different, with a markedly larger value for the peak and an overall higher normalisation. Given the larger distances of the A-star sample ($D \leqslant 75$ pc), the inner limit for data used to construct the A-star distribution is located at the third bin of the MinMs data (log $a_{\rm proj} = 1.6$). Considering the fits to the M-dwarf, solar-type and A-star surveys, the MinMs results provide further evidence to support the trend of a wider typical system separation as a function of host star mass that has been noted in previous studies. The MinMs study refines the population statistics for low-mass stars with the large sample and comprehensive mass and separation sensitivity.

5.4 Mass ratio distribution

Based on the survey completeness shown in Figure 13, the systems included in the mass ratio distribution have a mass ratio of $q \geqslant 0.2$. The shape of the observed mass ratio distribution is consistent with a flat distribution, as shown in Figure 17. Because the target masses are close to the stellar limit, all targets are not sensitive to the full range of mass ratios ($q \geqslant 0.2$). The median mass of a star in the sample is ∼0.44 $M_\odot$ and the mass ratio limit for the median star corresponds to a secondary mass limit of 0.09 $M_\odot$. For the lowest-mass stars in the sample, the bottom of the main sequence occurs at a mass ratio greater than $q > 0.2$. As the lowest-mass primaries in our sample have masses in the $0.12 - 0.18$ $M_\odot$ range, corresponding to a companion at the stellar/substellar boundary with $q \sim 0.6$, the two lowest mass ratio bins are affected by this potential bias.

The mass ratio values were sorted by the separation of the pair and split into two sets by a range of dividing separations, and the inner and outer distributions were compared to each other with a Kolmogorov-Smirnov (KS) test. The inner and outer distributions were not found to be significantly different, regardless of the dividing separation used. This result is different from what was found for both G-star (Raghavan et al. 2010) and A-star binaries (De Rosa et al. 2014). Since there was no difference in the mass ratio distributions, the full set of companions was used to investigate the shape of the true underlying distribution. In order to estimate the expected shape of the mass ratio distribution, taking into account the distribution of primary masses, we performed a series of Monte Carlo simulations to construct comparison mass ratio distributions from pairing the MINMS primaries with secondaries of different companion mass ratio functions (Figure 17).

We have assumed that the full mass range of the MINMS primaries can be described as a simple population with a single underlying mass ratio distribution. The pairing simulations were based on a population of 1×10^5 primary stars with a distribution of masses matching the primaries in the MINMS survey. For each primary, a companion mass was drawn randomly from rising, falling, or uniform mass ratio distributions over the full stellar companion mass range of $0.08M_\odot$ to the given primary mass, producing 1×10^5 companions. We then divided the masses of the secondaries by the masses of the primaries to obtain the corresponding mass ratios. From this analysis, only those stars with $M_\odot < 0.4$ were biased against detecting mass ratios of $q < 0.2$ (making up 35 per cent of the sample) and given that the sample stars fall off quickly toward lower-mass primaries, only 10 per cent of primaries $< 0.3M_\odot$ were similarly biased, resulting in a bias in half of the $q = 0.2 - 0.4$ bin. In this way, the rising, falling and uniform distributions are compared with similar completeness to the mass ratio distribution of the observed companions. This is similar to previous analyses for higher-mass primaries, and statistical analyses of companion mass ratio distributions (Reggiani & Meyer 2011, 2013). In light of our implicit assumption that the q-distribution is the same for the full range of MINMS primaries, the observed mass ratio distribution is thus consistent with companions drawn from a distribution flat in mass ratio ($f(q) \propto q^0$).

5.5 Companion and total system mass distributions

Given the high level of completeness to the bottom of the main sequence, the distributions of primary and companion mass were constructed for all pairs with >3 au projected separation. Unlike the flat mass ratio distribution, the companion mass distribution shown in Figure 18 rises continuously with decreasing mass. Similarly, the total system mass distribution in Figure 19 rises to smaller masses. For comparison, a KS test was performed to compare the mass distribution of single stars and that of primaries in binary systems; with a p-value of 0.34, no intrinsic difference was found between the two populations, indicating no preference for massive primaries having more companions (or vice versa). For triple and quadruple systems, all companions and the primary are summed to determine the system mass included in Figure 18. For comparison with the total system distribution, the target star mass distribution is also plotted in Figure 19.

5.6 Frequency of companions

There are two quantities that define the multiplicity of the sample. The multiplicity fraction (MF) quantifies the number of multiple

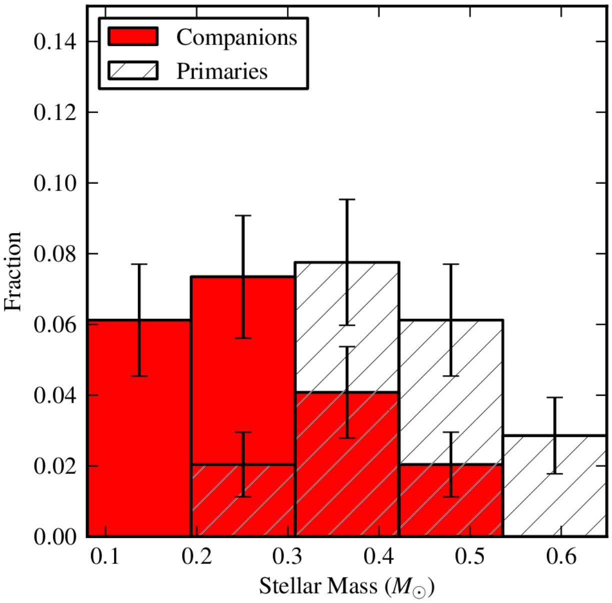

Figure 18. The distribution of primary masses and companion masses for all stellar companions and hosts found within the MINMS study, shown in fractions of the total sample. A KS test performed on the single star masses against the masses of primaries in binaries showed no preference toward stellar mass correlating with presence of companions over the K7-M6 spectral type range of our sample.

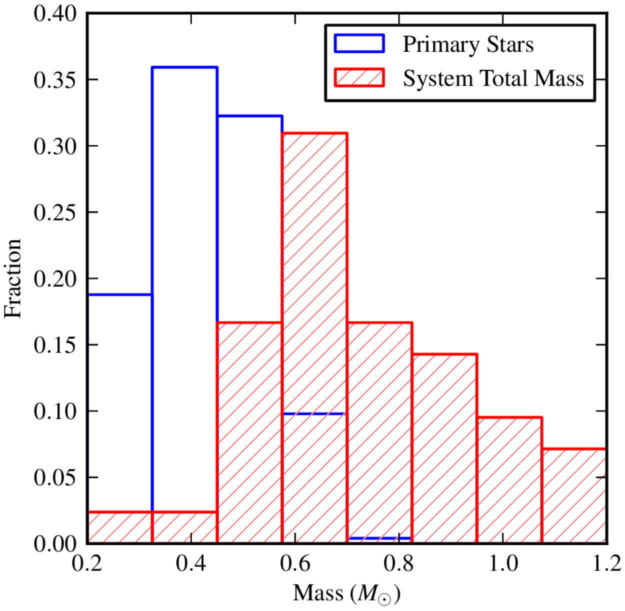

Figure 19. The distribution of total system mass, calculated as the sum of all components within a given multiple system, including all companions with separations of $a_{\rm proj} \geqslant 3$ au and $q \geqslant 0.2$, normalised by the number of such companions (red hatched histogram). Plotted for reference is the distribution of primary masses given in Figure 4, normalised by the overall sample size (blue histogram).

systems within the sample:

$$MF = \frac{b + t + q + ...}{s + b + t + q + ...}, \quad (3)$$

where s is the number of singles, b the number of binaries, t the number of triples, q the number of quadruples, and so forth (e.g. Reipurth & Zinnecker 1993; Goodwin, Whitworth & Ward-Thompson 2004). The companion star fraction (CSF) quantifies the total number of companions within the sample as the following:

$$CSF = \frac{b + 2t + 3q + ...}{s + b + t + q + ...}, \quad (4)$$

(Patience et al. 2002). As described in Section 5.1, AO data exist for a subsample of 196 stars within the 245-star MinMs sample. Therefore, the multiplicity fraction can be calculated for separate subsamples, accounting for selection effects over different ranges of projected separation. Of the AO data, which forms a subsample searching projected separations in the 1-100 AU range, we find 41 binaries of the 196 stars with AO imaging, corresponding to a MF of 21 ± 3 per cent. For the plate data, we find 17 wide binaries covering the 100-10000 au range within the full 245 star sample with plate imaging, corresponding to a MF for the wide subsample of 7 ± 2 per cent. This is consistent with the tighter semi-major axis distribution and lower multiplicity seen in comparison to higher-mass primaries.

The CSF over $3 - 10,000$ au is calculated by summing the fraction in each separation bin of Figure 16, since each bin is already corrected for incompleteness. The resulting $\mathrm{CSF}_{3-10,000\mathrm{au}}$ value is 23.5 ± 3.2 per cent, as shown in Figure 20. For closer separations, the survey is not fully sensitive to the bottom of the main sequence, but a lower limit on the total CSF can be estimated by combining the bound companions resolved within this study with those reported within the WDS catalogue and the Ninth catalogue of Spectroscopic Binary Orbits (SB9; Pourbaix et al. 2004). The resulting CSF $_{\mathrm{total}}$ is $34.7^{+2.9}_{-3.2}$ per cent. (Similarly, the lower limit on the total multiplicity of the sample was estimated as $\mathrm{MF}_{\mathrm{total}} = 28.6^{+2.7}_{-3.1}$ per cent.)

To place the MinMs results in a broader context, the CSF is compared with samples with different primary star masses. Two separation ranges are considered: the full $3 - 10,000$ au range and the more restrictive $30 - 10,000$ au range. The $3 - 10,000$ au range requires samples of nearby field objects to reach the smaller projected separations, so the MinMs value is compared with field Solar-type stars (Raghavan et al. 2010) and field brown dwarfs (Burgasser et al. 2006). As shown in Figure 20, the CSF calculated over both separation ranges shows a decline with primary mass. The solar-type star study was sensitive to the bottom of the main sequence as is the case for the MinMs survey, while the surveys of brown dwarfs were typically sensitive to $q \gtrsim 0.5$. Over the restricted $30 - 10,000$ au range, for which a $\mathrm{CSF}_{30-10,000\mathrm{au}} = 12.4 \pm 2.3$ per cent was measured for the M-dwarf primaries within this study, it is possible to include the results from the more massive A-stars (De Rosa et al. 2014). Due to the paucity of wide companions to brown dwarfs, there is only an upper limit on the brown dwarf companion star fraction over this separation range (Allen et al. 2007).

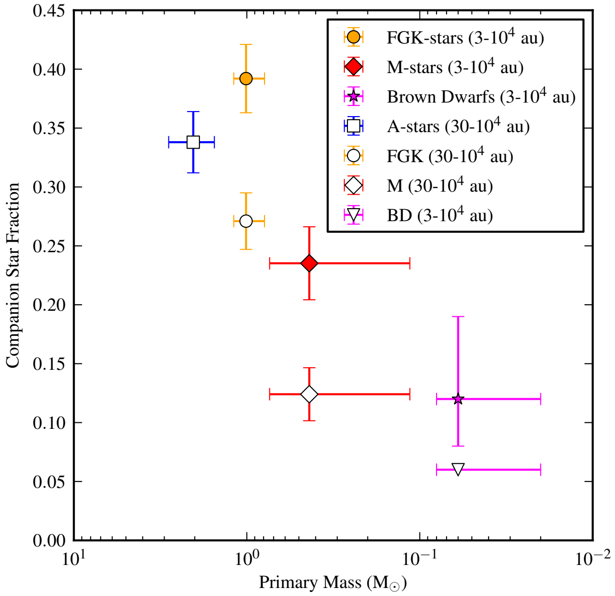

Figure 20. The companion star fractions measured over the full $3 - 10,000$ au (filled symbol) and restricted $30 - 10,000$ au (open symbol) separation ranges. Comparison values for both ranges, from left to right, are shown for solar-type stars (yellow circles, Raghavan et al. 2010), and M-dwarfs (red diamonds, this study). Over the $3 - 10,000$ au range, a measured value exists for brown dwarf primaries (pink star, Burgasser et al. 2006). Over the restricted $30 - 10,000$ au range, additional comparison values are available for field A-type stars (blue square, De Rosa et al. 2014), as well as an upper limit to the $\mathrm{CSF}_{30-10,000\mathrm{au}}$ for brown dwarf primaries (pink downward triangle, Allen et al. 2007), demonstrating the decreasing trend of multiplicity with later spectral type.

5.7 Higher order multiple systems

Since the MinMs companions include a large range of separations from a minimum of 0.2 au to a maximum of 2,952 au, and ∼200 stars have both AO and wide field imaging, it is possible to detect higher order multiple systems within the survey. A total of three triple and two quadruple systems were identified. All the triple systems are in hierarchical arrangements and the ratio of inner to outer projected separations ranges from 347:1 to 27:1. The threshold for stability of multiple systems is considered to be a separation ratio for the outer to inner pair of 5:1 (Eggleton 2006), suggesting that all the triple systems are likely stable. For the two quadruples, one system consists of two widely separated close pairs, while the other system is composed of a close pair and two wider and lower mass stars. For a full accounting of the frequency of higher order multiples, radial velocity measurements of the sample with AO and wide field imaging are required.

To determine whether any spectroscopic systems were previously known within the sample, we cross-referenced the SB9 catalogue and the 70 star M-dwarf spectroscopic survey by (Marcy & Benitz 1989, hereafter MB89) against our sample. Among the 50 MinMs stars within the MB89 study, only two spectroscopic binaries are known. From the cross-reference with SB9, an additional 10 spectroscopic binaries were identified within our sample from the following surveys, listed in Table 6: Nidever et al. 2002 (N02), Evans 1959 (E59), Tomkin & Pettersen 1986 (TP86), Tokovinin 1997 (T97), Mazeh et al. 2001 (M01), and Herbig & Moorhead 1965 (HM65). Of these spectroscopic systems, one was resolved in archival AO imaging (HIP 9724). As the completeness of the SB9 catalogue is unknown since non-detections are not reported, we do not include these binaries in our analysis. The incompleteness of the spectroscopic results underscores the need for a comprehensive

Table 6. Summary of known spectroscopic binaries in the MinMs sample

HIP	Reference	SB Type	Period (days)	AO Resolved?
9724	N02	1	6818	Yes
11964	E59	1	1.962	No
25953	MB89	2	-	No
34603	TP86	1	10.428	No
38082	MB89	2	-	No
65011	T97	1	200.26	No
76901	N02	1	62.628	No
80346	N02	1	1366.1	No
82809	M01	1	2.9655	No
82817	M01	1	2.9655	No
111802	HM65	1	4.0832	No

spectroscopic companion survey of nearby M-dwarfs, such as the CARMENES survey (Quirrenbach et al. 2010). By building upon the current results, the MinMs sample represents an ideal target set for developing a comprehensive understanding of the frequency and properties of higher-order multiple systems with low-mass primaries.

6 SUMMARY AND CONCLUSIONS

With a combination of multi-epoch adaptive optics and wide-field imaging, we have conducted a companion search program targeting 245 late K and early M-dwarfs which are within 15 pc with *Hipparcos* parallax uncertainties of < 10 per cent, $M_V > 8$, and which are not companions to earlier spectral type primaries. Companions with projected separations as small as 0.2 au were resolved, and beginning at a separation of 3 au and continuing to 10,000 au, the observations were sensitive to the companions down to the stellar/substellar limit. Within this complete range, a total of 65 co-moving companions were detected, 47 with AO observations and 18 from wide-field imaging data, of which four are newly resolved within this study.

Over the complete $3 - 10,000$ au separation range, the companion star fraction is 23.5 ± 3.2 per cent. With the large sample size, the uncertainties are reduced by a factor of $\sim$2 relative to previous studies, which makes it possible to determine that the M-dwarf CSF is distinctly lower than the solar-type value (Raghavan et al. 2010) and higher than the corresponding brown dwarf fraction (Burgasser et al. 2006). By considering the separation range of $30 - 10,000$ au to enable a comparison with the more distant and more massive A-stars (De Rosa et al. 2014), a $\mathrm{CSF}_{30-10,000au} = 12.4 \pm 2.3$ was measured, and a systematic decline in CSF as a function of primary mass is observed.

Dividing the observed range of companion separations into six bins, the separation distribution is seen to rise continuously toward the smallest separations to which the survey is sensitive. When compared to the results of a previous lucky imaging survey of M-dwarfs (Janson et al. 2012), the MinMs distribution appears to have a wider spread, likely due to the enhanced coverage that enabled a direct measurement of the widest systems. The mass ratio distribution is flat across the $q = 0.2 - 1.0$ range, similar to that observed for companions to solar-type stars (Raghavan et al. 2010), but different from the rise toward lower mass ratios seen for higher-mass stars (De Rosa et al. 2014).

The MinMs study can serve as a benchmark dataset for comparisons with the companion star properties of more distant populations of young low-mass stars. Given the existing large coverage, the MinMs sample is also an ideal set to pursue radial velocity searches for the closest companions to complete the separation distribution, and to provide the first complete accounting of high order multiplicity of M-dwarfs.

ACKNOWLEDGMENTS

The authors wish to thank the anonymous referee for providing a thorough review and helpful comments which improved this manuscript. KWD is supported by the National Science Foundation Graduate Research Fellowship under Grant No. DGE-1311230. RJDR acknowledges support from Science and Technology Facilities Council grants ST/H002707/1 and ST/K005588/1. RJP acknowledges support from the Royal Astronomical Society in the form of a research fellowship. We are grateful to the MMT Observatory staff for their excellent support of these observations. We also thank B. Svoboda for valuable programming discussions. This research has made use of the SIMBAD database, operated at CDS, Strasbourg, France. This research makes use of data products from the Two Micron All Sky Survey, which is a joint project of the University of Massachusetts and the Infrared Processing and Analysis Center/California Institute of Technology, funded by the National Aeronautics and Space Administration and the National Science Foundation. This research has made use of the Washington Double Star catalogue maintained at the US Naval Observatory. This research used the facilities of the Canadian Astronomy Data Centre operated by the National Research Council of Canada with the support of the Canadian Space Agency. Results are based on data obtained from the ESO Science Archive Facility. This research has made use of data obtained from the SuperCOSMOS Science Archive, prepared and hosted by the Wide Field Astronomy Unit, Institute for Astronomy, University of Edinburgh, which is funded by the UK Science and Technology Facilities Council.

REFERENCES

Allen P. R., Koerner D. W., McElwain M. W., Cruz K. L., Reid I. N., 2007, AJ, 133, 971
Andrews S. M., Wilner D. J., Hughes A. M., Qi C., Dullemond C. P., 2009, ApJ, 700, 1502
Artymowicz P., Lubow S. H., 1994, ApJ, 421, 651
Baraffe I., Chabrier G., Allard F., Hauschildt P. H., 1998, A & A, 337, 403
Bastian N., Covey K. R., Meyer M. R., 2010, ARA & A, 48, 339
Bergfors C. et al., 2010, A & A, 520, A54
Bertin E., Arnouts S., 1996, 117, 393
Beuzit J.-L. et al., 2004, A & A, 425, 997
Browning M. K., Basri G., Marcy G. W., West A. A., Zhang J., 2010, AJ, 139, 504
Burgasser A. J., Kirkpatrick J. D., Cruz K. L., Reid I. N., Leggett S. K., Liebert J., Burrows A., Brown M. E., 2006, ApJS, 166, 585
Cutri R. M. et al., 2003, 2MASS All Sky Catalog of point sources.
De Rosa R. J. et al., 2011, MNRAS, 415, 854
De Rosa R. J. et al., 2014, MNRAS, 437, 1216
Doyon R., Nadeau D., Vallee P., Starr B. M., Cuillandre J. C., Beuzit J.-L., Beigbeder F., Brau-Nogue S., 1998, in Society of Photo-Optical Instrumentation Engineers (SPIE) Conference Series, Vol. 3354, Society of Photo-Optical Instrumentation

Engineers (SPIE) Conference Series, Fowler A. M., ed., pp. 760–768

Eggleton P., 2006, Evolutionary Processes in Binary and Multiple Stars

ESA, 1997, VizieR Online Data Catalog, 1239, 0

Evans D. S., 1959, MNRAS, 119, 526

Fischer D. A., Marcy G. W., 1992, 396, 178

Gaidos E., Mann A. W., 2014, ApJ, 791, 54

Gini C., 1955, Memorie di metodologica statistica, 1, 156

Goodwin S. P., 2010, Royal Society of London Philosophical Transactions Series A, 368, 851

Goodwin S. P., Whitworth A. P., Ward-Thompson D., 2004, A & A, 423, 169

Gray R. O., Corbally C. J., Garrison R. F., McFadden M. T., Bubar E. J., McGahee C. E., O'Donoghue A. A., Knox E. R., 2006, AJ, 132, 161

Hambly N. C. et al., 2001, 326, 1279

Hawley S. L., Gizis J. E., Reid I. N., 1996, 112, 2799

Heintz W. D., 1986, 65, 411

Henry T. J., Jao W.-C., Subasavage J. P., Beaulieu T. D., Ianna P. A., Costa E., Méndez R. A., 2006, AJ, 132, 2360

Herbig G. H., Moorhead J. M., 1965, ApJ, 141, 649

Hodapp K. W. et al., 2008, in Society of Photo-Optical Instrumentation Engineers (SPIE) Conference Series, Vol. 7014, Society of Photo-Optical Instrumentation Engineers (SPIE) Conference Series

Houk N., Cowley A. P., 1975, University of Michigan Catalogue of two-dimensional spectral types for the HD stars. Volume I. Declinations -90 to -53.

Janson M. et al., 2012, ApJ, 754, 44

Kenyon S. J., Hartmann L., 1995, 101, 117

King R. R., Goodwin S. P., Parker R. J., Patience J., 2012a, 427, 2636

King R. R., Parker R. J., Patience J., Goodwin S. P., 2012b, 421, 2025

Kobayashi N. et al., 2000, in Society of Photo-Optical Instrumentation Engineers (SPIE) Conference Series, Vol. 4008, Optical and IR Telescope Instrumentation and Detectors, Iye M., Moorwood A. F., eds., pp. 1056–1066

Koen C., Kilkenny D., van Wyk F., Marang F., 2010, MNRAS, 403, 1949

Kozai Y., 1962, AJ, 67, 591

Lenzen R. et al., 2003, in Society of Photo-Optical Instrumentation Engineers (SPIE) Conference Series, Vol. 4841, Society of Photo-Optical Instrumentation Engineers (SPIE) Conference Series, Iye M., Moorwood A. F. M., eds., pp. 944–952

Lépine S., Gaidos E., 2011, 142, 138

Lidov M. L., 1962, Planet. Space Sci., 9, 719

Luhman K. L., Allen P. R., Espaillat C., Hartmann L., Calvet N., 2010, ApJS, 186, 111

Luhman K. L., Stauffer J. R., Muench A. A., Rieke G. H., Lada E. A., Bouvier J., Lada C. J., 2003, ApJ, 593, 1093

Marcy G. W., Benitz K. J., 1989, 344, 441

Mason B. D., Wycoff G. L., Hartkopf W. I., Douglass G. G., Worley C. E., 2001, 122, 3466

Mazeh T. et al., 2001, MNRAS, 325, 343

McCarthy D. W., Burge J. H., Angel J. R. P., Ge J., Sarlot R. J., Fitz-Patrick B. C., Hinz J. L., 1998, in Society of Photo-Optical Instrumentation Engineers (SPIE) Conference Series, Vol. 3354, Infrared Astronomical Instrumentation, Fowler A. M., ed., pp. 750–754

Metchev S. A., Hillenbrand L. A., 2009, ApJS, 181, 62

Murakawa K. et al., 2004, pasj, 56, 509

Murakawa K. et al., 2003, in Society of Photo-Optical Instrumentation Engineers (SPIE) Conference Series, Vol. 4841, Instrument Design and Performance for Optical/Infrared Ground-based Telescopes, Iye M., Moorwood A. F. M., eds., pp. 881–888

Neves V., Bonfils X., Santos N. C., Delfosse X., Forveille T., Allard F., Udry S., 2014, A & A, 568, A121

Newton E. R., Charbonneau D., Irwin J., Berta-Thompson Z. K., Rojas-Ayala B., Covey K., Lloyd J. P., 2014, AJ, 147, 20

Nidever D. L., Marcy G. W., Butler R. P., Fischer D. A., Vogt S. S., 2002, ApJS, 141, 503

Parker R. J., Goodwin S. P., 2009, MNRAS, 397, 1041

Parker R. J., Meyer M. R., 2014, ArXiv e-prints

Parker R. J., Quanz S. P., 2013, MNRAS, 436, 650

Patience J. et al., 2002, ApJ, 581, 654

Perryman M. A. C. et al., 1997, 323, L49

Pourbaix D. et al., 2004, A & A, 424, 727

Poveda A., Allen C., Costero R., Echevarría J., Hernández-Alcántara A., 2009, ApJ, 706, 343

Quirrenbach A. et al., 2010, in Society of Photo-Optical Instrumentation Engineers (SPIE) Conference Series, Vol. 7735, Society of Photo-Optical Instrumentation Engineers (SPIE) Conference Series

Raghavan D. et al., 2010, 190, 1

Reggiani M., Meyer M. R., 2013, A & A, 553, A124

Reggiani M. M., Meyer M. R., 2011, ApJ, 738, 60

Reid I. N., Gizis J. E., 1997, AJ, 113, 2246

Reid I. N., Hawley S. L., Gizis J. E., 1995, 110, 1838

Reipurth B., Zinnecker H., 1993, A & A, 278, 81

Robin A. C., Reylé C., Derrière S., Picaud S., 2003, A & A, 409, 523

Roeser S., Demleitner M., Schilbach E., 2010, AJ, 139, 2440

Rojas-Ayala B., Covey K. R., Muirhead P. S., Lloyd J. P., 2012, ApJ, 748, 93

Rousset G. et al., 2003, in Society of Photo-Optical Instrumentation Engineers (SPIE) Conference Series, Vol. 4839, Society of Photo-Optical Instrumentation Engineers (SPIE) Conference Series, Wizinowich P. L., Bonaccini D., eds., pp. 140–149

Tokovinin A., 2008, MNRAS, 389, 925

Tokovinin A. A., 1997, A & A, 121, 71

Tokunaga A. T. et al., 1998, in Society of Photo-Optical Instrumentation Engineers (SPIE) Conference Series, Vol. 3354, Infrared Astronomical Instrumentation, Fowler A. M., ed., pp. 512–524

Tomkin J., Pettersen B. R., 1986, AJ, 92, 1424

Torres C. A. O., Quast G. R., da Silva L., de La Reza R., Melo C. H. F., Sterzik M., 2006, A & A, 460, 695

van Leeuwen F., 2007, 474, 653

Worley C. E., 1962, AJ, 67, 396

Wu Y., Murray N., 2003, ApJ, 589, 605

APPENDIX

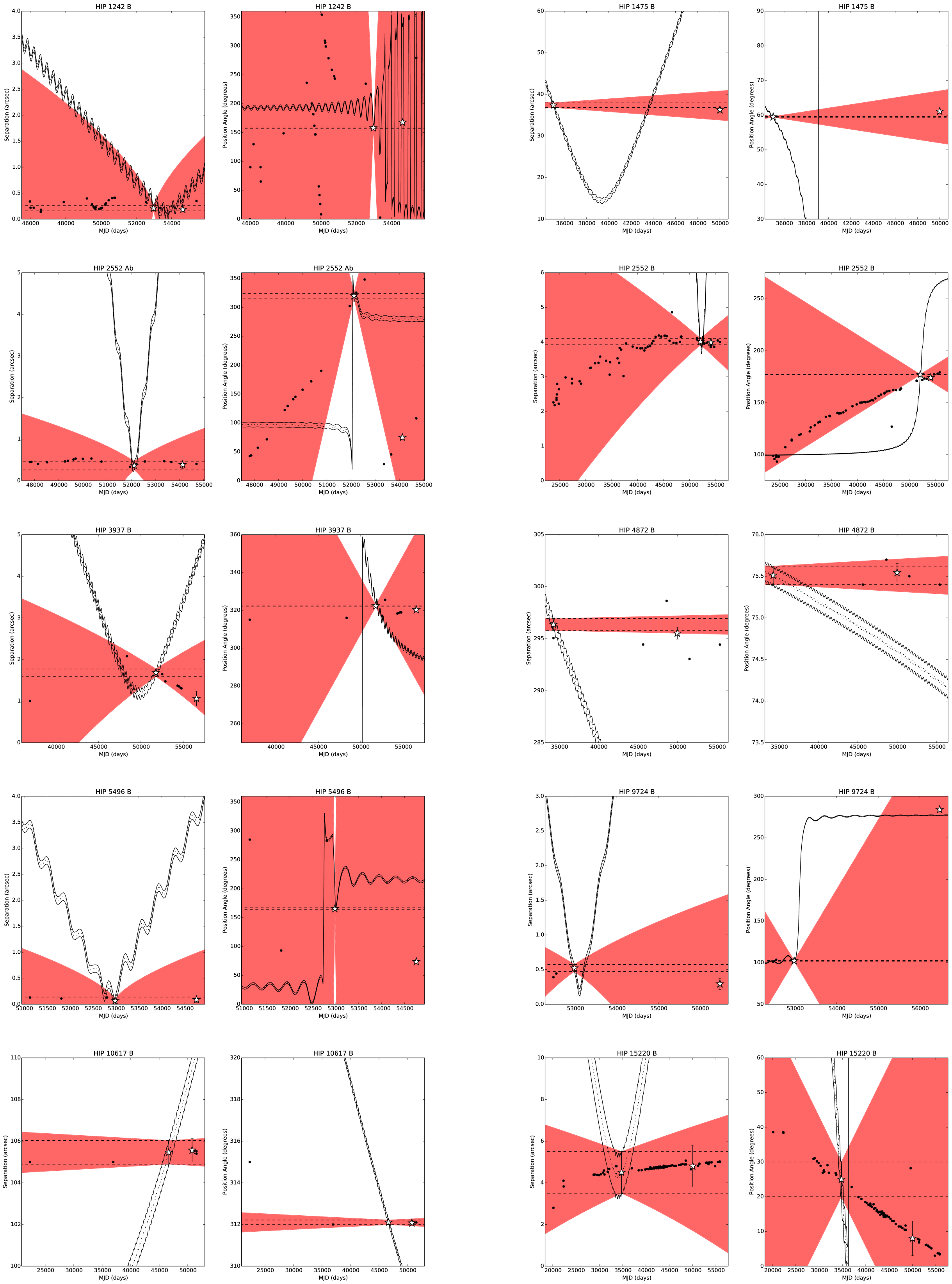

Figure 21. Sample proper motion diagrams of the bound companions identified within this study. Symbols, curves, and shading are as with Figure 6. The full set of proper motion diagrams for each of the detected companion candidates in this study is available in the electronic edition of the journal.

Table 7: Companion detection limits

	AO Δm (mag) at $\rho = (arcsec)$									ρ sensitive to full MS		
HIP	0.05	0.15	0.25	0.50	1.00	1.50	2.00	5.00	10.00	$\rho_{\rm AO,max}$ (arcsec)	$\rho_{\rm Plate,min}$ (arcsec)	$\rho_{\rm Plate,max}$ (arcmin)
HIP428	...	0.64	1.87	4.33	6.67	8.08	8.71	9.18	9.17	34.00	5.64	14.81
HIP439	0.02	3.87	5.04	6.23	6.41	6.39	6.40	6.36	4.11	14.00	21.58	38.40
HIP1242	0.01	2.70	2.09	6.34	7.04	7.04	7.07	7.01	4.48	13.00	2.50	33.42
HIP1475	...	0.89	1.91	4.37	6.16	7.88	8.20	8.51	8.51	35.00	12.49	46.46
HIP2552	...	0.63	1.49	2.36	5.14	6.76	7.75	6.47	7.90	39.00	5.37	16.56
HIP3937	...	0.61	0.87	1.89	2.55	1.35	1.64	7.50	8.79	36.00	6.30	14.07
HIP4569	...	...	...	...	...	...	...	...	...	...	5.40	13.49
HIP4856	...	0.69	1.94	4.28	6.90	8.02	8.63	9.52	9.34	38.00	7.93	20.24
HIP4872	...	1.10	2.00	4.46	6.58	8.29	8.65	9.02	8.94	35.00	8.46	16.73
HIP5496	0.08	1.09	3.48	4.93	6.82	7.25	7.29	7.22	6.71	13.00	8.09	20.34
HIP5643	...	0.58	1.31	2.61	4.39	5.81	6.86	7.64	7.44	39.00	10.62	45.17
HIP8051	...	1.16	2.12	5.25	7.24	8.47	8.60	8.71	8.64	36.00	16.39	14.60
HIP8768	...	0.65	1.87	4.62	7.02	8.37	9.05	9.49	9.45	35.00	11.74	15.14
HIP9291	...	0.84	1.77	3.79	5.96	7.59	8.07	8.52	8.26	40.00	4.30	13.61
HIP9724	0.04	3.71	5.02	4.65	7.44	7.44	7.58	7.52	4.94	13.00	7.15	18.23
HIP9786	...	2.62	3.64	5.96	6.60	6.60	6.61	6.57	5.62	13.00	4.86	17.97
HIP10279	...	0.46	1.81	4.70	6.84	8.18	8.75	8.67	8.62	35.00	20.82	16.00
HIP10395	...	0.60	1.80	4.40	6.69	7.89	8.44	8.69	8.69	35.00	8.09	13.28
HIP10617	...	2.28	4.36	6.16	8.14	8.66	8.87	9.04	9.00	26.00	9.31	11.64
HIP10812	...	-0.05	1.28	4.81	7.35	8.24	9.20	10.54	8.69	74.00	5.53	11.84
HIP11048	...	0.66	1.93	4.66	6.96	8.39	9.04	9.33	9.33	36.00	9.94	13.96
HIP11964	...	3.29	5.10	7.00	8.83	9.24	9.51	9.42	8.80	14.00	12.82	14.36
HIP12097	...	...	...	...	...	...	...	...	...	...	7.12	12.26
HIP12781	...	0.63	1.80	4.12	6.62	7.99	8.68	9.14	9.01	38.00	6.31	22.19
HIP13218	...	...	...	...	...	...	...	...	...	...	6.88	12.87
HIP13389	0.05	3.51	5.13	6.52	7.27	7.32	7.36	7.22	5.08	14.00	6.21	14.31
HIP15220	...	...	...	...	...	...	...	...	...	...	6.18	11.59
HIP15638	...	...	...	...	...	...	...	...	...	...	5.64	11.87
HIP16536	...	2.74	3.85	5.90	7.37	7.34	7.52	7.45	6.38	13.00	5.40	15.52
HIP17609	...	0.57	3.52	4.85	6.79	6.87	6.91	6.89	6.87	58.00	8.33	11.30
HIP19337	...	...	...	...	...	...	...	...	...	...	10.61	12.40
HIP19394	...	...	...	...	...	...	...	...	...	...	5.54	11.12
HIP21088	...	0.66	1.76	4.27	6.65	7.91	8.96	9.18	9.11	36.00	5.91	29.88
HIP21556	...	0.70	1.81	4.74	7.18	8.28	8.78	9.13	8.88	40.00	6.72	15.02
HIP21932	...	1.81	4.27	6.55	8.55	9.00	9.06	9.21	9.28	24.00	6.98	17.97
HIP22627	...	3.17	4.68	5.54	5.67	5.64	5.43	5.22	4.77	17.00	6.58	13.56
HIP22738	0.06	2.63	3.82	5.04	5.76	5.76	5.76	5.45	5.19	15.00	6.89	15.00
HIP22762	...	...	...	...	...	...	...	...	...	...	6.34	13.75
HIP23452	...	0.69	1.73	4.18	3.58	6.84	8.37	9.36	9.10	40.00	11.47	19.43
HIP23512	...	0.63	1.83	4.11	6.55	7.95	8.60	8.97	8.79	38.00	4.72	18.10
HIP23518	...	0.50	2.98	4.51	7.08	7.34	7.40	7.44	7.41	53.00	7.66	12.24
HIP23932	...	0.16	2.36	5.05	7.05	7.23	7.28	7.34	7.29	25.00	7.96	17.98
HIP24186	0.02	4.48	5.85	7.51	8.33	8.34	8.35	8.20	5.58	15.00	25.91	42.61
HIP24284	...	...	...	...	...	...	...	...	...	...	6.45	13.56
HIP25578	...	1.97	4.10	6.08	8.45	8.99	9.17	9.18	9.21	25.00	3.90	18.92
HIP25878	...	0.83	1.80	4.51	6.43	8.57	8.79	9.73	9.59	41.00	10.75	29.46
HIP25953	...	...	...	...	...	...	...	...	...	...	5.51	13.03
HIP26801	...	...	...	...	...	...	...	...	...	...	8.06	13.40
HIP26857	...	1.17	2.13	5.20	7.24	8.58	8.72	8.86	8.75	35.00	10.75	28.59
HIP28035	...	...	...	...	...	...	...	...	...	...	6.61	11.43
HIP28368	...	...	...	...	...	...	...	...	...	...	7.12	12.32
HIP29052	...	2.95	4.21	6.02	6.25	6.20	6.23	6.12	4.16	15.00	5.13	14.69
HIP29277	...	1.11	2.01	4.95	6.85	8.64	9.03	9.39	9.22	37.00	6.31	17.78
HIP29295	...	0.72	1.79	4.15	6.20	7.13	7.44	7.57	7.42	36.00	14.17	28.97
HIP29316	...	0.56	1.74	3.86	5.88	3.95	4.21	8.94	8.70	40.00	7.26	15.28
HIP30920	...	3.54	5.28	6.76	7.10	5.90	7.27	7.07	6.14	14.00	13.03	40.39

Table 7: continued.

	AO Δm (mag) at $\rho = (arcsec)$									ρ sensitive to full MS		
HIP	0.05	0.15	0.25	0.50	1.00	1.50	2.00	5.00	10.00	$\rho_{\rm AO,max}$ (arcsec)	$\rho_{\rm Plate,min}$ (arcsec)	$\rho_{\rm Plate,max}$ (arcmin)
HIP31292	0.00	2.82	4.37	5.84	7.07	7.12	7.22	7.16	3.71	13.00	4.86	19.20
HIP31293	0.08	2.40	3.74	5.28	6.85	6.89	7.19	7.07	5.65	14.00	6.75	18.48
HIP31635	0.07	3.95	5.18	6.09	6.32	6.29	6.28	6.13	3.99	13.00	7.39	17.10
HIP31862	...	...	...	...	...	...	...	...	...	...	9.04	12.53
HIP33142	...	0.87	1.31	4.18	6.36	7.94	8.80	9.07	8.83	41.00	6.45	15.91
HIP33226	...	1.18	2.09	5.03	7.13	8.46	8.57	8.65	8.48	35.00	6.98	29.84
HIP33499	0.04	3.41	4.57	4.64	3.87	5.73	5.79	5.80	4.09	14.00	6.08	20.81
HIP34115	...	...	...	...	...	...	...	...	...	...	5.24	11.16
HIP34603	...	1.10	2.04	5.17	7.31	9.11	8.82	9.72	9.44	39.00	6.31	26.48
HIP35191	...	1.78	3.90	4.88	5.03	5.00	5.02	3.37	4.39	14.00	7.66	13.85
HIP35353	...	...	...	...	...	...	...	...	...	...	8.19	11.50
HIP36208	0.00	2.85	5.04	6.29	6.78	6.77	6.78	6.76	2.80	10.00	3.76	43.83
HIP36338	...	...	...	...	...	...	...	...	...	...	5.37	13.56
HIP36626	...	0.63	1.60	3.20	4.29	6.22	7.59	8.33	8.30	35.00	6.18	14.04
HIP36627	...	0.54	1.42	2.92	4.63	6.00	7.06	7.63	7.58	35.00	4.97	13.91
HIP36834	...	...	...	...	...	...	...	...	...	...	6.45	14.53
HIP36915	...	...	...	...	...	...	...	...	...	...	5.91	13.02
HIP36985	...	...	...	...	...	...	...	...	...	...	9.67	11.76
HIP37217	0.00	3.44	5.17	6.50	6.92	6.94	6.94	6.81	4.44	13.00	5.67	15.72
HIP37288	...	3.86	5.50	6.66	7.75	7.70	7.74	7.17	7.02	16.00	8.73	11.43
HIP37766	...	3.45	5.34	6.97	7.63	7.74	7.73	7.57	6.85	13.00	5.37	27.98
HIP38082	...	...	...	...	...	...	...	...	...	...	5.64	11.28
HIP38956	...	0.66	1.69	4.11	6.14	7.39	7.82	8.09	8.06	36.00	5.37	19.34
HIP40501	0.02	3.55	4.90	6.39	7.16	7.22	7.21	7.06	5.93	15.00	16.93	18.27
HIP41824	...	0.59	1.85	4.05	6.32	7.90	8.64	8.94	5.67	41.00	4.70	15.06
HIP42220	...	...	...	...	...	...	...	...	...	...	8.33	12.10
HIP42762	...	...	...	...	...	...	...	...	...	...	5.51	11.16
HIP44722	...	...	...	...	...	...	...	...	...	...	11.01	11.45
HIP45908	0.00	2.99	4.29	5.79	6.74	6.79	6.86	6.80	3.56	13.00	8.77	15.93
HIP46655	...	1.21	2.18	5.28	6.88	8.07	8.05	8.12	7.85	41.00	12.63	17.24
HIP46706	...	0.94	1.37	0.62	3.26	5.43	6.90	8.93	9.07	39.00	5.51	16.65
HIP46769	...	0.12	1.75	3.45	6.22	7.87	8.43	8.76	8.71	43.00	27.68	11.99
HIP47103	0.00	3.48	5.22	6.77	8.59	8.83	8.94	8.58	7.95	14.00	5.26	18.47
HIP47425	0.03	2.91	3.99	5.54	7.40	7.64	7.67	7.61	6.21	14.00	7.02	17.61
HIP47513	0.01	3.29	5.14	6.30	6.64	6.59	6.62	6.54	4.78	13.00	24.58	14.80
HIP47620	...	0.38	2.18	3.56	6.17	7.67	8.03	8.14	8.02	54.00	6.58	13.56
HIP47650	...	...	...	...	...	...	...	...	...	...	11.55	14.68
HIP47741	...	...	...	...	...	...	...	...	...	...	3.36	11.88
HIP47780	0.07	2.92	4.54	5.93	7.76	8.08	8.14	7.92	4.31	15.00	8.10	16.89
HIP48336	...	...	...	...	...	...	...	...	...	...	8.06	12.15
HIP48659	...	3.05	4.76	7.01	8.80	9.44	9.64	9.55	8.95	13.00	5.13	14.72
HIP48714	...	1.06	1.99	4.30	6.77	8.30	8.49	9.89	9.81	37.00	24.31	15.78
HIP49969	0.05	1.13	3.84	6.80	7.89	7.94	7.94	7.77	6.38	14.00	23.51	13.51
HIP49986	...	0.76	1.76	3.46	5.62	7.09	7.69	8.06	7.94	36.00	24.85	21.18
HIP50341	...	...	...	...	...	...	...	...	...	...	6.45	12.22
HIP51007	...	1.10	2.07	4.80	6.74	8.21	8.34	8.46	8.21	41.00	6.58	13.50
HIP51317	...	0.00	1.66	5.00	7.37	8.86	9.50	11.33	11.58	46.00	24.32	23.58
HIP52190	...	...	...	...	...	...	...	...	...	...	6.34	11.92
HIP52596	...	...	...	...	...	...	...	...	...	...	6.07	11.90
HIP53020	...	0.59	2.63	4.59	6.58	8.27	9.15	10.84	11.24	24.00	4.57	24.65
HIP53985	...	0.66	1.78	4.13	6.46	7.80	8.88	9.20	9.10	36.00	9.14	14.16
HIP54035	...	1.02	1.87	4.30	6.58	7.94	8.21	8.61	8.51	36.00	44.59	65.44
HIP54211	...	0.68	1.87	4.31	6.75	8.11	8.64	9.05	8.84	39.00	8.86	34.38
HIP54532	...	0.63	1.62	3.36	5.42	6.06	6.23	6.17	5.93	42.00	7.69	15.50
HIP55042	...	...	...	...	...	...	...	...	...	...	2.50	13.15
HIP55360	...	1.10	2.06	4.96	7.15	8.89	8.68	9.41	9.12	38.00	9.94	18.69
HIP56157	...	...	...	...	...	...	...	...	...	...	6.04	12.63

Table 7: continued.

	AO Δm (mag) at $\rho = (arcsec)$									ρ sensitive to full MS		
HIP	0.05	0.15	0.25	0.50	1.00	1.50	2.00	5.00	10.00	$\rho_{\rm AO,max}$ (arcsec)	$\rho_{\rm Plate,min}$ (arcsec)	$\rho_{\rm Plate,max}$ (arcmin)
HIP56244	...	3.09	4.80	6.63	9.06	10.32	10.78	11.34	10.45	15.00	5.80	16.09
HIP56528	...	1.16	2.14	5.37	6.90	8.50	9.02	9.36	9.26	35.00	8.37	18.76
HIP57050	...	0.51	1.70	3.38	5.50	6.79	7.31	8.34	8.09	41.00	5.37	15.01
HIP57087	...	0.78	2.67	6.32	8.60	8.96	9.11	9.18	8.88	36.00	14.64	16.44
HIP57544	...	0.72	1.79	4.36	6.65	7.56	8.29	8.91	8.71	38.00	5.78	31.14
HIP57548	...	1.08	2.03	4.54	6.47	7.54	7.70	7.77	7.50	41.00	15.45	49.67
HIP57802	...	1.12	2.01	4.80	7.11	8.83	8.67	9.40	9.10	39.00	25.39	19.41
HIP59406	...	2.83	4.58	6.80	7.77	7.84	7.85	7.65	6.78	15.00	4.45	13.24
HIP60444	...	...	...	...	...	...	...	...	...	...	6.31	12.92
HIP60559	...	0.93	1.87	4.22	6.48	7.97	8.08	8.62	8.26	39.00	5.13	18.83
HIP60910	...	2.71	5.16	7.19	9.14	9.78	10.35	10.58	9.73	12.00	13.43	12.64
HIP61094	...	0.01	2.32	4.23	6.27	7.24	7.64	10.03	11.76	23.00	9.00	12.21
HIP61629	...	2.38	4.73	6.85	8.65	9.32	9.57	10.36	10.35	27.00	6.48	17.20
HIP61706	...	...	...	...	...	...	...	...	...	...	5.78	11.60
HIP61874	0.00	3.06	4.34	5.77	5.97	5.95	5.98	5.82	3.01	15.00	3.92	21.42
HIP62452	...	0.96	1.96	4.33	6.40	7.58	7.73	7.81	7.54	41.00	5.91	19.91
HIP62556	...	1.01	1.15	2.55	5.42	7.10	7.93	8.48	8.25	37.00	6.31	16.32
HIP63510	...	3.40	4.54	6.71	7.02	7.03	7.01	6.74	5.22	14.00	7.93	14.26
HIP65011	...	0.08	1.25	2.52	4.86	6.53	7.29	7.72	7.66	42.00	9.54	12.56
HIP65026	...	0.48	1.81	3.98	3.49	3.47	6.62	9.14	9.03	41.00	30.49	15.57
HIP65714	...	...	...	...	...	...	...	...	...	...	5.37	12.00
HIP65859	...	0.11	1.29	3.49	5.82	7.03	7.52	9.25	9.87	36.00	26.73	21.77
HIP66625	...	0.23	1.44	2.83	5.26	7.00	7.78	8.06	8.02	41.00	8.06	12.81
HIP66906	...	0.63	1.72	3.97	6.31	7.54	8.39	8.57	8.48	36.00	5.64	17.96
HIP67155	...	3.46	5.72	7.40	7.84	8.03	8.06	7.85	7.08	14.00	11.82	30.92
HIP67164	...	0.62	1.63	3.53	5.83	7.26	8.00	8.22	8.02	38.00	4.99	16.27
HIP68469	...	0.66	1.80	4.08	6.35	7.77	8.65	8.85	8.74	36.00	6.72	16.62
HIP69454	0.00	3.44	4.11	6.35	8.19	8.14	8.54	8.40	5.46	20.00	8.10	14.27
HIP70475	...	...	...	...	...	...	...	...	...	...	5.10	11.67
HIP70865	...	...	...	...	...	...	...	...	...	...	14.51	11.90
HIP70890	0.00	3.27	4.98	6.65	8.45	9.01	9.17	9.05	8.30	14.00	4.86	128.61
HIP70975	...	3.59	4.46	4.51	4.52	4.55	4.54	4.45	3.08	13.00	4.43	15.41
HIP71253	...	0.65	1.67	4.09	6.41	7.45	8.18	8.87	8.62	39.00	11.42	27.50
HIP71898	...	0.65	1.86	4.52	7.21	8.31	8.77	9.05	8.86	39.00	7.52	15.53
HIP72896	...	3.21	5.30	6.60	1.93	7.04	7.22	7.01	6.32	14.00	4.97	16.40
HIP72944	...	3.20	4.94	7.06	8.27	8.50	8.57	6.50	7.84	17.00	7.52	17.27
HIP73470	...	0.45	1.50	2.98	4.96	3.08	5.39	8.44	8.28	41.00	11.69	14.13
HIP74190	...	...	...	...	...	...	...	...	...	...	6.31	11.53
HIP74995	...	2.00	4.35	5.99	8.05	8.63	8.74	8.81	8.63	28.00	19.22	26.82
HIP75187	...	0.66	1.96	4.51	6.90	8.39	8.89	9.24	9.10	38.00	7.79	14.61
HIP76074	0.00	4.10	5.32	7.31	8.99	8.61	9.43	9.33	8.52	14.00	8.09	28.11
HIP76832	...	0.12	1.00	2.57	5.14	6.86	7.59	7.78	7.75	54.00	3.49	12.52
HIP76901	...	0.64	1.69	3.68	6.06	7.47	8.22	8.47	8.37	36.00	4.99	15.98
HIP78353	...	...	...	...	...	...	...	...	...	...	7.25	11.99
HIP79431	...	...	...	...	...	...	...	...	...	...	5.80	11.58
HIP79755	...	1.13	2.10	4.68	7.10	7.93	8.28	8.45	8.27	37.00	11.69	15.60
HIP79762	...	0.43	1.63	3.62	6.02	7.46	8.46	8.55	8.51	36.00	6.85	15.52
HIP80018	0.15	2.95	4.38	6.04	8.04	8.24	8.88	6.27	2.26	14.00	8.09	19.98
HIP80346	...	0.57	1.37	2.69	4.12	5.39	6.49	7.65	7.37	40.00	7.12	20.69
HIP80459	...	1.36	2.76	5.04	7.67	8.65	8.83	9.01	9.00	35.00	7.79	25.58
HIP80824	...	0.68	1.89	4.16	6.80	7.89	8.11	8.27	8.08	37.00	16.13	38.83
HIP82809	0.03	3.13	4.46	5.69	6.06	6.05	6.08	5.90	3.66	14.00	4.97	24.82
HIP82817	...	0.54	0.33	4.24	6.72	6.77	7.13	7.17	7.14	22.00	14.24	26.90
HIP83043	...	0.65	1.72	3.65	6.03	7.45	8.13	8.79	8.59	42.00	8.33	16.11
HIP83599	0.00	3.39	4.64	5.62	5.93	5.94	5.94	5.86	3.49	14.00	8.60	15.77
HIP83762	...	0.33	2.94	4.37	7.05	7.51	7.50	7.53	7.55	50.00	7.39	12.47
HIP83945	...	0.65	1.89	4.48	6.58	8.14	8.83	9.12	9.09	34.00	5.51	22.39

Table 7: continued.

	AO Δm (mag) at $\rho = (arcsec)$									ρ sensitive to full MS		
HIP	0.05	0.15	0.25	0.50	1.00	1.50	2.00	5.00	10.00	$\rho_{\mathrm{AO,max}}$ (arcsec)	$\rho_{\mathrm{Plate,min}}$ (arcsec)	$\rho_{\mathrm{Plate,max}}$ (arcmin)
HIP84051	...	...	...	...	...	...	...	...	...	...	8.50	13.36
HIP84099	...	0.55	3.27	4.69	7.75	8.18	8.17	8.15	8.15	53.00	5.91	13.89
HIP84140	...	0.25	0.17	2.11	5.24	6.93	8.08	8.92	8.91	37.00	9.27	27.88
HIP84521	...	...	...	...	...	...	...	...	...	...	6.31	11.18
HIP84790	...	0.44	2.79	4.34	7.27	7.83	7.92	7.92	7.86	51.00	6.04	13.46
HIP84794	...	...	...	...	...	...	...	...	...	...	6.85	14.38
HIP85523	...	2.29	4.48	7.06	9.17	9.41	9.50	9.48	9.37	28.00	9.31	36.71
HIP85665	...	0.15	1.20	3.28	5.62	7.00	7.75	9.16	9.32	42.00	8.86	16.71
HIP86057	0.00	3.22	5.32	7.31	8.91	8.43	9.29	9.25	8.12	13.00	7.56	17.14
HIP86087	...	0.34	2.43	3.95	6.91	8.46	8.73	8.77	8.75	38.00	7.79	11.82
HIP86162	...	0.65	1.91	4.57	6.81	8.28	8.87	9.09	9.07	35.00	8.46	36.81
HIP86214	0.05	3.12	4.89	6.74	8.12	8.42	8.48	8.25	7.43	14.00	5.40	32.82
HIP86287	...	0.62	1.60	3.32	5.60	7.07	8.24	8.93	8.95	36.00	8.46	20.61
HIP86776	...	0.53	1.96	4.05	7.00	7.84	8.24	9.00	8.82	38.00	7.52	17.58
HIP86990	0.08	3.10	4.07	4.50	4.62	4.65	4.64	4.46	2.80	16.00	9.04	28.58
HIP87937	...	-0.13	0.65	3.76	5.75	6.77	7.44	8.59	8.44	25.00	6.85	91.39
HIP87938	...	0.39	2.52	4.14	6.82	7.53	7.55	7.62	7.56	45.00	5.51	11.83
HIP88574	...	0.64	1.70	3.86	6.13	7.54	8.69	9.13	9.09	36.00	8.06	21.48
HIP91430	...	...	...	...	...	...	...	...	...	...	20.82	12.93
HIP91699	...	0.45	1.63	3.38	5.45	6.77	7.10	7.99	7.74	41.00	6.31	14.56
HIP91768	...	0.68	1.86	4.23	6.95	7.84	8.06	8.13	7.93	39.00	6.18	46.70
HIP91772	...	0.61	1.82	4.40	6.86	8.54	8.60	9.16	9.05	36.00	8.33	46.70
HIP92403	...	2.23	4.35	6.49	8.17	8.49	8.63	8.66	8.31	28.00	4.99	56.12
HIP92871	...	0.68	1.95	4.62	7.47	8.43	8.83	9.23	9.01	42.00	7.66	14.16
HIP93069	...	...	...	...	...	...	...	...	...	...	12.14	13.57
HIP93101	...	1.27	2.63	4.78	7.09	5.54	8.37	8.83	8.64	38.00	9.27	15.28
HIP93206	...	...	...	...	...	...	...	...	...	...	6.75	11.83
HIP93873	...	0.62	1.60	3.67	5.79	7.11	8.07	8.52	8.40	36.00	6.98	19.58
HIP93899	...	1.85	0.07	1.55	3.41	4.82	5.95	8.14	9.05	50.00	5.91	19.04
HIP94349	0.00	1.19	2.95	5.54	7.69	7.50	8.35	8.33	7.44	13.00	19.48	16.31
HIP94761	...	0.61	1.74	3.98	6.28	7.73	8.55	9.02	8.99	34.00	9.94	28.39
HIP97241	...	1.15	2.08	4.92	6.92	8.55	8.94	9.28	9.08	39.00	7.92	14.50
HIP97292	...	0.44	2.16	3.41	5.79	6.85	7.17	4.96	7.30	54.00	9.54	12.24
HIP99150	...	1.73	3.40	4.92	7.27	8.30	8.60	9.34	9.27	27.00	4.32	11.18
HIP99701	0.01	3.28	4.72	5.54	5.90	5.92	5.95	5.73	4.98	15.00	13.63	26.89
HIP100923	...	...	...	...	...	...	...	...	...	...	6.21	11.23
HIP101180	...	0.65	1.71	4.18	6.63	7.97	8.67	8.96	8.82	36.00	6.18	20.85
HIP102141	...	3.19	5.00	6.33	7.30	7.30	6.55	7.34	6.70	14.00	7.43	15.58
HIP102401	...	0.50	3.37	4.90	7.44	7.81	7.89	7.88	7.76	52.00	7.52	13.53
HIP102409	...	3.52	5.37	6.74	6.88	6.89	6.84	6.49	5.38	14.00	11.87	16.82
HIP103039	...	0.66	1.90	4.66	7.07	8.42	8.96	9.23	9.18	35.00	11.42	29.17
HIP103096	...	0.68	1.90	4.52	6.89	8.20	8.66	8.99	8.98	34.00	10.21	23.65
HIP103441	0.02	4.67	6.01	6.85	7.05	7.04	7.05	6.65	5.26	14.00	4.16	12.10
HIP103800	...	...	...	...	...	...	...	...	...	...	15.18	11.59
HIP103910	...	...	...	...	...	...	...	...	...	...	4.86	13.10
HIP104432	...	...	...	...	...	...	...	...	...	...	6.85	13.70
HIP104644	...	...	...	...	...	...	...	...	...	...	6.21	11.26
HIP106106	...	0.81	1.94	4.20	6.45	8.08	8.54	8.97	8.96	36.00	5.24	24.86
HIP106255	0.05	1.55	4.00	7.13	8.68	8.58	8.94	8.82	7.90	14.00	4.57	20.09
HIP106440	...	2.06	4.38	6.54	8.78	9.37	9.43	9.48	9.37	28.00	10.39	33.65
HIP106811	...	...	...	...	...	...	...	...	...	...	6.85	12.52
HIP108159	...	0.07	0.29	2.03	3.65	5.17	5.85	6.01	5.99	20.00	6.07	11.39
HIP108569	...	...	...	...	...	...	...	...	...	...	10.12	13.91
HIP108706	...	1.23	2.48	4.61	7.09	5.44	8.30	8.71	8.48	39.00	4.84	18.72
HIP108782	...	0.63	1.81	4.19	6.56	8.01	8.83	9.34	9.31	35.00	9.14	16.27
HIP109388	...	2.09	4.56	6.44	7.30	7.33	7.35	7.30	7.14	28.00	7.26	18.32
HIP109555	...	1.07	2.04	4.57	6.75	8.33	8.58	8.95	8.87	36.00	6.99	14.35

Table 7: continued.

	AO Δm (mag) at $\rho = (arcsec)$									ρ sensitive to full MS		
HIP	0.05	0.15	0.25	0.50	1.00	1.50	2.00	5.00	10.00	$\rho_{\rm AO,max}$ (arcsec)	$\rho_{\rm Plate,min}$ (arcsec)	$\rho_{\rm Plate,max}$ (arcmin)
HIP109638	...	...	...	...	...	...	...	...	...	...	6.85	11.14
HIP110893	...	0.59	1.71	4.00	6.14	7.35	6.64	8.61	8.64	35.00	8.06	41.66
HIP111313	...	...	...	...	...	...	...	...	...	...	8.33	13.11
HIP111766	...	2.36	4.90	5.97	5.72	8.32	9.31	9.95	9.89	27.00	6.07	12.65
HIP111802	...	3.56	4.90	7.27	8.56	9.35	9.58	9.72	9.23	14.00	28.46	19.17
HIP112460	...	1.04	2.00	4.52	6.59	8.12	8.42	8.68	8.65	35.00	6.99	32.54
HIP112774	...	...	...	...	...	...	...	...	...	...	21.36	11.80
HIP112909	...	0.47	2.64	4.36	7.12	7.81	7.91	8.00	7.94	57.00	5.91	11.46
HIP113020	...	0.61	1.80	4.20	6.34	7.87	8.76	9.34	9.34	35.00	17.60	35.55
HIP113229	0.04	3.91	4.72	4.90	4.92	4.89	4.84	4.77	1.29	13.00	7.15	19.35
HIP113296	...	0.66	1.84	4.33	6.77	8.18	8.74	9.09	8.93	36.00	10.88	24.35
HIP114046	0.03	3.27	4.72	6.23	6.90	6.97	7.00	6.97	4.01	13.00	33.86	50.88
HIP115332	0.04	4.08	5.37	6.98	7.43	7.29	7.46	7.18	6.59	14.00	5.91	15.17
HIP115562	...	0.19	1.82	3.38	5.97	7.56	8.05	8.33	8.29	42.00	11.28	12.86
HIP116132	...	0.63	1.85	4.32	7.00	8.26	8.76	4.99	9.03	37.00	6.85	26.96
HIP116317	...	...	...	...	...	...	...	...	...	...	13.43	11.92
HIP117473	...	0.75	1.73	4.64	6.48	8.34	8.88	9.43	9.32	39.00	32.51	27.88
HIP117828	0.00	3.61	5.10	6.68	7.47	7.42	7.49	7.42	3.35	13.00	8.77	16.68

This paper has been typeset from a TEX/ LATEX file prepared by the author.